



UNIVERSITAT DE BARCELONA

Bioengineering approach to study the role of cell migration during zebrafish heart regeneration

Işil Tekeli

ADVERTIMENT. La consulta d'aquesta tesi queda condicionada a l'acceptació de les següents condicions d'ús: La difusió d'aquesta tesi per mitjà del servei TDX (www.tdx.cat) i a través del Dipòsit Digital de la UB (diposit.ub.edu) ha estat autoritzada pels titulars dels drets de propietat intel·lectual únicament per a usos privats emmarcats en activitats d'investigació i docència. No s'autoritza la seva reproducció amb finalitats de lucre ni la seva difusió i posada a disposició des d'un lloc aliè al servei TDX ni al Dipòsit Digital de la UB. No s'autoritza la presentació del seu contingut en una finestra o marc aliè a TDX o al Dipòsit Digital de la UB (framing). Aquesta reserva de drets afecta tant al resum de presentació de la tesi com als seus continguts. En la utilització o cita de parts de la tesi és obligat indicar el nom de la persona autora.

ADVERTENCIA. La consulta de esta tesis queda condicionada a la aceptación de las siguientes condiciones de uso: La difusión de esta tesis por medio del servicio TDR (www.tdx.cat) y a través del Repositorio Digital de la UB (diposit.ub.edu) ha sido autorizada por los titulares de los derechos de propiedad intelectual únicamente para usos privados enmarcados en actividades de investigación y docencia. No se autoriza su reproducción con finalidades de lucro ni su difusión y puesta a disposición desde un sitio ajeno al servicio TDR o al Repositorio Digital de la UB. No se autoriza la presentación de su contenido en una ventana o marco ajeno a TDR o al Repositorio Digital de la UB (framing). Esta reserva de derechos afecta tanto al resumen de presentación de la tesis como a sus contenidos. En la utilización o cita de partes de la tesis es obligado indicar el nombre de la persona autora.

WARNING. On having consulted this thesis you're accepting the following use conditions: Spreading this thesis by the TDX (www.tdx.cat) service and by the UB Digital Repository (diposit.ub.edu) has been authorized by the titular of the intellectual property rights only for private uses placed in investigation and teaching activities. Reproduction with lucrative aims is not authorized nor its spreading and availability from a site foreign to the TDX service or to the UB Digital Repository. Introducing its content in a window or frame foreign to the TDX service or to the UB Digital Repository is not authorized (framing). Those rights affect to the presentation summary of the thesis as well as to its contents. In the using or citation of parts of the thesis it's obliged to indicate the name of the author.



FACULTAD DE FÍSICA

PROGRAMA DE DOCTORADO DE BIOMEDICINA

TESIS DOCTORAL

**Bioengineering approach to study the role of
cell migration during zebrafish heart
regeneration**

Işıl Tekeli

2015



FACULTAD DE FÍSICA

PROGRAMA DE DOCTORADO DE BIOMEDICINA

2015

TESIS DOCTORAL

Bioengineering approach to study the role of cell migration during zebrafish heart regeneration

Memoria presentada por

Işıl Tekeli

Para obtener el grado de

Doctora

Tesis doctoral realizada bajo la dirección del Dr. Ángel Raya Chamorro en el Instituto de Bioingeniería de Cataluña (IBEC) y en el Centro de Medicina Regenerativa de Barcelona (CMRB)

Firmado,

El Director:

El Tutor:

La Doctoranda:

Dr. Ángel Raya Chamorro

Dr. Albert Tauler Girona

Işıl Tekeli

Contents

Abstract	v
List of Figures	vii
List of Tables	viii
List of abbreviations	xi
1 Introduction	1
1.1 Overview of regeneration	1
1.2 Heart regeneration	3
1.2.1 The limits of heart regeneration in humans and mammals	3
1.2.2 Heart regeneration in neonatal mice	5
1.2.3 Heart regeneration in urodeles	7
1.3 Heart regeneration in zebrafish	8
1.3.1 Zebrafish as a model organism	8
1.3.2 The zebrafish heart	10
1.3.3 Zebrafish heart regeneration and injury models	13
Amputation	13
Cryoinjury	14
Genetic Ablation	14
1.3.4 Cellular and molecular mechanisms during heart regeneration	15
Epicardial mechanisms	16
Endocardial mechanisms	16
Myocardial mechanisms	17
Mechanisms in larval cardiac regeneration	18

Contents

Cell migration	18
1.3.5 Lineage tracing methods in zebrafish heart regeneration	19
1.4 Multiphoton microscopy and its use in activation of molecules	23
2 Objectives	27
3 Materials and methods	29
3.1 Zebrafish husbandry	29
3.2 Methods related to lineage tracing of zebrafish cardiomyocytes	29
3.2.1 Transgenic zebrafish lines	29
3.2.2 Photoactivation in zebrafish embryos	30
Chemical inducers	30
Inhibition of pigmentation in the embryos	30
<i>In vivo</i> uncaging of caged-cyclofen by using a UV lamp	30
Screening and <i>in vivo</i> imaging	31
3.2.3 Ventricular amputation surgery	31
3.2.4 Labeling with BrdU	32
3.2.5 Heart tissue collection	32
3.2.6 Sample processing and immunohistochemistry	32
3.2.7 Microscopy and image processing	33
3.3 Methods related to three-photon uncaging	33
3.3.1 Set up for measuring three-photon cross-section	33
3.3.2 <i>In vitro</i> damage assay	33
3.3.3 Control experiments	34
3.3.4 Three-photon activation set up	34
3.3.5 Illumination experiments	35
3.4 Methods related to epicardium cell culture experiments	35
3.4.1 Transgenic zebrafish lines	35
3.4.2 Preparation of polyacrylamide gels	35
3.4.3 Heart seeding and epicardium cell culture	36
3.4.4 Microscopy and imaging	36
3.4.5 Measurement of cell migration velocity	37

4	Results	39
4.1	Lineage tracing of cardiomyocytes during zebrafish heart development and regeneration	39
4.1.1	Development of a photo-inducible <i>Cre/lox</i> -based genetic labeling method to specifically label one or a small group of adjacent cardiomyocytes	39
4.1.2	Lineage tracing of labeled cardiomyocytes during zebrafish heart development	44
4.1.3	Lineage tracing of labeled cardiomyocytes during zebrafish heart regeneration	48
4.2	Three photon-based cell photoactivation in living embryos	51
4.3	Development of an <i>ex vivo</i> method to study epicardial cell migration behavior during zebrafish heart regeneration	58
4.3.1	Optimization of epicardial cell culture conditions	58
4.3.2	Optimization of surface coating	60
4.3.3	Characterization of zebrafish epicardial cells from uninjured hearts	61
	Cell migration velocity and traction force measurements	61
	Characterization of cell movement through transgenic zebrafish lines	63
5	Discussion	65
5.1	Discussion of lineage tracing of zebrafish cardiomyocytes during development and regeneration	65
5.2	Discussion about three photon-based cell photoactivation in living embryos	67
5.3	Discussion about development of an <i>ex vivo</i> method to study epicardial cell migration behavior during zebrafish heart regeneration	69
5.4	General discussion	70
6	Conclusions	73
	Bibliography	75
	Appendix I	89

Contents

Appendix II	95
Resumen	115
Agradecimientos	119

Abstract

The zebrafish (*Danio rerio*) is one of the principal models for investigating heart regeneration due to their intrinsic capacity to restore large portions of the heart upon injury. A better understanding of the mechanisms underlying this complex process would help developing strategies to regenerate the human heart. With this aim, here, we set up novel bioengineering approaches to understand cell migration mechanisms of cardiomyocytes and epicardial cells during zebrafish heart regeneration.

The first approach involves the development of a cardiomyocyte-specific, photo-inducible *Cre/lox* genetic labeling system and its use in lineage tracing of embryonic cardiomyocytes during heart development and regeneration. By using this method we show that cardiomyocytes labeled in embryonic hearts survive and contribute to all three (primordial, trabecular, and cortical) layers of the adult zebrafish heart. Moreover, lineage tracing during regeneration show that only cardiomyocytes immediately adjacent to the injury site contribute to the regeneration, and cardiomyocyte fate is extensively predetermined, with cells from each myocardial layer giving rise to cells that retain their layer identity in the regenerated myocardium.

Then, we show that by coupling this labeling system to three-photon microscopy activation, we can perform prospective labeling, and increase the spatial resolution of our labeling system. Three-photon illumination has been used for *in vivo* imaging of deep structures, but whether it can be used for photo-activation had never been tested. Here we show, theoretically and experimentally for the first time, that three-photon illumination is suitable for activating molecules in deep tissues and improving our system in terms of spatial resolution and prospective labeling.

The final approach consists on developing an *ex vivo* experimental set up in order to investigate physical characteristics of epicardial cell migration during zebrafish heart

Abstract

regeneration. This method allows us to measure physical features that are essential for cell migration such as migration velocity and traction forces of the epicardial explants obtained from zebrafish hearts.

All the approaches developed in this thesis offer new bioengineering tools to study zebrafish heart regeneration, and reveal new insights on this process. Moreover, these techniques present wide applicability to perform lineage tracing of other cell types during zebrafish heart regeneration or in other biological processes.

List of Figures

1	Phylogenetic distribution of regeneration across the Metazoa and the Chordata	2
2	Zebrafish adults and larvae	9
3	Comparative morphology of adult atrial and ventricular chambers in the zebrafish and mouse	11
4	Cortical, primordial, and trabecular muscle layers in the juvenile zebrafish heart	12
5	Lineage tracing methods that revealed pre-existing cardiomyocytes are the source of new cardiomyocytes in zebrafish heart regeneration	22
6	Comparison of one, two, and three photon excitation	24
7	The mechanisms of multiphoton excitation	25
8	Chemical structures of 4-hydroxy-tamoxifen, 4-hydroxy-cyclofen, and caged cyclofen	40
9	<i>Cre/lox</i> recombination based genetic labeling system	41
10	Genetic labeling of zebrafish cardiomyocytes using a UV-inducible <i>Cre/lox</i> recombination system	42
11	Diameters of the labeled areas in 4dpf zebrafish hearts	43
12	Genetically labeled cardiomyocytes are found in all three myocardium layers	45
13	Labeled cortical area size	47
14	Cell fate of labeled cardiomyocytes during regeneration	49
15	Cardiomyocytes distant from the amputation site do not contribute to the regenerated tissue	50

List of Figures

16	Numerical results of the ratio between three- and two-photon uncaging rates for the caging group	53
17	Percentage of dead cells as function of laser flux for illumination at 1064 nm	54
18	Cardiomyocyte labeling using three-photon uncaging of cyclofen	55
19	Control experiments for three-photon illumination	56
20	Long-term <i>in vivo</i> lineage tracing of zebrafish cardiomyocytes	57
21	Epicardial explants from different hearts	59
22	Cell movement graphed through manual tracking by Image J	62
23	Average migration velocity of epicardial explants	63
24	Epicardial explants obtained from transgenic zebrafish lines	64

List of Tables

1	Comparison between different injury models for studying zebrafish heart regeneration	15
2	Distribution of the myocardium layers within the labeled areas of the adult hearts	46

List of abbreviations

^{14}C	carbon-14
BrdU	5-bromo-2'-deoxyuridine
<i>cmhc2a</i>	cardiac myosin light chain a (officially called <i>myl7</i>)
Cre	cyclic recombinase
DAPI	4',6-diamidino-2-phenylindole
DMNB	4,5 dimethoxy-2-nitrobenzyl
dpa	days post-amputation
dpc	days post-cryoinjury
dpf	days post-fertilization
DsRed	<i>Discosoma</i> red fluorescent protein
EdU	5-ethynyl-2'-deoxyuridine
EGFP	enhanced green fluorescent protein
<i>fgf17b</i>	fibroblast growth factor 17

List of abbreviations

FGF	fibroblast growth factor
<i>fgfr2</i>	fibroblast growth factor receptor2
<i>fgfr4</i>	fibroblast growth factor receptor 4
<i>gata4</i>	transcription factor gata4
GFP	green fluorescent protein
hpa	hours post-amputation
hpf	hours post-fertilization
<i>myl7</i>	myosin light polypeptide 7
PDGF	platelet-derived growth factor
PTU	1-phenyl 2-thiourea
<i>raldh2</i>	retinaldehyde dehydrogenase 2
RA	retinoic acid
<i>tbx18</i>	t-box transcription factor encoding gene
<i>tcf21</i>	transcription factor 21
UV	Ultraviolet
wpf	weeks post-fertilization

1 Introduction

1.1 Overview of regeneration

Regeneration is defined as the restoration of a lost body part [Bely and Nyberg, 2010]. It is a fascinating process, which involves the recognition of lost tissue or injury, followed by mechanisms that reconstruct this structure. Understanding how such mechanisms are initiated, regulated, and finalized is expected to have a remarkable impact for regenerative medicine.

The ability to regenerate is widespread in the animal kingdom, with representatives from most animal phyla displaying the ability to regrow missing body parts [Brockes et al., 2001, Sánchez Alvarado, 2000] (Fig. 1). Some well-known examples include cnidarians such as *Hydra*, annelids, molluscs, nemertean worms, platyhelminthes such as planarians, and chordates including vertebrates. The regenerative capacities of these animals vary. Planarians, for instance, are capable of regenerating missing heads or entire bodies from small fragments, whereas salamanders are capable of regrowing missing limbs.

The number of cell types to be replaced during a regenerative process varies depending on the tissue or organ. It may consist on replacing a single cell type, such as the case of the salamander lens, or replacing all the cells within a region of the body, such as in the case of planarian regeneration. In the case of salamander, the missing lens is regenerated by the unipotent dorsal iris, which can only give rise to lens cells [Reyer et al., 1973, Tsonis et al., 2004]. In contrast, a small piece of planarian tissue can be considered pluripotent because it can regenerate all cell types of the entire planaria [Reddien and Alvarado, 2004]. The regenerative pluripotency at the tissue scale could be achieved either by the action of individual pluripotent cells, or alternatively, through

1 Introduction

the collective action of multiple cell types that each has different, restricted potential [Tanaka and Reddien, 2011].

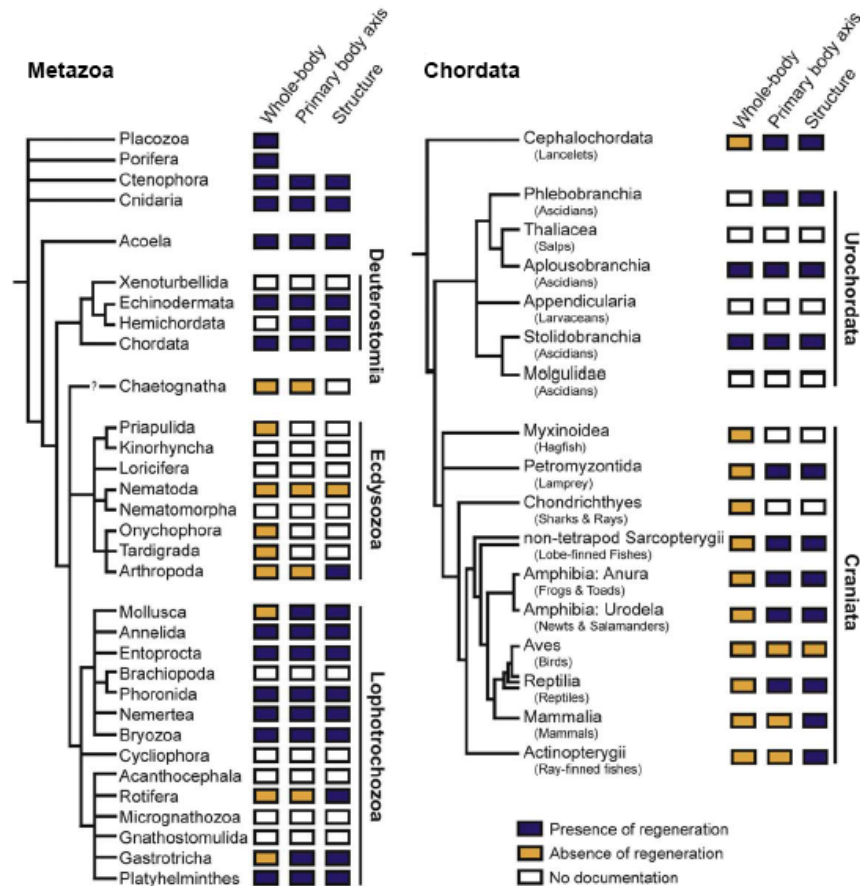


Figure 1. Phylogenetic distribution of regeneration across the Metazoa and the Chordata. ‘Presence of regeneration’ (blue boxes) indicates that at least one well-substantiated report exists for regeneration in that taxon and does not imply that all species in that taxon can regenerate. ‘Absence of regeneration’ (yellow boxes) indicates that there is at least one well-substantiated report for the lack of regeneration in that taxon (and none indicating the presence of regeneration). From Bely and Nyberg [2010].

There are multiple possible means by which new cells are produced for regeneration. They could be produced by resident stem cells, through de-differentiation, or transdifferentiation [Tanaka and Reddien, 2011]. Stem cells go through asymmetric cell division to produce more cells like themselves, and differentiated cells at the same time [Weissman et al., 2001]. In de-differentiation, the pre-existing cells lose their differentiated character, and gain the ability to divide, whereas in transdifferentiation one cell type

changes into another [Jopling et al., 2011]. Several of these mechanisms could act in concert to allow regeneration of a complex tissue in vertebrates.

Mammals, on the other hand, retain the mechanisms for replacing lost cells in a few organs such as the liver, gut, skin, and skeletal muscle [Hata et al., 2007, Masaki and Ide, 2007, Shi and Garry, 2006], however, this type of cell renewal is mostly considered as tissue repair due to natural homeostasis, rather than regeneration. These mechanisms cannot compensate for the tissue lost after an injury, and therefore they should not be confused with epimorphic regeneration [Raya et al., 2004, Tsonis, 2000].

1.2 Heart regeneration

Being able to regenerate the human heart has emerged as a worldwide challenge in recent years, especially since cardiovascular diseases have become the number one cause of death worldwide. According to the World Health Organization, 7.5 million people die annually due to cardiovascular diseases, and this represents almost 1/3 of all global deaths [Mendis et al., 2011]. Different strategies have been developed including stimulating regenerative capacity of cardiomyocytes, therapies involving progenitor or stem cells, cell therapy, and reprogramming, however none of them have succeeded in complete heart regeneration so far. Therefore, studying the natural heart regeneration that occurs in other organisms stands out as an alternative approach. Zebrafish are able to regenerate many parts of their bodies, as well as their heart [Shi et al., 2015]. Therefore, understanding the mechanisms underlying heart regeneration in zebrafish may lead to the development of successful clinical therapies to regenerate the human heart.

1.2.1 The limits of heart regeneration in humans and mammals

The human heart is one of the least regenerative organs of the body. After a myocardial infarction, approximately one billion cardiomyocytes are lost, and due to this extremely

1 Introduction

low regeneration capacity, dying cardiomyocytes are replaced by a non-contractile, fibrous scar tissue [Laflamme and Murry, 2011].

For many years, adult mammalian cardiomyocytes were thought to be terminally differentiated, and post-mitotic [Burton et al., 1999, Goldstein et al., 1974], so the postnatal heart growth was mainly due to hypertrophy (enlargement of cardiomyocytes) [Li et al., 1996]. However, a strong evidence showing that adult human cardiomyocytes can divide and form new cardiomyocytes was revealed [Bergmann et al., 2009]. Bergmann and colleagues exploited the pulse of atmospheric carbon-14 (^{14}C) occurred during the nuclear bomb testing in the cold war. Since ^{14}C entered into the human DNA through the plants, and food chain, the levels of ^{14}C in the cardiomyocytes corresponded to the ^{14}C levels of the atmosphere when these cells were born. The analysis showed that individuals born up to 22 years before the bombings had high ^{14}C levels indicating that human cardiomyocytes were capable of renewal during adulthood. Nevertheless, mathematical modeling based on this study estimated very low cardiomyocyte turnover. Approximately 1% of the cardiomyocytes were renewed at age 20, and 0.4% at age 75. According to this, around 45% of cardiomyocytes are renewed during a human's lifetime, while the remaining 55% remain since birth [Bergmann et al., 2009].

While it is not technically feasible to identify the origin of newly forming human cardiomyocytes, i.e. whether they come from pre-existing cardiomyocytes or from progenitor cells, this issue has been investigated in mice. Studies based on lineage tracing of differentiated cardiomyocytes and multi-isotope imaging mass spectrometry in mice concluded that pre-existing cardiomyocytes duplicate to generate new cardiomyocytes at a low rate during homeostasis and after an injury [Ali et al., 2014, Senyo et al., 2013]. However, another lineage tracing based study suggested that the progenitor cells are the ones that contribute to cardiomyocyte formation after an injury [Hsieh et al., 2007]. In this work, the authors genetically labeled mice cardiomyocytes and traced their progeny. Since they observed a reduction in the fraction of labeled cardiomyocytes after an injury, they concluded that the major contribution came from unlabeled progenitor cells [Hsieh et al., 2007]. Similarly, there are opposing conclusions regarding the contribution of c-kit-positive cardiac progenitor cells to cardiomyocyte production. While one study reported that c-kit-positive cells are necessary and sufficient for cardiac regeneration [Ellison et al., 2013], another study found that these cells form negligible numbers of

1.2 Heart regeneration

cardiomyocytes both during homeostasis and after injury [van Berlo et al., 2014]. Even though further studies are necessary to elucidate how new cardiomyocytes are formed in the adult mammalian heart, it is clear that the rate of new cardiomyocyte formation is too low to result in clinically meaningful myocardial regeneration [Senyo et al., 2014].

A possible reason for this insufficient proliferation of mammalian cardiomyocytes might be their DNA content. Most mammalian cardiomyocyte contain more than two sets of chromosomes. Rodent cardiomyocytes, starting from 4 days after birth, become binucleated with each nucleus remaining diploid [Li et al., 1996], while most human cardiomyocytes (about 74%) maintain a single nucleus, however increase their DNA content to tetraploidy or even higher ploidy [Adler, 1975, Adler and Friedburg, 1986]. Although some indirect evidence have been shown for the proliferation of binucleated cardiomyocytes [Naqvi et al., 2014], it is possible that the mononucleated cardiomyocytes are less differentiated than bi- or multinucleated cardiomyocytes and reenter cell cycle more readily to contribute to myocardial regeneration. Indeed, the majority of zebrafish cardiomyocytes are mononucleated [Poss, 2007], and this could be associated with their high proliferative capacity.

1.2.2 Heart regeneration in neonatal mice

The regenerative ability of the zebrafish heart encouraged scientists to study heart regeneration in mammalian models. In 2011, Porrello and colleagues reported that neonatal mice can regenerate their heart until 1 week after birth. They observed that 1-day-old neonatal mice regenerated their heart within the following 21 days when approximately 15% of the apex of the left ventricle was surgically removed [Porrello et al., 2011]. The series of regenerative events that they detected were highly similar to those described in zebrafish, such as initial formation of a blood clot at the injury site, early infiltration of inflammatory cells and fibroblasts, deposition of extracellular matrix, activation of epicardial genes, and the eventual replacement of the blood clot and fibrotic tissue with new cardiomyocytes. Lineage tracing experiments and 5-bromo-2'-deoxyuridine (BrdU) labeling together with the observation of sarcomeric disassembly in cardiomyocytes indicated that the majority of the newly formed cardiomyocytes came from pre-existing cardiomyocytes through cell proliferation [Porrello et al., 2011]. Interestingly,

1 Introduction

this regenerative potential was lost by the first week of age, since 7-day-old neonatal mice failed to regenerate lost cardiac tissue. Instead, a fibrotic scar tissue was observed in the wound, and the sarcomeric disassembly did not take place [Porrello et al., 2011]. Notably, this loss of cardiac regenerative capacity in neonatal mice coincides with when cardiomyocytes become binucleated and withdraw from the cell cycle [Li et al., 1996], supporting the view that proliferative capacity of cardiomyocytes are directly related with regenerative capacity of the heart.

A recent study by Andersen et al. questioned the regeneration of neonatal hearts upon ventricular resection. They found that extensive scarring occurred in apically resected hearts at 21 days post-surgery and found limited evidence for formation of new cardiomyocytes [Andersen et al., 2014]. Upon this publication, several laboratories claimed to have produced data supporting that the neonatal mouse heart does have regenerative capabilities and new cardiomyocytes form after myocardial injury [Sadek et al., 2014], and indicated that the controversial results were probably due to technical considerations as well as determining how regeneration was defined [Bryant et al., 2015, Sadek et al., 2014]. However, the discussions regarding this issue have continued in the cardiovascular community, with the aim of explaining the differences observed among different groups.

Meanwhile, in addition to the ventricular resection model, myocardial infarction [Haubner et al., 2012, Porrello et al., 2013] and cryoinjury [Darehzereshki et al., 2015, Jesty et al., 2012, Strungs et al., 2013] models have been developed in neonatal mice. In the infarction model, myocardial ischemia was induced by permanent ligation of the left anterior descending coronary artery, and regeneration of the injured heart muscle was observed in 1-day-old neonatal mice. Consistent with the studies using the ventricular resection model, 7- and 14-day-old mice failed to undergo cardiac regeneration following myocardial infarction [Porrello et al., 2013]. Also, histological and genetic lineage tracing studies demonstrated that the majority of regenerated cardiomyocytes were derived from pre-existing cardiomyocytes through cell proliferation, similar to what happens after ventricular resection in neonatal mice [Haubner et al., 2012, Porrello et al., 2013]. In the cryoinjury model, different results were obtained in various studies. Jesty et al. reported that cryoinjured mice at 1-3 days of age regenerated a large proportion of the injured tissue over a period of 94 days, however the regeneration was not complete.

1.2 Heart regeneration

In contrast with results from ventricular resection and infarction models, they observed contribution of c-kit⁺ cardiac progenitor cells to regeneration in addition to high amount of cardiomyocyte proliferation [Jesty et al., 2012]. However, a recent paper by Strungs et al. has reported complete regeneration of 1-day-old neonatal hearts following cryoinjury and that this regenerative potential is lost by day 7 after birth [Strungs et al., 2013]. Adding to the controversy, a third study that applied both transmural and non-transmural cryoinjury in neonatal mice indicated that after a transmural cryoinjury neonatal heart failed to regenerate due to lack of sufficient cardiomyocyte proliferation, whereas non-transmurally cryoinjured neonatal hearts fully regenerated [Darehzereshki et al., 2015].

In summary, many recent studies show that the neonatal mice can regenerate their heart through cardiomyocyte proliferation following different forms of tissue damage, including ventricular resection, myocardial infarction, and cryoinjury, and this regenerative potential is lost already at one week after birth. However, there are other studies indicating that neonatal mice do not fully regenerate. More studies remain to be done in order to clarify these differences obtained in regenerative capacity of the neonatal mice heart, and identify the molecular and cellular basis for neonatal heart regeneration.

1.2.3 Heart regeneration in urodeles

Urodele amphibians such as newts and axolotls can regenerate many parts of their body including limbs, tail, spinal cord, retina, lens, jaws, intestine, and brain tissue [Carlson, 2011]. The majority of the studies examining natural cardiac regeneration capacity in amphibians were done on newts, and these studies showed varying results over the years.

The proliferative potential of newt cardiomyocytes was first described by John Oberpriller and Jean C. Oberpriller at the beginning of 1970s. They carried out a series of studies that characterized cardiac regeneration in adult newt upon amputation of the ventricular apex. They observed mitotic cells in the wound area 16 to 22 days after injury, and based on the electron microscopy analysis they concluded that these cells were cardiomyocytes [Oberpriller and Oberpriller, 1971]. Later, in a detailed study they defined the events that take place after amputation, and concluded that newt hearts were capable

1 Introduction

of regeneration to some extent but failed to achieve it completely [Oberpriller and Oberpriller, 1974]. On the other hand, when the amputated cardiac tissue was minced and transplanted back to the wound site, functional integration occurred and the amputated ventricle was restored [Bader and Oberpriller, 1979]. More recently, it was reported that resection injuries at the base of the newt heart regenerated with much less scarring [Witman et al., 2011]. Additionally, experiments done with isolated newt cardiomyocytes showed that they were able to divide in culture conditions [Oberpriller et al., 1995], however mono and binucleated cardiomyocytes were heterogenous in terms of their proliferation [Bettencourt-Dias et al., 2003]. This finding, together with the difference in the regenerative responses towards an injury in the apex and in the base, raises the possibility that there may be different populations of cardiomyocytes in the newt heart with distinct regenerative potentials.

Despite these important findings, and their pioneering role as experimental model for regeneration, newt lost their place as protagonists in regeneration research since they lack genetic tools that are required for revealing cellular and molecular mechanisms of regeneration.

1.3 Heart regeneration in zebrafish

1.3.1 Zebrafish as a model organism

Zebrafish, *Danio rerio*, is a small, freshwater, teleost fish that originally comes from rivers in India (Fig. 2 a, b). It has become a widespread vertebrate model in research due to its advantageous features such as short generation time, the large numbers of eggs laid, and the fact that, because fertilization is external, and embryos remain transparent until 72 hours post-fertilization (hpf), most of the development stages are visible (Fig. 2 d, e).

The zebrafish has been used in developmental biology for many years [Creaser, 1934], but its current position as a model organism started with the pioneer work of Streisinger et al., who used molecular genetics techniques to study vertebrate embryology [Streisinger

1.3 Heart regeneration in zebrafish

et al., 1981], and Kimmel, who studied zebrafish embryonic development in detail, especially the nervous system [Kimmel, 1993, Kimmel et al., 1990, 1989].

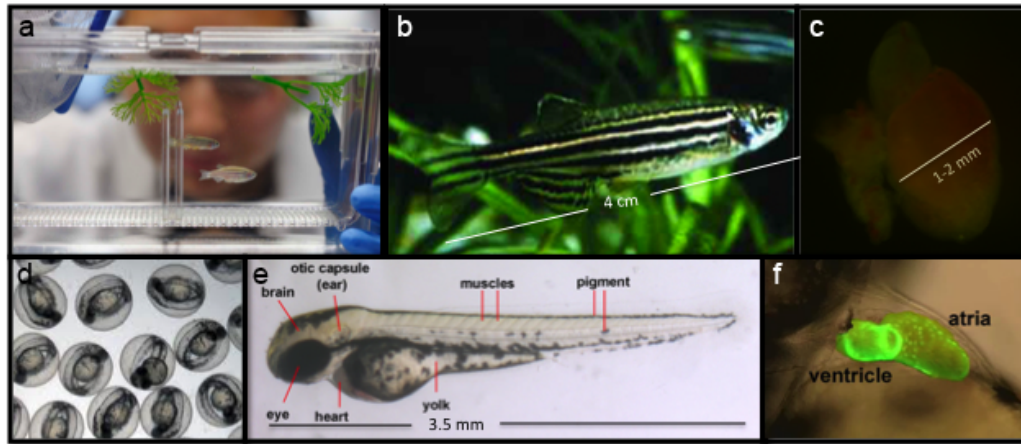


Figure 2. Zebrafish adults and larvae (a) Female and male adult zebrafish are put in a crossing tank to obtain eggs. The size of (b) an adult zebrafish is around 4 cm long, and (c) an adult heart is 1-2 mm. (d) Zebrafish eggs remain in their corion until 48-72 hpf. (e) At 72 hpf larvae have many organs developed, including the heart (f).

Zebrafish benefits from a powerful set of genetic tools developed initially for research on developmental biology [Driever et al., 1996]. In order to identify genes responsible for development, thousands of developmental and behavioral mutants were created by random chemical mutagenesis using N-ethyl-N-nitrosourea (ENU) [Solnica-Krezel et al., 1994]. Then in 2010, sequencing of the zebrafish genome was completed by the Sanger Institute [Howe et al., 2013], which facilitated genetic screens using insertional mutagenesis, through transposon- or viral-based methods, rather than random chemical mutations [Kettleborough et al., 2013].

Transposons are DNA sequences that can jump into or out of the genome, catalyzed by transposase enzymes. This property allows transposons to be used for transgenesis by flanking the sequence to be integrated with transposon sites and then co-injecting the DNA construct and transposase mRNA into a single cell embryo. Today, the adaptation of Tol2 transposon mutagenesis system to zebrafish [Kwan et al., 2007], together with the efficacy of expressing fluorescent reporters in a transparent animal accounts for the tens of thousands of transgenic zebrafish lines available (zfin.org).

1 Introduction

Another way to knockdown a gene function in zebrafish is through morpholino injection. Morpholinos are stable, modified oligonucleotides in which the deoxyribose ring has been replaced with a morpholine ring, designed to bind complementary sequences at a gene's transcription start or splicing sites, thus resulting in blockade of its translation or splicing [Summerton and Weller, 1997]. The effect of morpholinos is transitory, but usually efficient during the first 2 days of development when injected into one-cell stage embryo. However, different approaches have been used to introduce morpholinos into adult tissues, such as using *vivo*-morpholinos, a form of morpholino that can be readily taken into cells by endocytosis, by electroporation [Thummel et al., 2011], or implantation of morpholino-loaded beads [Becker and Becker, 2014]. Today, generating knockdown phenotypes by using morpholinos has largely been replaced by targeted genome editing techniques, which can produce heritable changes in the genome, such as Zinc finger nucleases (ZFNs), transcription activator-like effector nucleases (TALENs), or clustered regularly interspaced short palindromic repeats (CRISPRs) [Wyatt et al., 2015].

Currently there are more than 900 laboratories around the world that use zebrafish, and since the beginning of 21st century it has also become a new experimental model in regeneration studies due to its high regenerative capacity and the availability of molecular and genetic tools. Today it is known that adult zebrafish can regenerate many tissue and organs including fins [Johnson and Weston, 1995], optic nerves [Bernhardt et al., 1996], spinal cord [Becker et al., 1997], retinae [Vihtelic and Hyde, 2000], liver [Sadler et al., 2007], pancreas [Moss et al., 2009], kidney [Diep and Davidson, 2011], brain [Kroehne et al., 2011], and heart [Poss et al., 2002].

1.3.2 The zebrafish heart

In mammals, the heart is the first organ that develops, since embryo survival depends on the proper functioning of the heart [Bakkers, 2011]. The zebrafish embryos, however, are not completely dependent on a functional cardiovascular system in the early developmental stages. This is because the embryos can still obtain enough nutrients and oxygen through diffusion due to its small size [Hu et al., 2001]. This feature permits

1.3 Heart regeneration in zebrafish

analysis of mutants with cardiovascular defects [Stainier et al., 1996, 1993]. However, regarding the general aspects of cardiovascular development, and also heart structure and composition, zebrafish are comparable to mammals [Hu et al., 2001, Stainier, 2001](Fig. 3)

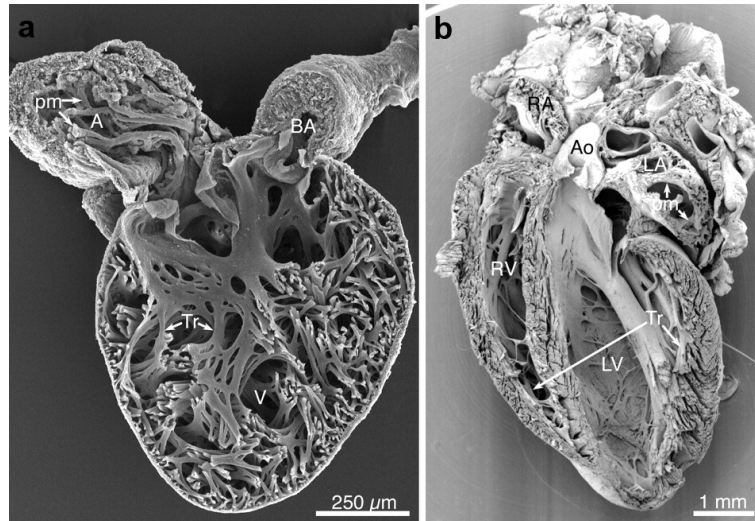


Figure 3. Comparative morphology of adult atrial and ventricular chambers in the zebrafish and mouse. Main features of chamber morphology (ventricles with trabeculae carneae, Tr; atria with pectinate muscles, pm) are conserved between (a) zebrafish and (b) mouse hearts. The differences are in higher proportion of trabeculated ventricular myocardium and presence of a single atrial and ventricular chamber in the fish. From Sedmera [2011].

The zebrafish heart, approximately 1 mm³ in size, has two chambers: one ventricle and one atrium [Stainier et al., 1993] (Fig. 2 c). In contrast to the double-circulation of the mammalian heart that works at high pressure, zebrafish has a single-circulation, not requiring the pulmonary circulation, and therefore has a simpler structure. In zebrafish, the single ventricle and atrium lack septa, and the outflow tract consists on a simple bulbus arteriosus. The blood enters the atrium through the sinus venosus, which collects blood from the body, then passes to the ventricle, and goes out through the outflow tract, which transfers the blood into the gills arches for oxygenation [Hu et al., 2001].

As in mammals, the zebrafish heart is composed of three tissue layers called the myocardium, epicardium, and endocardium. The myocardium is the heart muscle tissue that is composed of contractile cardiomyocytes, and is surrounded by one-thick cell

1 Introduction

layers both inside and outside, known as endocardium and epicardium, respectively. Similar to mammalian heart, in zebrafish, the myocardium has been recognized to be divided into a peripheral wall of compact muscle, and an inner trabecular muscle [Hu et al., 2001]. However, recently within the compact muscle two different heart muscle lineages were identified: primordial, and cortical muscle [Gupta and Poss, 2012].

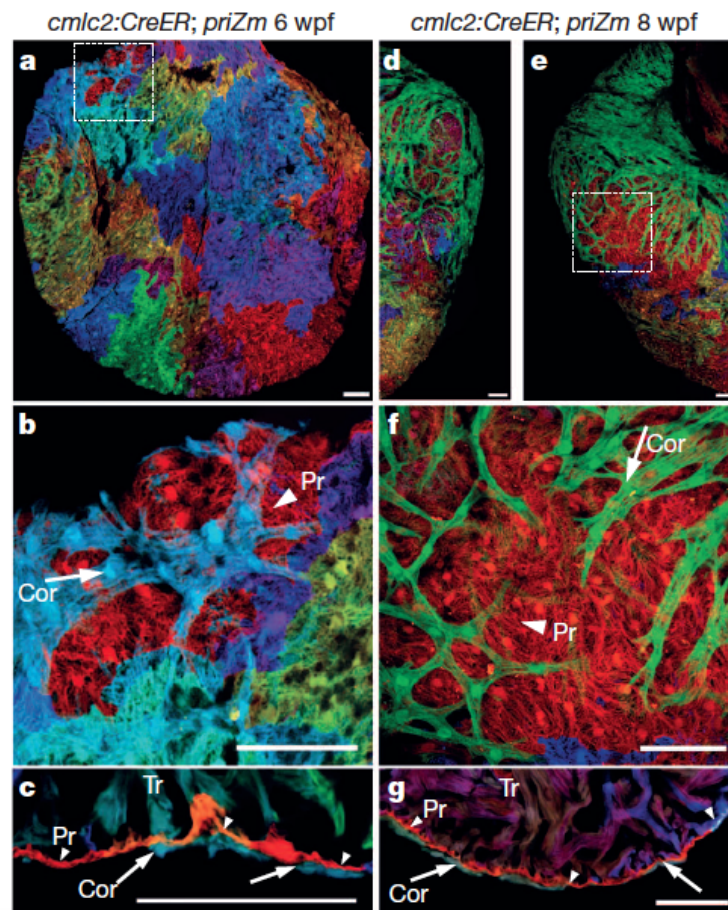


Figure 4. Cortical, primordial, and trabecular muscle layers in the juvenile zebrafish heart. (a, b) 6 wpf ventricular surface, and (c) confocal slice indicating cortical (Cor; arrow), primordial (Pr; arrow-head) and trabecular (Tr) muscle. 8 wpf ventricular surface indicating (d-f) a large green basal cortical clone, and (g) section indicating all three muscle types. Dashed boxes in a and e are shown in higher magnification in b and f, respectively. Adapted from Gupta and Poss [2012].

During development, individual myocardial cells begin to contract irregularly around 20 hpf, and the heart beats in a coordinated fashion, at a rate of about 25 beats/minute

1.3 Heart regeneration in zebrafish

at 22 hpf, which increases to 90 beats/minute by 24 hpf, and, shortly after that circulation starts [Stainier et al., 1993]. By 2 days post-fertilization (dpf) the zebrafish heart is looped, and consists of 250-300 cardiomyocytes which form a single-cell thick wall [Gupta and Poss, 2012]. Starting from 3 dpf these cardiomyocytes start forming protrusions, and delaminate to form the trabecular myocardium [Liu et al., 2010, Staudt et al., 2014]. This single-cardiomyocyte thick wall, called primordial muscle, retains its thickness throughout the life of the fish, and around 6 weeks post-fertilization (wpf) another layer of cardiomyocytes emerge externally on top the primordial layer. This late-emerging layer, which can be several cells thick, is termed as cortical muscle [Gupta and Poss, 2012] (Fig. 4). Upon multicolor clonal labeling analysis, it was suggested that only a few cardiomyocytes, around 8 per ventricle, formed the entire cortical layer [Gupta and Poss, 2012].

1.3.3 Zebrafish heart regeneration and injury models

Amputation

The regeneration capacity of the adult zebrafish heart was first discovered in the beginning of 2000's by using the amputation model, in which around 20% of the ventricle apex is removed surgically [Poss et al., 2002, Raya et al., 2003].

After amputation a very rapid blood clot seals the wound and prevents massive blood loss. The days following the amputation, this blood clot turns into a fibrin clot and further compacts. Eventually the fibrin clot gets gradually invaded by new cardiomyocytes. Around 30 days post-amputation (dpa) almost all of the missing myocardium is reconstructed and at 60 dpa the amputated heart becomes indistinguishable from a non-injured heart [Poss et al., 2002, Raya et al., 2003].

The amputation model has been used to study zebrafish heart regeneration for more than a decade now, and the majority of findings have been achieved by using this model. However, recently some alternative methods have been developed.

1 Introduction

Cryoinjury

A few years ago, cryoinjury emerged as an alternative to amputation, in order to better mimic the events that take place after a myocardial infarction such as tissue-wide cell death, inflammatory responses, cleaning of the cell debris, and scar formation [Chablais et al., 2011, Gonzalez-Rosa et al., 2011, Schnabel et al., 2011]. In this model, necrosis is provoked in 20-25% of the ventricle by applying dry ice [Schnabel et al., 2011] or a thin probe cooled by liquid nitrogen [Chablais et al., 2011, Gonzalez-Rosa et al., 2011]. In cryoinjured hearts, inflammatory response is evident. The wound area is infiltrated with leukocytes at 1 day post-cryoinjury (dpc), and at 3 and 7 dpc, both neutrophil and eosinophil granulocytes are found in the wound [Schnabel et al., 2011]. This inflammatory response triggers the fibrosis that leads to collagen deposition, and as a result a large collagen scar can form after cryoinjury, in contrast to what happens after amputation. Interestingly, the scar is later absorbed or resolved and the zebrafish heart still fully regenerates after cryoinjury [Chablais et al., 2011, Gonzalez-Rosa et al., 2011]. However, in hearts damaged by this method, full regeneration takes between 60 and 130 days, much longer than in amputated hearts probably due to the clearing of the necrotic cells, and resolution of the scar tissue [Lien et al., 2012]. After regeneration, even though the heart function is restored completely, some morphological alterations such as a rounded ventricle, a thicker ventricular wall, and arrhythmic ventricular contractions are observed [Gonzalez-Rosa et al., 2011].

Genetic Ablation

Alternatively, an inducible genetic ablation system for cardiomyocytes has been created in order to kill high amount of cardiomyocytes without damaging other cell types of the heart [Wang et al., 2011]. In this system, two transgenic fish lines are crossed to obtain the expression of the diphtheria toxin A chain in the Cre recombinase expressing cardiomyocytes upon induction by tamoxifen.

The genetic ablation method causes the depletion of 60% of ventricular cardiomyocytes, triggering signs of heart failure including reduced swimming performance, limited exercise tolerance, and even sudden death when exposed to stress, that are not detected

1.3 Heart regeneration in zebrafish

in other injury models. Despite severe muscle damage, in this model cardiomyocytes proliferate rapidly and full muscle regeneration and functional recovery are observed at 30 and 45 days post-depletion, respectively.

The comparison of these three models is found in table 1

Type of injury	Ventricular amputation	Cryo-injury	Genetic ablation
Method of damage	Removal of cells	Cell damage caused by freezing and thawing	Cardiomyocyte-specific cell death caused by expression of diphtheria toxin A chain (DTA)
Size of injury	Removal of cells	15-25% of the ventricle	>60% of the myocardium
Mortality after the procedure	20% of the ventricle	5%	Dose dependent
Cell death	10%	Apoptosis and necrosis throughout the heart	Apoptosis throughout the ventricle uniformly at 3 and 5 dpi
Inflammation	Some apoptosis and necrosis along the amputation plane	Yes	Yes
Cardiomyocyte proliferation	Yes	Yes	Yes
Epicardial activation	Yes	Yes	Yes
Initial collagen deposition	Yes	Yes/No	No

Table 1. Comparison between different injury models for studying zebrafish heart regeneration. From Lien et al. [2012].

1.3.4 Cellular and molecular mechanisms during heart regeneration

An injury to the zebrafish heart, induced by any of the interventions explained above, provokes organ-wide responses in all three tissue layers of the heart: epicardium, endocardium, and myocardium, and activates different cellular and molecular mechanisms.

1 Introduction

Epicardial mechanisms

The epicardium of the regenerating heart shows an organ-wide activation as early as 1-2 dpa and starts to express embryonic epicardial markers such as *raldh2* which encodes for the retinoic acid (RA) synthesizing enzyme, and *tbx18* which encodes a T-box transcription factor [Kikuchi et al., 2011b]. Epicardial cells proliferate from 3 to 7 dpa, and activated epicardial cells become localized to the apex by 14 dpa [Lepilina et al., 2006].

It was thought that epicardial derived cells might give rise to myocardial lineages during regeneration [Lepilina et al., 2006]. However, genetic fate-mapping experiments using inducible Cre recombinase driven by the promoter of an epicardial marker, *tcf21*, showed that *tcf21*-expressing epicardial cells gave rise to perivascular cells but not to cardiomyocytes after surgery [Kikuchi et al., 2011a]. This finding was further supported by transplantation experiments, and it was shown that epicardial cells give rise to myofibroblasts, but not to cardiomyocytes [Gonzalez-Rosa et al., 2012].

Another important event during heart regeneration is the formation of new blood vessels. Epicardial cells appear to play a role in neovascularization through paracrine mechanisms. During regeneration members of fibroblast growth factor (FGF) signaling pathway were shown to be upregulated: The expression of FGF ligand gene *fgf17b* was induced in the injured myocardium, whereas FGF receptor genes *fgfr2* and *fgfr4* were upregulated in the epicardial cells. The inhibition of FGF signaling blocked both the integration of epicardial cells into the wound, and neovascularization, causing a regeneration arrest [Lepilina et al., 2006]. Similarly, inhibition of platelet-derived growth factor (PDGF) signaling blocked epicardial cell proliferation and coronary vasculature formation [Kim et al., 2010].

Endocardial mechanisms

Upon amputation, endocardial cells respond to the injury even faster than epicardial cells do, as early as 1 hour post-amputation (hpa). According to transmission electron microscopy, the endocardial cells near the amputation plane, which normally have elongated nuclei and thin cell bodies attached to the cardiomyocytes, round up and detach from the cardiomyocytes [Kikuchi et al., 2011b].

1.3 Heart regeneration in zebrafish

In addition, by 3 hpa *raldh2* gets upregulated in all endocardium as well, as an organ wide response, and starting from 1 dpa its expression becomes localized to the endocardial cells near the amputation plane. Inhibition of RA synthesis by expressing a dominant-negative retinoid acid receptor alpha or the RA-degrading enzyme Cyp26, impairs cardiomyocyte proliferation, while RA injection does not induce cardiomyocyte proliferation. These findings indicate that RA produced by endocardial and epicardial *Raldh2* is a permissive, rather than instructive, signal for regeneration [Kikuchi et al., 2011b].

Even though the research done on the field indicates that epicardium and endocardium have important roles during heart regeneration, it is still unclear why and how their organ-wide activation is triggered, as well as their molecular interactions with cardiomyocytes.

Myocardial mechanisms

Myocardium, the heart muscle, makes up the largest part of the zebrafish heart. Therefore, replacing the damaged or lost cardiomyocytes is the most crucial part of heart regeneration. Initial experiments based on the BrdU incorporation into proliferative cells suggested that the proliferating cells could be cardiomyocytes [Poss et al., 2002, Raya et al., 2003]. Later, an opposite argument was proposed by Lepilina et al. suggesting that a set of cardiac progenitor or stem cells were the source of the newly formed cardiomyocytes [Lepilina et al., 2006]. Detection of the expression of some of the cardiac progenitor markers such as *hand2*, *nkx2.5*, *tbx20* and *tbx5* also supported this suggestion [Lepilina et al., 2006]. However, eventually two independent experiments of cardiomyocyte lineage tracing demonstrated that new cardiomyocytes came from pre-existing cardiomyocytes through cell proliferation [Jopling et al., 2010, Kikuchi et al., 2010]. As additional evidence, histological analyses using transmission electron microscopy and immunofluorescence staining showed that cardiomyocytes near the injury site acquired less organized sarcomeres with reduced Z-bands, undergoing DNA synthesis and mitosis [Jopling et al., 2010, Kikuchi et al., 2010]. Cell proliferation assays such as BrdU or EdU (5-ethynyl-2'-deoxyuridine) incorporation demonstrated that cardiomyocyte proliferation started around 7dpa, and peaked at 14 dpa [Poss et al., 2002,

1 Introduction

Raya et al., 2003], and these proliferating cardiomyocytes were mainly found at the injury site (between 65-75%), but they were also present in other areas throughout the myocardium (from 10% up to 30%) [Itou et al., 2012, Jopling et al., 2010, Sallin et al., 2015]. Overall, strong evidences have shown that myocardium regenerates by proliferation of already existing cardiomyocytes, however whether all cardiomyocytes can contribute to the regenerated tissue or whether this potential is restricted to a subpopulation or cardiomyocytes from a specific area requires further investigation.

Mechanisms in larval cardiac regeneration

Zhang et al. studied cardiac regeneration in 3-4 dpf zebrafish larvae through a genetic ablation model [Zhang et al., 2013]. In this model, the bacterial enzyme Nitroreductase is expressed only in the ventricular muscle under the control of ventricular myosin heavy chain (*vmhc*) promoter. Nitroreductase can cause cell death by converting a prodrug into a cytotoxic agent [Curado et al., 2007], thus its transgenic expression in a specific cell type provokes controlled cell ablation. Using this model, the researchers analyzed regenerative responses, particularly the atrial ones. The results suggested that upon ablation of ventricular cardiomyocytes in 3-4 dpf larvae, new ventricular cardiomyocytes arise from the area adjacent to the atrioventricular canal, and expand across the whole ventricle to restore the lost ventricular heart muscle. Lineage tracing using the atrium specific atrial myosin heavy chain (*amhc*) promoter and live imaging showed that *amhc*⁺ atrial cardiomyocytes acquired ventricular fates and migrated into the ventricular to repair lost cardiomyocytes [Zhang et al., 2013]. However, when ablation was induced in the adult heart, *amhc*⁺ cardiomyocytes did not give rise to ventricular muscle [Zhang et al., 2013], suggesting that the atrial-to-ventricular transdifferentiation can be age-dependent.

Cell migration

Lineage tracing studies have shown that new cardiomyocytes are generated through proliferation of pre-existing ones; however, it is not well understood how these proliferating cardiomyocytes integrate into the injury site. To understand this issue, Itou et al.

1.3 Heart regeneration in zebrafish

investigated cardiomyocyte migration during zebrafish heart regeneration and showed that cardiomyocytes migrated to the injury site through the interaction of the chemokine ligand *cxcl12a* expressed by epicardial cells, and its receptor *cxcr4b* expressed by the cardiomyocytes. Heart regeneration was impaired when cardiomyocytes migration was inhibited through pharmacological blocking of *cxcr4b* function [Itou et al., 2012]. This demonstrated that cardiomyocytes migrate toward the regenerating area through this signaling pathway, however it is still unknown where these cardiomyocytes involved in the regeneration process come from, or whether the cardiomyocytes proliferating in distant zones of the heart may migrate until the wound and contribute to the newly formed tissue.

Similarly, immediately after cardiac amputation, the epicardium is quickly activated and migrates toward the injury site [Lepilina et al., 2006]. Proliferation of epicardial cells is detected from 3 to 7 dpa, and by 7 dpa, the migrated epicardium covers the apex and starts to invade the fibrin clot in order to contribute to the vessel formation to vascularize the regenerated tissues [Kikuchi et al., 2011b, Kim et al., 2010, Lepilina et al., 2006]. It was also shown that genetic ablation of the zebrafish epicardium during regeneration, inhibited cardiomyocyte proliferation and delayed regeneration [Wang et al., 2015]. These evidences combined indicate that epicardial migration is also essential for heart regeneration, and warrants further investigation.

In order to study cell migration during zebrafish heart regeneration, transgenic zebrafish lines, lineage tracing methods, or a combination of these techniques with bioengineering tools are necessary. The work presented in this thesis aims to create these tools to understand some of the mechanisms during zebrafish heart regeneration.

1.3.5 Lineage tracing methods in zebrafish heart regeneration

Lineage tracing, the combination of methods that allow monitoring the destiny of a cell and its progeny, was pioneered in the 19th century by Charles Whitman (1887) and Edmund Wilson (1892) [Whitman, 1887, Wilson, 1892]. Their studies based on direct observations of the individual cells during early cleavages of leech and annelid embryos

1 Introduction

under light microscopy led to the formulation of term “cell lineage”. However, cell tracing by direct observation is limited to the transparency of the organism or structure of interest. So, in the early 20th century, *vital dyes*, dyes that label cells without killing them, were used to systematically mark cells in amphibian embryos and follow their progeny during gastrulation [Vogt, 1929]. Also, tissue transplantation between differentially pigmented newt species was used as a pioneering tool to achieve important advances in vertebrate fate mapping during the same period [Spemann and Mangold, 1924].

Later, with the development of genetic markers and techniques to introduce them into the cells, vital dyes were replaced by reporters such as green fluorescent protein (GFP) from the jellyfish *Aequorea victoria* [Chalfie et al., 1994], or beta-galactosidase from *Escherichia coli*. These genetic markers can be introduced by direct injection, transfection, or viral infection. However, the efficiency of introducing the gene is usually very low [Kretzschmar and Watt, 2012]. In zebrafish, this limitation is overcome by using Tol2 transposon mutagenesis system for introducing transgenes [Kwan et al., 2007]. In this way, transgenic fish that express a fluorescent reporter gene in the cell type of interest can be created.

Today, the preferred lineage tracing approach in most situations is induced cell labeling by genetic recombination. In this approach, the expression of the reporter gene is driven in an inducible manner, thanks to a binary genetic switch system engineered into the genome. To achieve genetic labeling, two site-specific recombination systems Cre/lox, and FLP-FRT, adapted from bacteriophage P1, and *Saccharomyces cerevisiae* respectively, are commonly used in different model organisms, however in zebrafish the Cre/lox recombination system is more frequently used [Mosimann and Zon, 2011]. Cyclic recombinase (Cre) recognizes specific sequences, called *loxP* sites (34 base-pair-long sequences). Head-to-head orientation of the *loxP* sites causes inversion of the DNA between the two sites, whereas head-to-tail orientation results in the excision of the DNA sequence, rejoining the ends. This can be used to stop expression of a gene by excising it, to express a gene by excising a stop site which precedes the gene, or both simultaneously so switching off one gene and on another [Bailey et al., 2009, Sauer, 1998]. This excision is permanent and heritable by any daughter cells, thus making this a perfect tool for lineage tracing. Since *loxP* sites are not naturally found in zebrafish

1.3 Heart regeneration in zebrafish

genome, and Cre acts only on the transgene that contains these sites, so other parts of the genome remain unaffected by this recombination [Nagy, 2000].

In the *Cre/lox* based cell labeling, two transgenes must be introduced into the organism: an “effector” transgene that codes for Cre, and a “target” transgene that codes for the expression of a fluorescent reporter protein upon recombination by Cre. The reporter is usually expressed following the excision of a “stop” cassette placed between two *lox* sites, which blocks mRNA transcription until Cre functions in the nucleus. To control the activity of Cre several strategies have been developed. For spatial control, Cre is often targeted to a promoter in order to be expressed in a cell- or tissue-specific manner. For temporal control, a clever approach is fusing Cre to a modified form of the estrogen receptor that only binds to the synthetic analog of estrogen called tamoxifen or 4-hydroxy-tamoxifen (4-OHT). This form of the Cre is usually denominated as CreER^{T2}. By this way, the fusion protein that contains Cre is sequestered in the cytoplasm by a chaperone complex until tamoxifen is administered, which releases the fusion protein, allowing it to enter the nucleus and mediate recombination [Feil et al., 1997]. This approach, originally developed in mice, was successfully adapted to zebrafish in 2009 [Hans et al., 2009].

In zebrafish, *Cre/lox*-based lineage tracing has been used to identify various cellular processes during heart regeneration and development. To explore whether newly formed cardiomyocytes derive from existing differentiated cardiomyocytes or from undifferentiated progenitor cells, two similar *Cre/lox*-based lineage tracing approaches were used. In both studies, the researchers generated transgenic zebrafish in which the cardiomyocyte specific promoter cardiac myosin light chain 2 (*cmlc2/myl7*) drives the expression of tamoxifen-inducible Cre recombinase [Jopling et al., 2010, Kikuchi et al., 2010]. These fish were crossed with two different reporter lines, however in both Cre-mediated excision of a *loxP*-flanked stop sequence induces GFP expression when treated with tamoxifen (Fig. 5). In the offspring of this cross, almost all pre-existing cardiomyocytes and their progeny were labeled with GFP after tamoxifen treatment. If the regenerated myocardium were derived from undifferentiated progenitor cells, the new ventricular apex should be GFP-. Instead, the results clearly showed that the regenerated myocardium displayed GFP expression, indicating that the new cardiomyocytes were derived from pre-existing ones [Jopling et al., 2010, Kikuchi et al., 2010] (Fig. 5).

1 Introduction

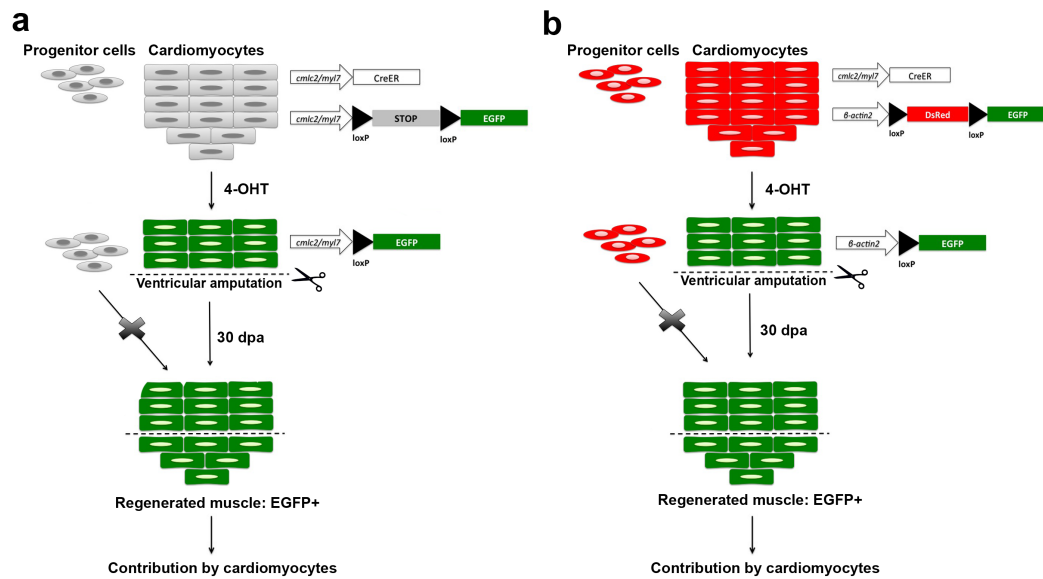


Figure 5. Lineage tracing methods that revealed pre-existing cardiomyocytes are the source of new cardiomyocytes in zebrafish heart regeneration. (a) In one transgene, the cardiomyocytes-specific *cmlc2* promoter drives the expression of tamoxifen-inducible Cre recombinase. This Cre acts on the second transgene by excising loxP-flanked stop sequence, causing the expression of EGFP. Thus, when tamoxifen is given to this transgenic zebrafish, all of its cardiomyocytes and their descendants express EGFP. EGFP positive apex after regeneration indicates that pre-existing cardiomyocytes form the new cardiomyocytes. (b) This approach is very similar to approach in a. As a difference, in the reporter transgene, the constitutive β -actin promoter initially drives the expression of the red fluorescent DsRed protein. When the Cre recombinase excises the stop sequence, EGFP starts to be expressed only in the cardiomyocytes due to *cmlc2* promoter, and the progenitor cells should remain DsRed+ and EGFP-. As in the case a, EGFP positive apex after regeneration indicates that pre-existing cardiomyocytes form the new cardiomyocytes.

Other examples in which Cre/lox-based cell labeling was used for cell tracking in zebrafish heart regeneration include *gata4*-expressing cardiomyocytes [Kikuchi et al., 2010], and *tcf21*-expressing epicardial cells [Kikuchi et al., 2011a]. Recently, in addition to these conventional Cre/lox-based lineage tracing methods, multicolor labeling systems have been developed. The Brainbow system originally developed for brain tissue in mouse [Livet et al., 2007], was later adapted to zebrafish, and used in zebrafish heart studies [Gupta et al., 2013, Gupta and Poss, 2012]. In this system, stochastic choice between distinct recombination events results in switching the default red reporter expression to yellow or cyan in a transgene integrated in multiple copies. By this way, the combination of different reporters is able to generate many different colors [Livet

1.4 Multiphoton microscopy and its use in activation of molecules

et al., 2007], and it is possible to label many cells and their progeny at the same time with different colors. However, the interpretation of the colors must be done carefully in order to be able to differentiate the origin of each clone correctly.

In this technique, imprecision in the timing of tamoxifen activation can be a general problem. Also, tamoxifen causes a general Cre recombinase activation in all of the cells containing the specific promoter which drives the Cre expression. In order to control timing and only activate a single cell within the same tissue, a photoactivable, caged form of a tamoxifen analog was synthesized. In this method, this compound called cyclofen was uncaged by ultraviolet (UV) light, successfully producing Cre recombinase activation only in the uncaged cells of a 24 hpf zebrafish embryo [Sinha et al., 2010b]. This method would be very advantageous to track individual cells in a complex process such as heart regeneration.

1.4 Multiphoton microscopy and its use in activation of molecules

Typical fluorescence microscopy is based on linear interactions between light and matter. It works as follows: when one photon is absorbed by the fluorescent molecule, it emits a single fluorescent photon. As this absorption-emission interaction is linear, when the excitation power is doubled, fluorescence produced doubles as well. In contrast, multiphoton microscopy, where two or three photons may be involved, is based on nonlinear interactions between photons and matter. In order to generate multiphoton excitation multiple photons must be absorbed simultaneously by the same molecule: two photons for two-photon microscopy or three photons for three-photon microscopy. Since the energy of a photon is inversely proportional to its wavelength, the two or three absorbed photons must have a wavelength about twice or third time that required for one-photon excitation (Fig. 6). For example, a fluorophore that normally absorbs UV light (approximately 350 nanometers wavelength) can also be excited by two photons of near-infrared light (approximately 700 nanometers wavelength) or by three photons of far-infrared light (approximately 1050 nanometers wavelength) if all photons reach the

1 Introduction

fluorophore at the same time. In order to produce a significant number of two- or three-photon absorption events, high photon fluxes in the range of 10^{20} – 10^{30} photons/(cm^2 s) concentrated in a time interval less than 10^{-15} s are necessary since under normal illumination the possibility to observe such an interaction is practically zero [Ustione and Piston, 2011].

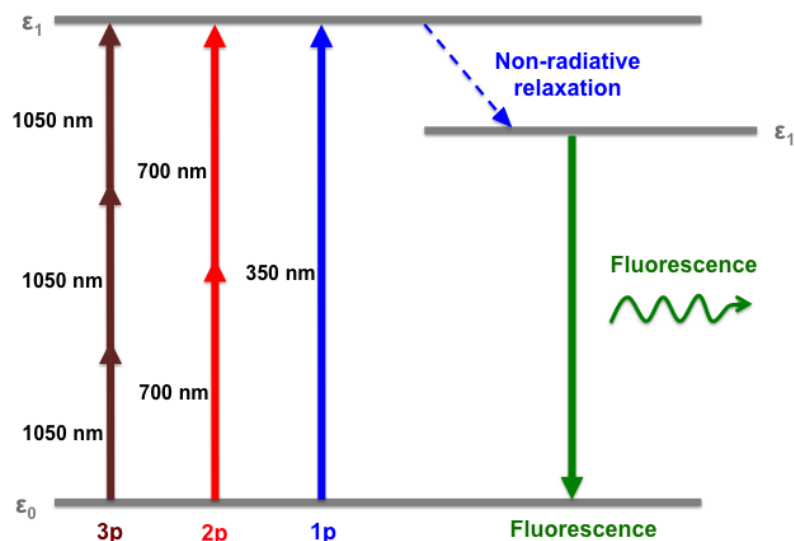


Figure 6. Comparison of one, two, and three photon excitation. In order to reach the energy level of one photon of 350 nm wavelength, two photons of 700 nm, or three photons of 1050 nm must be absorbed at the same time.

Two-photon excitation was predicted in 1931 [Göppert-Mayer, 1931] and first realized by detection of $\text{CaF}_2 : \text{Eu}^{2+}$ crystals using 0.5 ms pulses of a ruby laser in 1961 [Kaiser and Garrett, 1961]. However, the first two-photon excited fluorescence imaging of living specimens was published almost 30 years later when it was possible to generate high photon densities with the use of subpicosecond pulse mode-locked lasers [Denk et al., 1990]. Today, tuneable mode-locked Ti : sapphire lasers, compact turn-key solid-state Ti : sapphire lasers, Cr : LiSaF or fiber lasers are typically used in multiphoton microscopy [Konig, 2000]. The mode-locked (pulsed) lasers compress the laser power in small time packets so that photons are very crowded in time. In addition, high numerical aperture objectives which concentrate the light in a diffraction limited focal volume with a size of $\sim 1 \mu\text{m}^3$ are used in a multiphoton excitation set-up to compress the pho-

1.4 Multiphoton microscopy and its use in activation of molecules

tons in space [Williams et al., 1994]. The combination of the two effects generates an extremely high photon flux in a very small volume, so that the probability of a non-linear excitation event is greatly increased in a precised region of the sample (Fig. 7). Combination of such a laser with a scanning system would give the ability to produce multiphoton excitation in a thin optical section of the sample, without affecting other regions of the sample [Ustione and Piston, 2011].

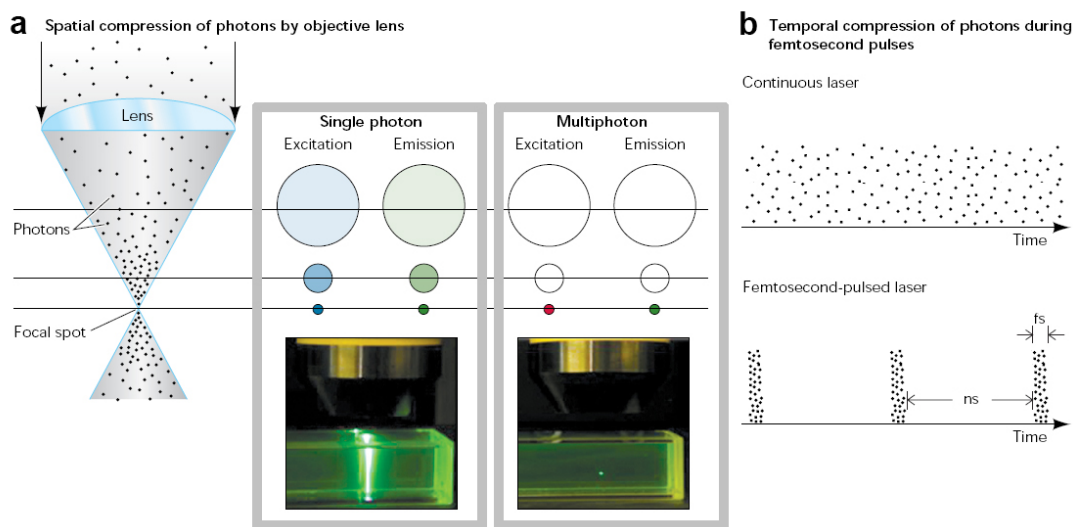


Figure 7. The mechanisms of multiphoton excitation. In multiphoton excitation high amounts of photons are concentrated (a) spatially using a high numerical aperture objective lens, and (b) temporally by pulsing them in femtoseconds of time. As a result, more than one photon can be absorbed simultaneously. Adapted from <http://parkerlab.bio.uci.edu>

Even though two-photon is the most commonly used type of multiphoton excitation, three-photon excitation, which was first demonstrated in the 1990s, is becoming a popular tool especially for *in vivo* studies involving deep structures [Hell et al., 1996, Horton et al., 2013, Xu et al., 1996]. Since in three-photon excitation the energies of three photons sum up to reach the same energy level of one-photon excitation, longer wavelengths are used. Using longer wavelengths provide two significant advantages: first, longer wavelength photons do not suffer from scattering as much as shorter wavelength photons, thus can penetrate deeper into the specimen; second, in when the focal volume is reduced it is much more effective compared to two-photon excitation [Xu et al., 1996].

1 Introduction

Although multiphoton excitation is typically used to generate fluorescence, it is the best option to produce *in vivo* photoactivation reactions such as uncaging of photolabile compounds or photoswitching of fluorescent molecules inside a living animal. First of all, it can reach deeper in the tissue compared to one-photon excitation, a huge advantage for *in vivo* activation. Furthermore, most photoactivation processes use UV light, and whenever UV excitation needs to be applied on cells or living organisms, the intensity of the UV source must be regulated very carefully. UV photons have very high energy and they can easily produce cell or tissue damage when high intensity is used. In addition, UV lasers are not commonly available with confocal systems, and when they are, special objectives are necessary for proper focusing of the UV light. More importantly, UV photons are subjected to severe scattering, which reduces the amount of photons that eventually reaches the specimen. Using infrared wavelengths (700-1100 nm) for two or three-photon excitation reduces both damage and scattering, and helps overcome these disadvantages [Ustione and Piston, 2011].

All these benefits are very important, however there is one crucial advantage of using multiphoton for *in vivo* photoactivation. In contrast to one-photon absorption, multiphoton absorption occurs only in the focal plane, so it is possible to produce a photoactivation only inside a cell, without affecting the surrounding cells. This is a great advantage compared to one-photon activation by using a single beam light source or laser, where the photo-activation occurs in all of the cells along the entire penetration length.

For all these reasons, multiphoton excitation is generally the preferred method whenever *in vivo* imaging or activation needs to be performed, and whenever the excitation wavelength is in the UV range, three-photon excitation is more advantageous over two-photon excitation [Wang et al., 2010].

2 Objectives

The general objective of this thesis was to develop strategies based on bioengineering approaches to study the role of cell migration during zebrafish heart regeneration. In this aspect, the specific objectives were:

1. To develop a lineage tracing system for zebrafish cardiomyocytes based on inducible genetic labeling techniques.
2. To perform lineage tracing of cardiomyocytes by using the technique developed in Objective 1, during zebrafish heart development and regeneration.
3. To assess the migration abilities of cardiomyocytes by using the data obtained by lineage tracing of cardiomyocytes in Objective 2.
4. To develop a method to analyze epicardial cell migration during zebrafish heart regeneration.

3 Materials and methods

3.1 Zebrafish husbandry

AB stain zebrafish, both wild type and transgenic lines were raised according to standard methods [Westerfield, 2000]. They were maintained in fish tanks in a closed system at 28.5°C. The fish were fed 2 times a day with special fish food (SDS, Essex, UK), and 2 times a day with brine shrimp.

All experiments were conducted following procedures approved by the Ethics Committee on Experimental Animals of the Barcelona Science Park and/or the Barcelona Biomedical Research Park.

3.2 Methods related to lineage tracing of zebrafish cardiomyocytes

3.2.1 Transgenic zebrafish lines

For Cre/lox based genetic labeling, a double transgenic line was created by crossing lines Tg(*myl7*:ERT2-Cre-ERT2) and Tg(-*1myl7*:LOXP-STOP-LOXP-EGFP). The generation and characterization of these lines were previously described [Jopling et al., 2010]. Both transgenes were expressed under the *myl7* cardiomyocyte specific promoter.

3 Materials and methods

3.2.2 Photoactivation in zebrafish embryos

Chemical inducers

4-Hydroxy-cyclofen (cyclofen) and caged 4-hydroxy-cyclofen (caged-cyclofen) were synthesized and prepared by the laboratory of Prof. Ludovic Jullien (Département de Chimie, Ecole Normale Supérieure, Paris, France) as described previously [Sinha et al., 2010b]. 4-Hydroxy-tamoxifen (4-OHT) was purchased from Sigma.

Cyclofen, and caged-cyclofen were solubilized in DMSO, and 4-OHT in ethanol (20 mg/mL) to a concentration of 10 mM; these stock solutions were stored at -20°C. Aliquots of those solutions were added to the embryo medium containing the zebrafish embryos to reach a concentration of 2 μ M. Control experiments were done by adding the same volume of pure DMSO to the samples.

The embryos were incubated overnight without dechorionization with 2 μ M caged-cyclofen in embryo medium prior to UV irradiation which was performed at 2 dpf. After incubation, the embryos were washed with fresh embryo medium prior to UV irradiation to avoid any possible interference, which could originate from photoreleasing the inducer in the incubating solution. Cyclofen and 4-OHT were used as controls, and same as caged-cyclofen, 2 μ M concentration of each was used to incubate embryos overnight.

Inhibition of pigmentation in the embryos

In order to facilitate UV light reaching to the embryo heart properly, pigmentation of the embryos were inhibited by treating them with 75 μ M 1-phenyl 2-thiourea (PTU) starting at 22 hpf (26 somite stage), as suggested [Karlsson et al., 2001], and until screening of the larvae was complete.

In vivo uncaging of caged-cyclofen by using a UV lamp

Prior to UV exposure, 2 dpf zebrafish were anesthetized using 4.2 ml of 0.4% tricaine methanesulfonate (tricaine for short) solution per 100 ml of embryo medium to prevent

3.2 Methods related to lineage tracing of zebrafish cardiomyocytes

them from moving [Westerfield, 2000]. UV irradiation was done at room temperature using a bench-top UV lamp (365 nm, Spectroline FC-100) above a plastic Petri dish without lid, containing 40-50 embryos in tricaine added medium for 4 min.

Screening and *in vivo* imaging

Each day following the uncaging experiment, screening for the GFP+ areas of the larvae heart was done by using a Stereomicroscope (Leica). Larvae containing GFP+ areas were imaged *in vivo* using a PerkinElmer UltraView ERS Spinning-Disk microscopy system mounted on a Zeiss Axiovert 200M microscope equipped with a Hamamatsu C9100-50 EMCCD camera. The videos were recorded by using Volocity software.

3.2.3 Ventricular amputation surgery

To study heart regeneration, published ventricular amputation protocol was used [Raya et al., 2003]. According to this protocol, fish were anesthetized in 4.2 ml 4% tricaine solution per 100 ml of fish water. Then, the fish were placed in a sponge with the ventral side facing up. Scales on the surface were removed using watchmaker forceps and a small opening made in the pericardial sac. With one hand, the apex were grabbed by using forceps, and with the other hand, a slight force was exerted on the body of the fish by using scissors to make the apex go out, and the tip of the apex was cut. The wounds were pressed with tissue tampons for a few seconds to accelerate blood clotting. Finally, the fish were returned to fish tanks, and were aided for respiration by sending air through gills with a plastic pipette.

In order to check the location of GFP+ areas, the hearts were visualized under the fluorescent stereomicroscope Leica MZ16 before amputating the ventricles, and the cut pieces of the apex were separated for further imaging.

3 Materials and methods

3.2.4 Labeling with BrdU

For the pulse-chase experiments with BrdU, zebrafish that went through ventricular amputation were anesthetized in 4.2 ml 4% tricaine solution per 100 ml of fish water, and injected intraperitoneally with 20 μ L of 2.5 mg/mL BrdU (Sigma) en PBS. BrdU injection was repeated everyday between 7 and 14 dpa.

3.2.5 Heart tissue collection

Regenerating hearts at 30 dpa were collected for analysis. Before heart collection, 20 μ L of 1000 U/mL heparin (Sigma) in PBS was injected intraperitoneally by a fine needle syringe (27G) to prevent blood coagulation. For this, first the fish were anesthetized by immersing them in 4.2 ml 4% tricaine solution per 100 ml of fish water, and after heparin injection they were euthanized by immersing them in overdose of tricaine for 10 minutes more (20 ml 4% tricaine solution per 100 ml of fish water).

To collect the hearts, the fish were placed in a sponge with the ventral side facing up. Scales on the surface were removed using watchmaker forceps and the pericardial sac was opened. When the heart was visible, it was carefully detached by first separating the atrium from the sinus venosus, and then by separating the outflow tract from the aorta with the aid of forceps. Once the heart was out, it was washed with PBS with 10 U/mL heparin to minimize the blood coagulation.

3.2.6 Sample processing and immunohistochemistry

Collected hearts were fixed overnight in 4% paraformaldehyde (Electron Microscopy Sciences) at 4°C, washed with PBS several times, equilibrated in 30% sucrose (Sigma) in PBS overnight, and frozen in OCT (Tissue-Tek) for cryosectioning. The frozen samples were cut into 10 μ m sections using the Cryostat Leica CM3050S. The sections were placed on six Superfrost Plus slides (Fisher Scientific) in a serial manner, so that each slide would have a representation of the whole heart in a similar manner. The sections

3.3 Methods related to three-photon uncaging

were dried overnight in room temperature, and then kept in -20°C until their use for immunohistochemistry.

Immunohistochemistry was performed on these cryosections using MF20 (DSHB), anti-GFP (GFP-1020; Aves Labs), and anti-BrdU (Accurate) primary antibodies; and DyLight 488 (Jackson Immuno Research Laboratories), Cy3 and Cy5 (Jackson Immuno Research Laboratories) as secondary antibodies. The nuclei were stained with DAPI (4',6-diamidino-2-phenylindole).

3.2.7 Microscopy and image processing

The images of the dissected hearts and cut apex were taken by a fluorescent stereomicroscope Leica MZ16 coupled with a camera Leica DFC300 FX. The heart sections were imaged using Leica SP5 confocal microscope. Images were processed with Adobe Photoshop software.

3.3 Methods related to three-photon uncaging

3.3.1 Set up for measuring three-photon cross-section

The set up used for the measurement of the cross-sections was the following: the 280 fs pulses at 1064 nm (~ 20 nm bandwidth) with repetition rate 20 MHz generated by a fiber laser (Femtopower, Fianium It) were sent to an inverted microscope, through a telescope to overfill the back aperture of the objective. The light was focused with a 60x NA = 1.0 water objective to a femtoliter volume. The emission fluorescence was collected in epifluorescence configuration using a photon counting (H9319, Hamamatsu).

3.3.2 *In vitro* damage assay

Fibroblasts cells were plated on glass-bottom dishes (MatTek) and imaged for 100 s using 280 fs pulses at 1064 nm, to study cell damage. After 24 hours dead cells were

3 Materials and methods

counted and the *damage threshold* was defined as the power where more than 60% of the cells survived.

3.3.3 Control experiments

Control experiments were done by exposing 48 hpf zebrafish to three conditions: 2 μ M cyclofen incubation overnight without illumination, 280 fs pulses illumination without previous treatment with caged-cyclofen, and 2 μ M caged-cyclofen incubation overnight without illumination. Later, these fish were grown in separate fish tanks until they were 3 months old.

3.3.4 Three-photon activation set up

The photoactivation of the caged-cyclofen was performed using 280 fs duration pulses at 1064 nm, with a repetition rate of 20 MHz, generated by a fiber laser (FemtoPower, Fianium It.). The pulses were sent by a set of galvo-scanners (Thorlabs, GVSM002/M) through a telescope, in order to fulfill the back aperture of the objective, to an inverted microscope (Olympus) equipped with a motorized xy-stage (Marzhauser, SCAN IM 120 x 80) and a motorized objective holder (Marzhauser, MA42). The usual objective used was a 40x with 1.3 NA (Olympus, UPLFLN 40 XO). Targeting the specific tissue was achieved with a custom software (Labview) and a PCI board (National Instrument, NI PCI-6024E) by controlling the galvo-scanners and the motorized stage. A CCD (EverFocus, EQ200E) was used for widefield imaging of the animal during the experiment. A custom software make the focal spot follow a 3D sinusoid. Typical patches targeted at the heart were of 15x15, 15x20, 20x20 μm^2 with 0.1 patch/s, by raster scanning. To minimize the accumulative increment in temperature inside the focal volume generated by femtosecond pulses, we combined the heart beating rate with the movement of the beam, by adding z-oscillation of the objective, to produce a pulsed photoactivation, with \sim 25-50 ms pulse width and \sim 2-3 Hz repetition rate.

3.3.5 Illumination experiments

48-80-hpf zebrafish embryos were placed in a glass-bottom petri dish (MatTek) after 1 min in embryo medium with anesthesia. The illumination experiment consisted in the three-photon activation by using the dedicated software with parameters described above, and it lasted 2 to 4 min. After illumination, embryos were transferred to individual tanks for further follow up. 24 hours later, they were imaged under a fluorescence microscope, classified according to GFP expression, and transferred to rearing tanks.

3.4 Methods related to epicardium cell culture experiments

3.4.1 Transgenic zebrafish lines

For the epicardium culture, the following transgenic lines were used: Tg(*actb2:myl12.1-EGFP*) that marks myosin 2 with EGFP (obtained from the laboratory of Dr. Elisa Marti Gorostiza from CSIC), Tg(*actb2:myl12.1-mCherry*) that marks myosin 2 with mCherry, and Tg(*actb2:lifeact-EGFP*) that marks F-actin with EGFP (obtained from the laboratory of Dr. Cristina Pujadas from UPF), and the double transgenic line created by crossing these last two lines.

3.4.2 Preparation of polyacrylamide gels

Polyacrylamide gel preparation was adapted from the protocol previously described [Serra-Picamal et al., 2012]. Glass-bottom dishes were activated for 30 minutes by using a 1:1:14 solution of acetic acid/bind-silane/ethanol. The dishes were washed twice with ethanol and air-dried for 10 minutes. For 12 kPa gels, a stock solution containing a concentration of 7.5% acrylamide, 0.14% bisacrylamide, 0.5% ammonium persulphate, 0.05% tetramethylethylenediamine and 2.4% of 200-nm-diameter red, green or far-red fluorescent carboxylate-modified beads (Fluospheres, Invitrogen) was prepared in a 10

3 Materials and methods

mM HEPES solution. 18 μ l from the mix was put as drop to the center of the glass-bottom dishes, and the solution was covered with a 18-mm-diameter coverslip. Gels were allowed to polymerize for 1 hour and then deionized water was added to peel off the coverslips. The surface was then activated with Sulfo-SANPAH under ultraviolet light (254 nm wavelength at a distance of 5–8 cm for 5 min). After thoroughly washing with Milli-Q water and PBS, gels were incubated with 200 μ l of a collagen I solution (0.1 mg/ml, Millipore) overnight at 4°C. Gels were washed afterwards with PBS, and equilibrated with epicardial cell culture medium.

3.4.3 Heart seeding and epicardium cell culture

The steps used to for heart tissue collection were followed to harvest hearts to obtain epicardial cell culture, but under sterile conditions. Hearts were seeded on collagen-coated polyacrylamide gels in a glass-bottom 35 mm cell culture plate (MatTek) with a cover slip, previously sterilized with UV, on top of them to facilitate attachment to the gel and incubated at 28°C without CO₂ in epicardial cell culture medium. The epicardial cell medium is L-15 cell culture medium (Invitrogen) supplemented with 2% FBS (Hyclone), 1% Glutamax (Thermo Fischer), 2% Pen/Strep (Thermo Fischer), and 2% Fungizone (250 μ g/mL) (Thermo Fischer). The media were changed daily.

3.4.4 Microscopy and imaging

Time-lapse images of the epicardial cell cultures were performed on an automated inverted microscope (Nikon Eclipse Ti) equipped with thermal control, using NIS element (Nikon) software. The interval between image acquisitions was 10 minutes and a typical experiment lasted for 15h. If multiple images were required to capture the expanding cell sheet, they were acquired at \times 20 for every time point, approximately overlapping laterally by 10% and later, these images were accurately stitched.

Epicardial cell cultures from transgenic fish containing fluorescently labeled F-actin, myosin, or both were imaged using a spinning disk microscope.

3.4 Methods related to epicardium cell culture experiments

3.4.5 Measurement of cell migration velocity

Cell migration velocities were measured by manually tracking each cell using Image J software.

4 Results

4.1 Lineage tracing of cardiomyocytes during zebrafish heart development and regeneration

As demonstrated by lineage-tracing approaches, cardiomyocyte proliferation appears to be the primary mechanism for heart muscle regeneration after amputation or injury [Jopling et al., 2010, Kikuchi et al., 2010]. It has been shown that newly generated cardiomyocytes arise from pre-existing ones, however it is not known which ones contribute to the new myocardium. In order to determine this, a cell tracing strategy was necessary. Therefore, we developed a genetic labeling method that allow labeling one or few cardiomyocytes within the embryonic heart to further trace them during development and regeneration.

4.1.1 Development of a photo-inducible *Cre/lox*-based genetic labeling method to specifically label one or a small group of adjacent cardiomyocytes

In order to label one or a small group of adjacent zebrafish cardiomyocytes, we developed a cardiomyocyte-specific, UV-inducible *Cre/lox* recombination-based genetic labeling strategy.

Cre/lox recombination based on the modified form of Cre recombinase, CreER^{T2}, provides a high temporal control, since its activation depends on tamoxifen administration.

4 Results

However the only spatial control in this system is conferred by the activity of the specific promoter, which can be therefore limited to a tissue or a cell type. In this work, our aim was to further control Cre activation to a limited area of the myocardium in order to label one or a small group of adjacent cardiomyocytes. For this, we used an analogue of 4-hydroxy-tamoxifen, called 4-hydroxy-cyclofen (cyclofen for short), which can be synthesized as in its inactive form by linking it to a caging group (Fig. 8), and can be activated by freeing it from this caging group upon UV illumination at the wavelength of 365 nm [Sinha et al., 2010a]. Therefore, our method is based on using caged-cyclofen as a CreER^{T2} activator, which penetrates the whole organism and tissue of interest, but only becomes functional where it is uncaged by the UV light. Cyclofen is nontoxic and as efficient as tamoxifen.

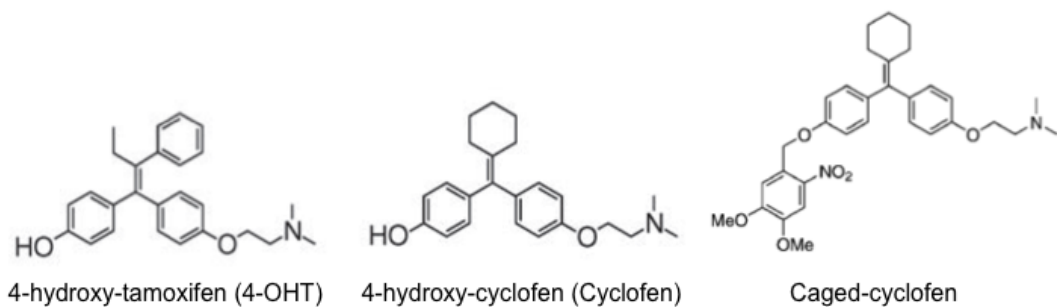


Figure 8. Chemical structures of 4-hydroxy-tamoxifen, 4-hydroxy-cyclofen, and caged cyclofen

This cyclofen-inducible approach was used to achieve cardiomyocyte labeling in a very small area of the myocardium. To do this, Cre expressing transgenic line Tg(*myl7*:ERT2-Cre-ERT2), and the reporter line Tg(-*1myl7*:LOXP-STOP-LOXP-EGFP) were used. In both of these transgenic lines, the cardiomyocyte specific *myl7* promoter drives the expression of the transgenes: inducible Cre recombinase, and the reporter sequence that Cre acts on. Therefore, when Cre recombination is activated in the progeny of these two lines, Cre excises the stop sequence between two *loxP* sites and as a result cardiomyocytes start expressing GFP (Fig. 9).

4.1 Lineage tracing of cardiomyocytes during zebrafish heart development and regeneration

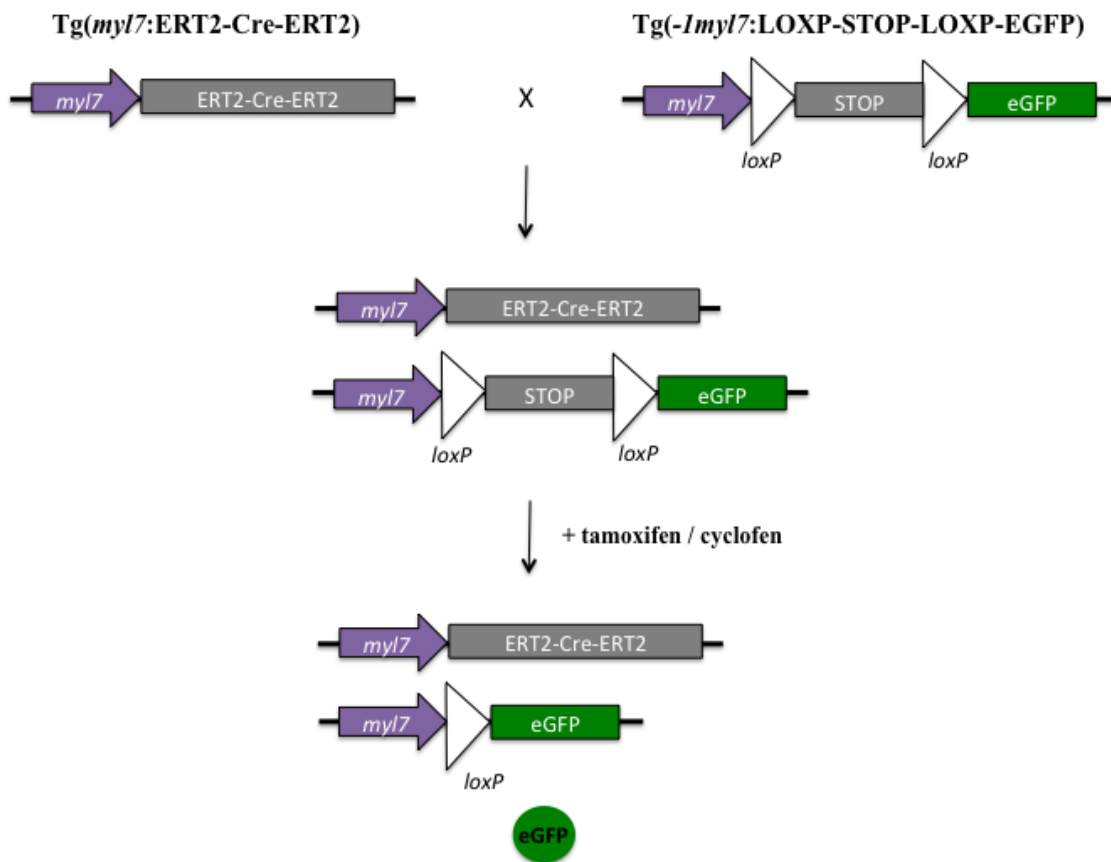


Figure 9. Cre/lox recombination based genetic labeling system. A double transgenic line was created by crossing following transgenic lines: (1) $Tg(myI7:ERT2-Cre-ERT2)$ in which Cre recombinase is expressed only in the cardiomyocytes under the cardiomyocyte specific promotor *myI7*, and (2) $Tg(-I myI7:LOXP-STOP-LOXP-EGFP)$ in which EGFP sequence is placed after a floxed stop sequence under *myI7* promotor. In the double transgenic fish, Cre recombinase becomes functional upon tamoxifen or cyclofen administration excises the stop sequence, enabling GFP expression only in the cardiomyocytes.

First, we tested whether cyclofen was able to induce Cre/lox recombination in our double transgenic system. To do this, we treated 2-dpf embryos with cyclofen and assessed GFP-expression two days later. After confirming that the recombination occurred successfully and specifically in cardiomyocytes (Fig. 10 a), these embryos were raised to adulthood to verify that GFP expression was permanent (Fig. 10 e, i). To test whether there was a leakage in our system, we treated 2-dpf embryos with caged-cyclofen and did not expose them to UV light. In those hearts, no recombination events were induced, as judged by the absence of GFP expression at 4 dpf (Fig. 10 b), and in adult animals

4 Results

(Fig. 10 f, j).

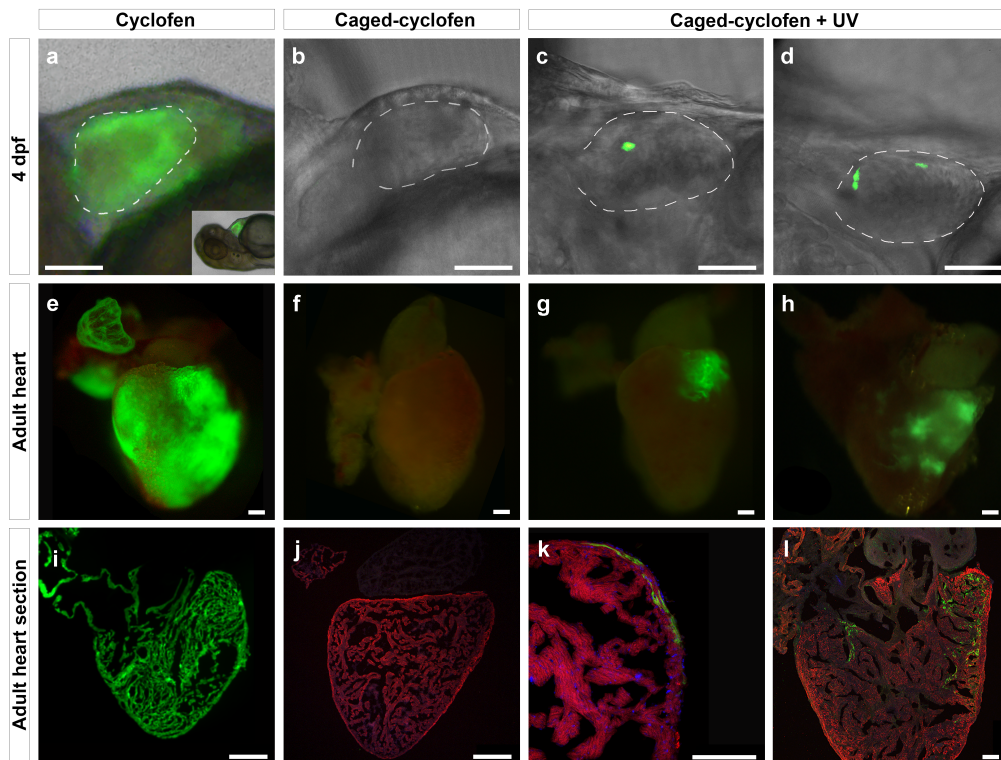


Figure 10. Genetic labeling of zebrafish cardiomyocytes using a UV-inducible *Cre/lox* recombination system. Double transgenic embryos [*Tg(myl7:ERT2-Cre-ERT2)* x *Tg(-1myl7:LOXP-STOP-LOXP-EGFP)*] were treated at 2 dpf with (a) uncaged cyclofen (n ~ 100), (b) caged-cyclofen without UV exposure (n ~ 100), and (c, d) caged-cyclofen followed by UV exposure (n ~ 100). One fish tank per condition (approximately 40 larvae) was raised to adulthood. Cyclofen works as a tamoxifen analogue and induces recombination in cardiomyocytes as observed by GFP expression at 4 dpf (a) and at adult stage (e, i). (b, f, j) Caged-cyclofen cannot induce recombination unless it is uncaged by UV exposure (c, d, g, h, k, l). Adult heart sections were processed for immunofluorescence with antibodies against MF20 and GFP. Nuclei were counterstained with DAPI. Scale bars: 150 μ m in a-d; 250 μ m in e-j; 100 μ m in k-l.

After doing these controls, we illuminated 2-dpf zebrafish embryos with 365 nm UV light, which were incubated in caged cyclofen-containing medium previously. We tried different concentrations of caged cyclofen (1 μ M, 2 μ M, 4 μ M) and different UV exposure times between 1 and 20 minutes. Among the various conditions used, optimizing illumination time to 4 minutes and caged cyclofen concentration to 2 μ M, we could obtain GFP expression in confined areas of embryonic zebrafish hearts: either a single labeled area or a few labeled areas within the same heart (Fig. 10 c, d).

4.1 Lineage tracing of cardiomyocytes during zebrafish heart development and regeneration

Among the illuminated embryos, we selected those with a single GFP-positive area within their hearts. The average diameter size of these GFP-labeled areas was calculated as $17.2 \mu\text{m}$ ($n=7$), indicating that each GFP-positive area comprised 1 or 2 cardiomyocytes (Fig. 11).

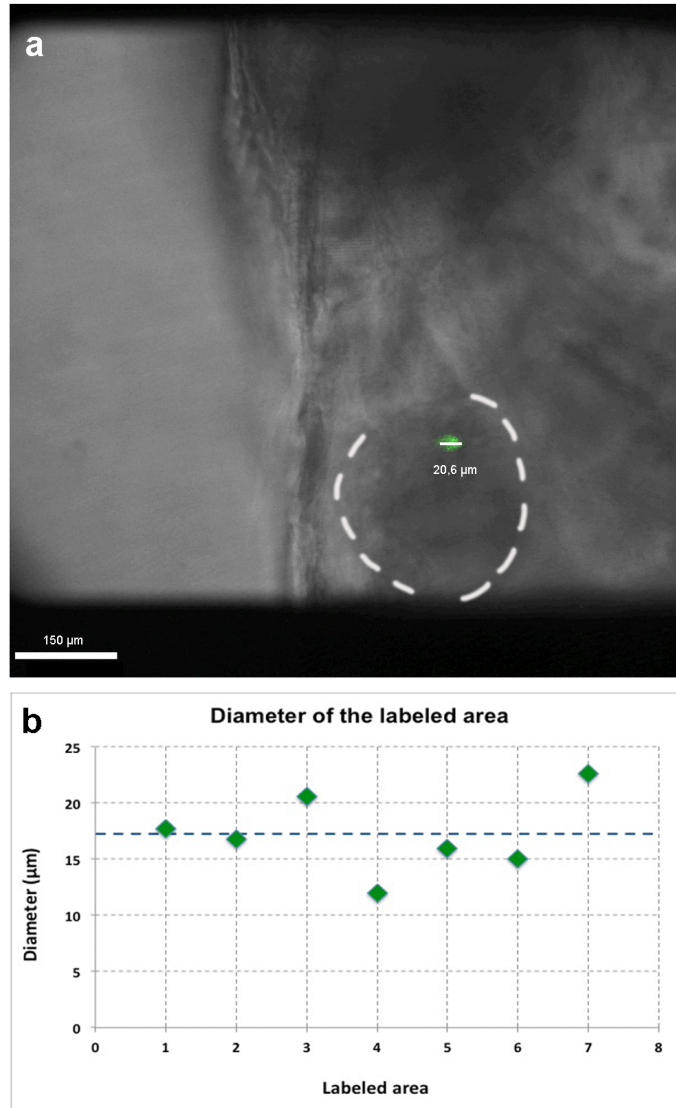


Figure 11. Diameters of the labeled areas in 4dpf zebrafish hearts. (a) Images of the labeled hearts were taken at 4 dpf and the diameters of the GFP-labeled areas were measured using Image J. (b) Measured diameters indicated that these labeled areas corresponded to one or two cardiomyocytes ($n=7$). Dashed line corresponds to the average diameter $17.2 \mu\text{m}$.

4 Results

As expected, these labeled embryos maintained GFP expression in their hearts as adults, demonstrating that labeled cardiomyocytes survived and passed the recombined construct onto their progeny (Fig. 10 g, k, h, l). These results showed that our myocardium-specific photoinducible genetic labeling system is suitable to label one or two cardiomyocytes in the embryonic zebrafish heart for further lineage tracing analysis during development and regeneration.

4.1.2 Lineage tracing of labeled cardiomyocytes during zebrafish heart development

The traditional view of the zebrafish ventricle consisting of two types of cardiac muscle, a peripheral wall of compact muscle and inner trabecular muscle, has been revised by the observation of primordial and cortical muscle lineages within the compact layer [Gupta and Poss, 2012]. Therefore, we wanted to assess the presence of different muscle lineages in the adult hearts labeled as embryos with our novel genetic labeling method described previously. In these labeled adult hearts we could observe GFP-positive cardiomyocytes in the innermost part of the compact myocardium forming a one-cell thick layer (Fig. 12 a, b), highly reminiscent of the primordial layer described by Gupta and Poss [Gupta and Poss, 2012]. Surprisingly, this structure was never found labeled alone in our labeled hearts, but always accompanied by labeled cardiomyocytes in the trabecular zone (n=16). This suggested that primordial cardiomyocytes gave rise to trabecular cardiomyocytes in all of the hearts analyzed, since by the time of labeling only primordial cardiomyocytes existed. Additionally, we could detect GFP-positive areas located in the outer part of the compact myocardium in adult hearts (Fig. 12 e, f), which would correspond to the cortical layer [Gupta and Poss, 2012]. Therefore, analyses of GFP-positive areas in labeled adult hearts provided further evidence for the existence of different myocardial layers (primordial, trabecular, and cortical) using a direct lineage tracing system, and demonstrated that cardiomyocytes labeled in embryonic hearts survive and contribute to all three layers in adult myocardium.

4.1 Lineage tracing of cardiomyocytes during zebrafish heart development and regeneration

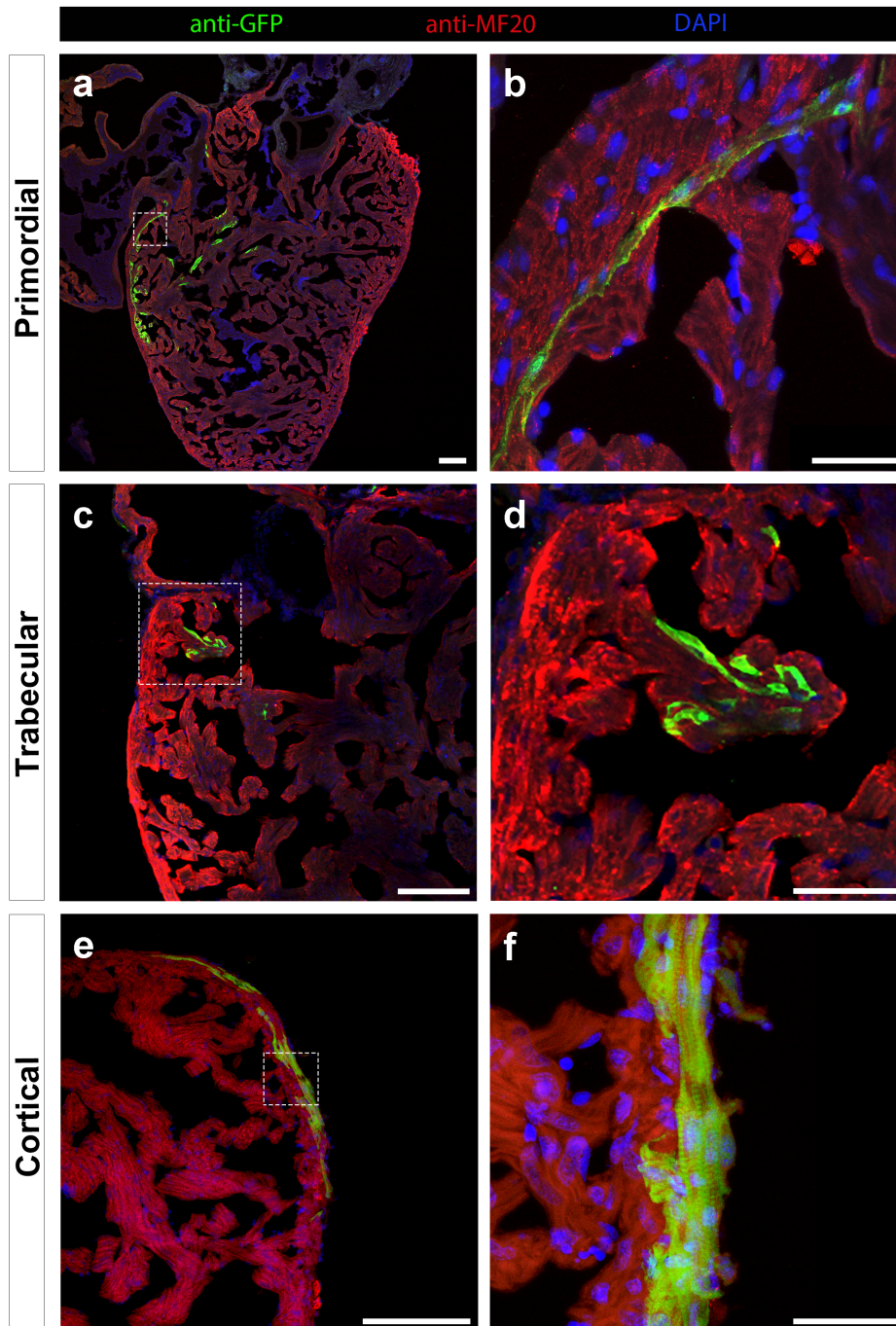


Figure 12. Genetically labeled cardiomyocytes are found in all three myocardium layers. Adult zebrafish hearts labeled at 2 dpf were sectioned and processed for immunofluorescence with antibodies against MF20 and GFP. (a, b) GFP-labeled cardiomyocytes were identified in the primordial layer, (c, d) the trabecular layer, and (e, f) the cortical layer. Nuclei were counterstained with DAPI. Scale bars: 100 μm in a, c, e; 25 μm in b, d, f.

4 Results

Detailed analyses of GFP-labeled hearts allowed us to draw other important conclusions. We observed that out of 30 hearts that were successfully labeled at 2 dpf and verified to contain GFP-positive cardiomyocytes at 4 dpf, when analyzed as adults, 23 hearts still maintained GFP-labeled areas (Table 2). The absence of GFP-positive cardiomyocytes in the remaining 7 hearts indicated that labeled cells either died before they could give rise to progeny, or that their progeny was not able to make it to the adult myocardium and died over time. Among the adult hearts that maintained GFP-labeled areas, approximately 1/3 (7 out of 23, 30%) showed labeled cardiomyocytes distributed along the three myocardial layers, whereas 40% (9 out of 23) occupied both primordial and trabecular layers, and the remaining 30% (7 out of 23) of GFP-positive areas contained exclusively trabecular cardiomyocytes (Table 2).

Labeled myocardium layer	Number of hearts
No label	7
Primordial only (P)	0
Trabecular only (T)	7
Cortical only (C)	0
P + T	9
P + C	0
T + C	0
P + T + C	7
TOTAL	30

Table 2. Distribution of the myocardium layers within the labeled areas of the adult hearts (n=30). GFP-labeled areas were composed of only trabecular layer (n=7), primordial and trabecular layer together (n=9), and all three layers together (n=7).

It is interesting to note that all labeled areas in adult hearts comprised trabecular muscle, even when no GFP-positive cardiomyocytes were found in the primordial layer. Previous studies have suggested that the trabecular heart muscle originates from primordial cardiomyocytes, which detach from the myocardial wall and then reattach, sometimes even at distant places, giving rise to trabeculae [Gupta and Poss, 2012, Liu et al., 2010, Staudt et al., 2014]. The relative distribution of GFP-labeled areas found in our studies is consistent with this scenario, and further points out that most primordial cardiomyocytes should be able to give rise to trabecular muscle, even though they do not contribute to the adult primordial layer. Finally, the GFP-positive areas comprising cortical myocardium

4.1 Lineage tracing of cardiomyocytes during zebrafish heart development and regeneration

detected in our studies ranged in size from 1.2% to 11% of the ventricular surface (Fig. 13), indicating that none of them had labeled a dominant clone in agreement with their reported low frequency [Gupta and Poss, 2012].

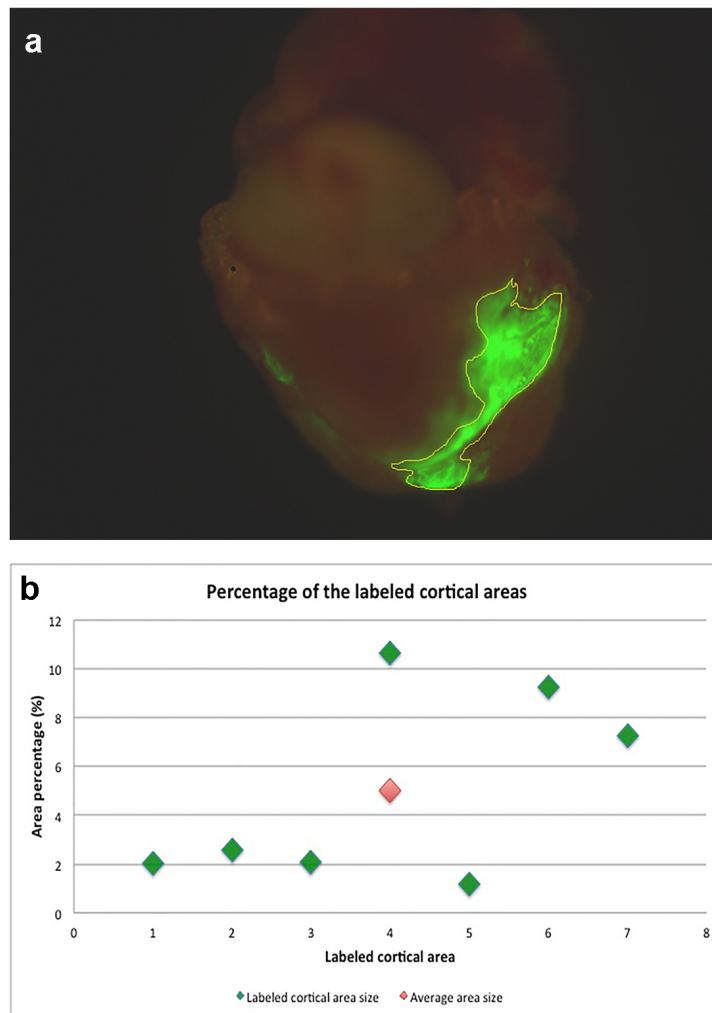


Figure 13. Labeled cortical area size. (a) Percentages of the cortical areas were calculated from the images of whole-mount hearts by using ImageJ. (b) Calculated areas ranged from 1.2% to 11% (n=7).

4 Results

4.1.3 Lineage tracing of labeled cardiomyocytes during zebrafish heart regeneration

To analyze the contribution of different GFP-labeled areas to regeneration, we amputated the ventricular apex of 3-month-old fish that had been labeled at 2 dpf and verified to contain GFP-positive cardiomyocytes at 4 dpf (n=21). We then analyzed the presence of GFP-labeled cardiomyocytes in the regenerated tissue at 30 dpa, a time when the regenerative process is well underway and most *de novo* cardiomyocytes have been produced [Poss et al., 2002, Raya et al., 2003]. In 6 of the 21 hearts processed and analyzed in this way, the amputation plane passed through a GFP-labeled area, as shown by the presence of GFP-positive cells in the piece of excised apex tissue (Fig. 14 a, d). In 4 of these 6 cases, the GFP-labeled areas affected by the amputation comprised trabecular and primordial myocardial layers, and the regenerated tissue after 30 dpa also contained GFP-positive cardiomyocytes in the same layers (Fig. 14 b, c). Similarly, the amputation plane cut through labeled trabecular and cortical layers in the remaining 2 hearts, and the regenerated tissue contained labeled cardiomyocytes from these two layers (Fig. 14 e, f). In all cases, the seamless continuation of labeled cells from the spared myocardium into the regenerated tissue indicates that cardiomyocytes in the primordial, trabecular, and cortical layers give rise to new cardiomyocytes in the corresponding layers of the regenerated myocardium.

With the aim of investigating the existence of specific regeneration-competent areas within the myocardium, and whether the migration of cardiomyocytes from such zones toward the injury site would occur during regeneration, we performed ventricular amputation in 15 adult zebrafish in which the GFP-labeled areas were located away from the apex. Taken together, the GFP-labeled areas in these hearts covered the vast majority of the ventricular surface, but the amputation plane did not cut through them (Fig. 15 a, b). When we analyzed the regenerated area at 30 dpa, we could not find GFP-labeled cardiomyocytes in any of these hearts (Fig. 15 d, e). Thus, our results indicated that cardiomyocytes proliferating at a distance from the regenerating area, which were found in several GFP-labeled clones (Fig. 15 f, g, h), do not contribute to the regenerated myocardium. Therefore, our findings did not support existence of any specific regeneration-competent area within the adult zebrafish myocardium.

4.1 Lineage tracing of cardiomyocytes during zebrafish heart development and regeneration

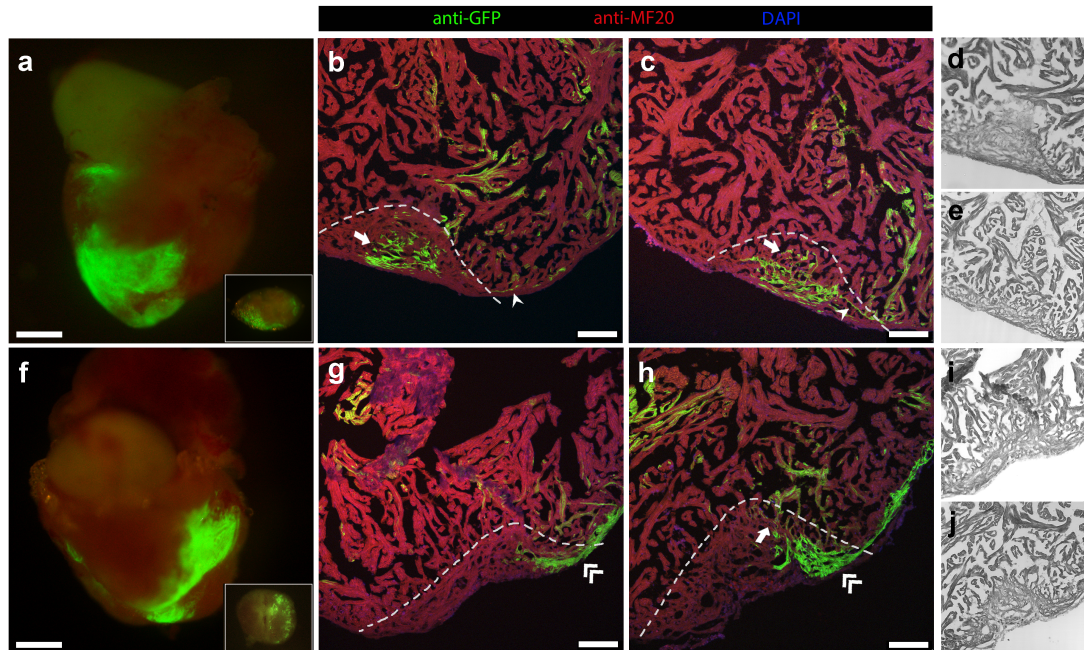


Figure 14. Cell fate of labeled cardiomyocytes during regeneration. 3-month-old adult zebrafish labeled at 2 dpf were subjected to ventricular amputation, and after 30 dpa the hearts were collected. (a, f) Epifluorescence images of representative hearts where the amputation plane passed through GFP-positive areas. The excised portion of tissue is shown in insert. (b, c, g, h) Collected hearts were sectioned, and processed for immunofluorescence with antibodies against MF20 and GFP. (b, c) Sections of the regenerated myocardium of the heart shown in (a), where primordial (arrowhead) and trabecular (arrow) labeled cardiomyocytes were observed. (g, h) Sections of the regenerated myocardium of the heart shown in (f), where trabecular (arrow) and cortical (double-arrowhead) GFP-positive cardiomyocytes were detected. (d, e, i, j) Bright-field images of the sections (b, c, g, h) in which the regenerating part can be differentiated due to Sudan Black staining. The amputation plane is indicated by dashed lines. Nuclei were counterstained with DAPI. Scale bars: 500 μm in whole-mount hearts; 100 μm in sections.

4 Results

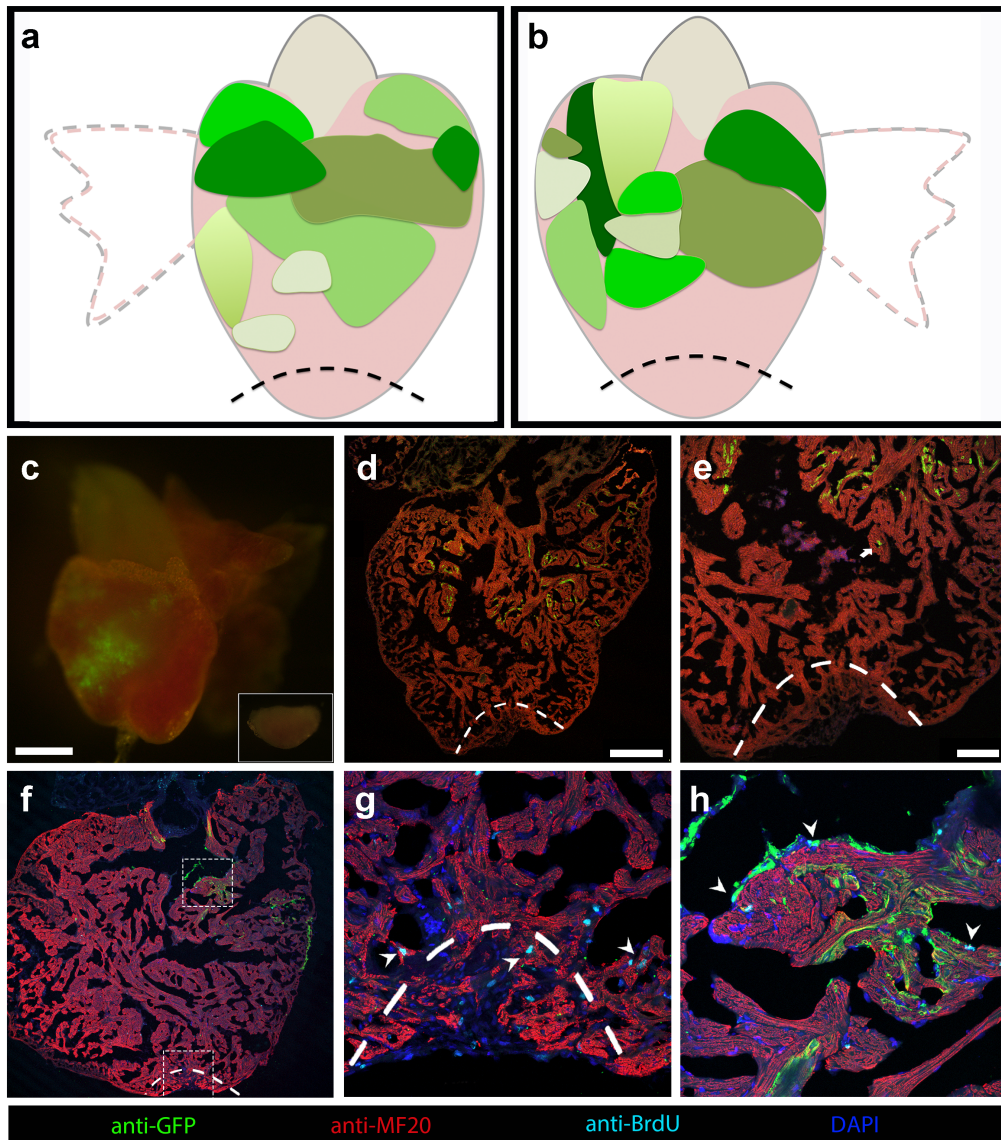


Figure 15. Cardiomyocytes distant from the amputation site do not contribute to the regenerated tissue. (a, b) Diagram summarizing the size and location of GFP-positive areas from different hearts, which did not contribute to regeneration (n=15). (c) Epifluorescence image of a representative heart where the amputation plane did not pass through the GFP-positive area. The excised portion of tissue is shown in insert. (d, e) Collected hearts were sectioned, and processed for immunofluorescence with antibodies against MF20 and GFP. GFP-labeled cardiomyocytes are absent in the regenerated area. (f, g, h) Sections processed for immunofluorescence with antibodies against BrdU showing the proliferating cardiomyocytes (g) in the injury site, and (h) in the GFP-positive area. The amputation plane is indicated by dashed lines. Nuclei were counterstained with DAPI. Scale bars: 500 μm in c; 250 μm in d; 100 μm in e.

4.2 Three photon-based cell photoactivation in living embryos

Uncaging of caged cyclofen can be achieved by UV illumination at 365 nm as shown in the previous section. However, in this set up, uncaging depends on which part of the heart receives the right dose of UV light, so labeling is random and not prospective. For prospective uncaging, a microscope-coupled laser system would be necessary. It was reported that by using femtosecond pulses at 750 nm, two-photon photolysis allowed 3D spatial resolution, successfully labeling single cells at the eye and somites in 24-hpf zebrafish embryos [Sinha et al., 2010a]. However, reaching the internal organs, such as the heart, requires deeper accessibility into the tissues. Therefore, we set out to evaluate whether three-photon illumination would be more efficient than two-photon illumination at deeper tissues. To do this, in collaboration with Dr. Dobryna Zalvidea from the Integrative Cell and Tissue Dynamics Group of IBEC, we theoretically calculated the ratio between caged-cyclofen uncaging rates for two- and three-photon excitation.

To address whether three-photon absorption at longer wavelengths is efficient at deeper tissues when excited with powers below the damage threshold, we first calculated the rate of n-uncaging as a function of the quantity of ballistic photons that reach the target cell. The power of the ballistic photons contributing to nonlinear absorption follows a Lambert-Beer like exponential decline,

$$P = P_0 e^{-z/l_s}$$

with depth z , characteristic length l_s calculated through Mie theory, and P_0 power at the surface of the sample. The n-photon uncaging rate when the laser illuminates a thick sample is k_{unc}^{np} [Xu and Webb, 1997].

$$k_{unc}^{np} = \frac{\sigma_{np} \eta_{np}}{n} \frac{\lambda^n}{h^n c^n} g_{np} \left(\frac{T}{\tau} \right)^{n-1} \frac{P_0^n}{(\pi w_0^2)^n} V F \cdot e^{-\frac{nz}{l_{np}}}$$

where σ^{np} is the n-photon absorption cross-section, η_{np} is the quantum efficiency of

4 Results

uncaging, and $\delta_{np} = \sigma_{np}\eta_{np}$ is the action uncaging cross-section, T the periodicity and τ the duration of the pulses, λ the central wavelength, h the Planck constant, c the velocity of light, w_0 the focal radius at the xy-plane, g_{np} is a measure of the n-order of temporal coherence of the excitation source, VF is the fraction of the excitation volume in the photolysis volume and l_{np} the scattering length at the wavelength for n-photon absorption. The uncaging rates depend on the molecule by δ_{np} , and on the illumination, through λ , τ , T , w_0 and P_0 . A compromise of the uncaging efficiency and damage constricts the illumination parameters for each tissue.

The caging molecule used to cage cyclofen, 4,5 dimethoxy-2-nitrobenzyl (DMNB), is likely to be photolysed around 1 μm when excited with three photons, since its optimal uncaging wavelength is 365 nm [Sinha et al., 2010a]. The choice of 1 μm excitation is based on minimization of scattering effects while using caged molecules that will not be one- and/or two-photon activated in the visible/very near-IR wavelength, allowing their combination with any fluorescent label that is excited within this range. The three-photon cross-section for DMNB was measured (see Appendix I. Three-photon illumination calculations), and found to be $\delta_{3p} = (4 \pm 2) \times 10^{-85} \text{cm}^6 (\text{s}/\text{photon})^2$. To our knowledge, there are no measurements of three-photon action uncaging cross-sections and only very few three-photon excitation cross-section values exist in the literature. This value, together with the two-photon uncaging cross-section $\delta_{2p} = 4 \times 10^{-53} \text{cm}^4 \text{s}/\text{photon}$ (see Appendix I. Three-photon illumination calculations), was necessary to calculate three-photon uncaging rate.

When uncaging rates of caged cyclofen for two- and three-photon excitations were calculated according to the formula stated above (For calculations see Appendix I. Three-photon illumination calculations), it was predicted that three-photon excitation for deeply embedded cells was up to 5 times more efficient than two-photon illumination, while being below the damage threshold and above a minimum production rate of the uncaged molecule (Fig. 16 a).

4.2 Three photon-based cell photoactivation in living embryos

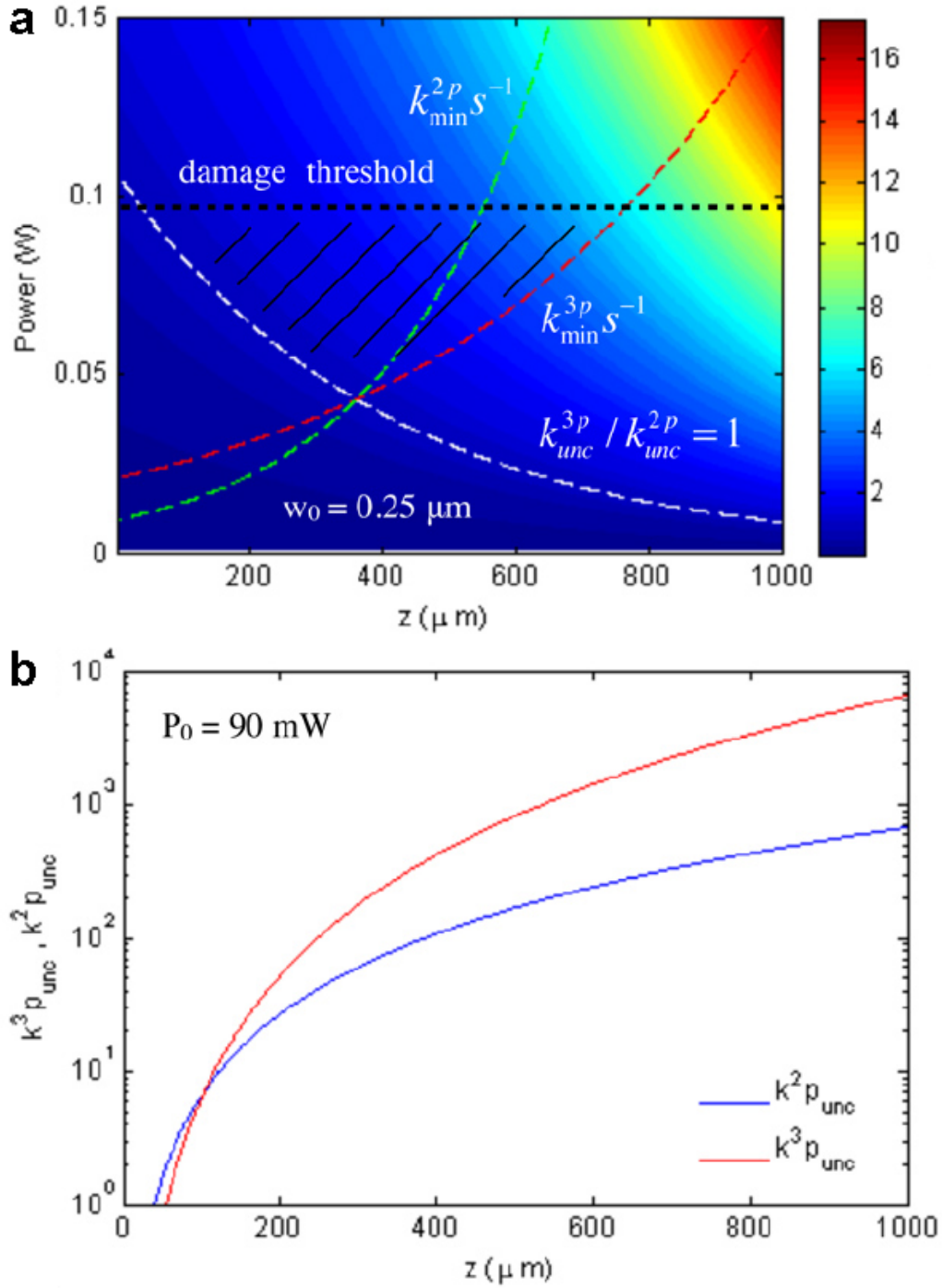


Figure 16. Numerical results of the ratio between three- and two-photon uncaging rates for the caging group. (a) Ratio between three- and two-photon uncaging rates as function of input power and depth inside the embryo. The curves represent: damage threshold (black), $k_{3p}^{unc}/k_{2p}^{unc} = 1$ (white), $k_{3p}^{unc}/k_{3p}^{min} s^{-1}$ (red) and $k_{2p}^{unc}/k_{2p}^{min} s^{-1}$ (green). (b) three- (red) and two- (blue) photon uncaging rates for the uncaging group for $P_0 = 90$ mW as function of depth.

4 Results

Specifically, even for powers still below the damage threshold, our calculations predict higher efficiency of three-photon uncaging as going deeper in the tissues, and more efficient two-photon uncaging in the superficial tissues (Fig. 16 b). For depths below 100 μm , two-photon uncaging is much more advantageous, but the difference between two- and three-photon uncaging efficiency is not very high. On the other hand, three-photon uncaging becomes much more advantageous in depths over 150 μm . Considering that the cells where uncaging occurs in our system are located within 150 to 200 μm , three-photon uncaging is more efficient compared to two-photon uncaging (Fig. 16 b). Moreover, higher efficiency of three- compared to two-photon uncaging can be achieved by decreasing the focal spot size, although limited by the damage threshold for a specific depth. In summary, our calculations predicted that three-photon uncaging at longer wavelengths could be a solution for photo-activation in tissues located deep inside the animal, where two-photon absorption suffers strong scattering that affects the efficiency of activation vs. damage threshold.

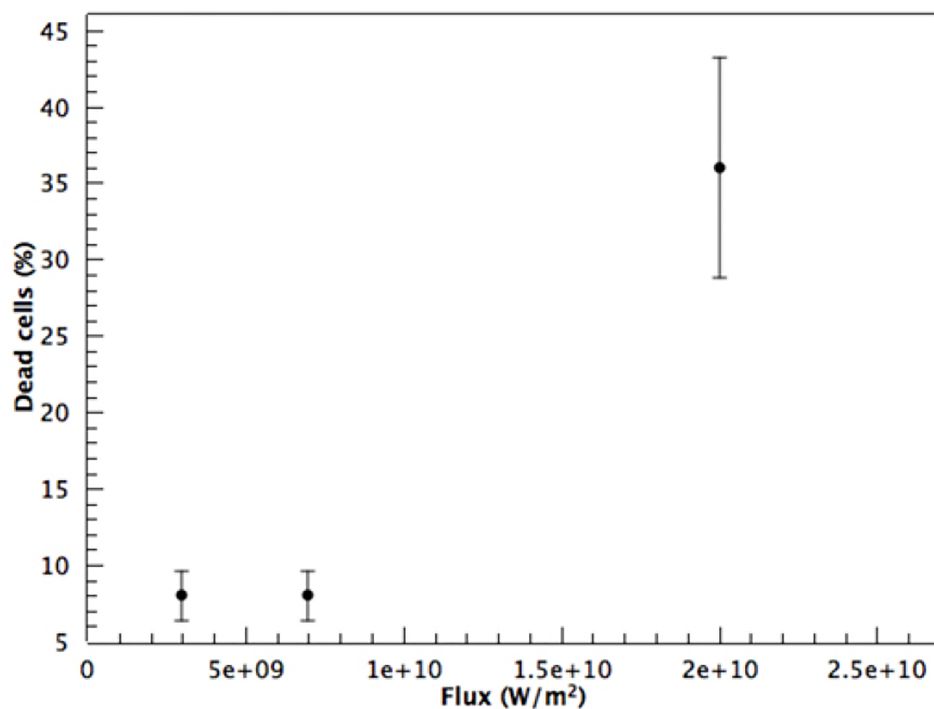


Figure 17. Percentage of dead cells as function of laser flux for illumination at 1064 nm

4.2 Three photon-based cell photoactivation in living embryos

The damage threshold was defined through a damage assay using fibroblasts. Fibroblasts plated on glass-bottom cell culture dishes were imaged for 100 s using 280 fs pulses at 1064 nm. After 24 hours dead cells were counted, and the “damage threshold” was defined as the power where more than 60% of the cells survived (Fig. 17)

After obtaining these conclusions from our mathematical model, we tested these predictions by investigating *in vivo* uncaging of caged cyclofen inside the hearts of 48-80 hpf zebrafish embryos by three-photon photolysis. These embryos were from the double transgenic line that allows cardiomyocyte labeling through an inducible *Cre/lox* system (Fig. 9). Successful uncaging of the caged cyclofen would initiate the *Cre/lox* recombination process, leading to the expression of GFP in photo-activated cardiomyocytes.

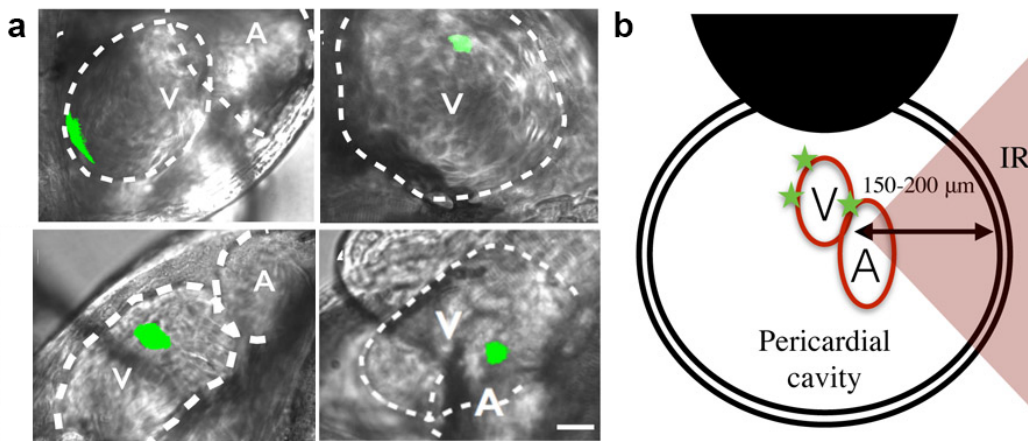


Figure 18. Cardiomyocyte labeling using three-photon uncaging of cyclofen (a) Selected areas were labeled in the hearts of zebrafish embryos, and (b) shows a labeled area behind inhomogeneous tissue, at $\sim 150 \mu\text{m}$.

To apply three-photon excitation based uncaging, we built a custom set up and designed a protocol with *ad hoc* photo-activation strategies for optimizing the quantity of molecules uncaged while avoiding tissue damage. Targeted cells found in different parts of the heart at varying depths more than $150 \mu\text{m}$ were successfully labeled and found to express GFP upon three-photon excitation (Fig. 18 a, b).

In parallel, we conducted control experiments to test *Cre/lox* recombination ability of cyclofen, and caged-cyclofen without three-photon excitation. These controls were

4 Results

done by exposing the animals to cyclofen without illumination, 280 fs pulses illumination without previous treatment with caged-cyclofen, and finally, caged-cyclofen without illumination. The uncaged form of cyclofen was able to induce *Cre/lox* recombination in our system, whereas caged cyclofen alone without three-photon illumination did not activate our system (Fig. 19). This indicated that caging of cyclofen was stable and did not uncage without its proper photolysis. Also, three-photon illumination alone did not have any affect on recombination (Fig. 19).

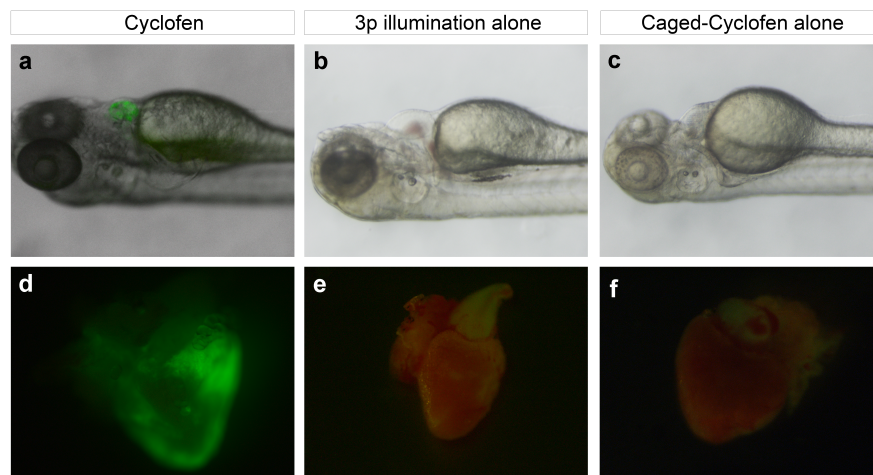


Figure 19. Control experiments for three-photon illumination showing recombined heart when the animal is exposed to cyclofen, non-recombined heart when the animal was illuminated with the three-photon source but not treated with caged-cyclofen, and when the animal was treated with caged-cyclofen.

To investigate the long-term survival of the labeled cells and their progeny, some of the fish were developed until adulthood (three months old), and their hearts were harvested for analysis. Figure 20 shows a heart harvested 3 months after three-photon illumination, which originally affected an area of 0.01 mm^2 in a central part of the heart ventricle. The final labeled area in the adult heart was $\sim 0.126 \text{ mm}^2$ with a signal to noise ratio (SNR_{dB}) of 20 dB (Fig. 20 c). Photoactivated cardiomyocytes and their progeny were identified in the adult myocardium, and shown to contribute to all three myocardium layers, primordial, cortical and trabecular (Fig. 20 b, c, e, f). Our results show that negligible damage occurred during three-photon uncaging in cardiomyocytes at the embryonic stage, as labeled cells were able to survive, divide and their progeny

4.2 Three photon-based cell photoactivation in living embryos

was found after 3 months in the hearts of the adult zebrafish, indistinguishable from unlabeled cardiomyocytes.

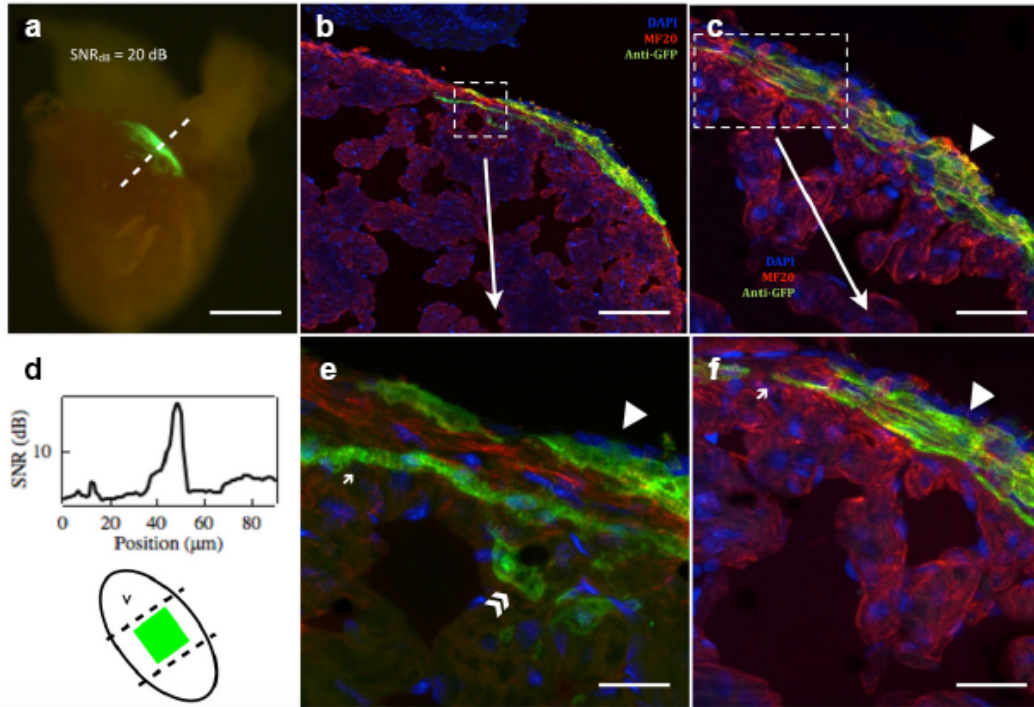


Figure 20. Long-term *in vivo* lineage tracing of zebrafish cardiomyocytes. (a) Excised heart of an adult zebrafish. The original $\sim 10\text{-}20\ \mu\text{m}^2$ labeled area was extended to $\sim 0.125\ \text{mm}^2$ (scale bar is $250\ \mu\text{m}$) (d) shows a fluorescence SNR ~ 20 dB and the position of the original labeled zone. (b, c, e, f) immunostaining images of the adult zebrafish heart sections showing the participation of the photoactivated cardiomyocytes in the three layers of the heart wall (scale bar: b: $50\ \mu\text{m}$, c: $20\ \mu\text{m}$, e: $5\ \mu\text{m}$ and f: $10\ \mu\text{m}$).

4.3 Development of an *ex vivo* method to study epicardial cell migration behavior during zebrafish heart regeneration

Epicardial migration is one of the most important mechanisms during zebrafish heart regeneration. In response to heart damage, epicardial cells activate quickly, and migrate to the injury site [Lepilina et al., 2006]. It was shown that blocking of epicardial signals or migration, impairs proper heart regeneration [Itou et al., 2012, Wang et al., 2015]. These findings encouraged us to study the migratory behavior of zebrafish epicardial cells, with the aim of comparing this behavior in control hearts and regenerating hearts. In collaboration with Marina Uroz from Dr. Xavier Trepats' lab, we focused on setting up an experimental approach to study physical features that are essential for migration such as migration velocity and traction forces, as well as characterizing zebrafish epicardial cells using transgenic zebrafish lines.

4.3.1 Optimization of epicardial cell culture conditions

The first experiments done with zebrafish hearts aimed at finding suitable culture conditions and heart collection protocols. To culture zebrafish hearts we opted to use a cell culture medium not based on CO₂ for buffering, Leibovitz L-15, supplemented with 2% fetal bovine serum and 1% glutamax. To prevent bacterial and fungal contaminations, 1% penicillin/streptomycin and 1% amphotericin B were also added. The hearts were seeded on six-well tissue culture plates.

In these experiments the success rate of cell explantation was as low as 1 out of 12 hearts (8.3%) even though the hearts kept beating during culture. We reasoned that this could be improved by establishing strong, lasting contacts with the surface in order to explant epicardial cells. In order to increase surface contact and cell explantation, we put a sterile coverslip on top of each heart. This modification increased the contact areas of the heart and the surface, and improved the cell explantation frequency up to 60%.

4.3 Development of an ex vivo method to study epicardial cell migration

The cells on average explanted 4 or 5 days after seeding, and continued expanding over time (Fig. 24).

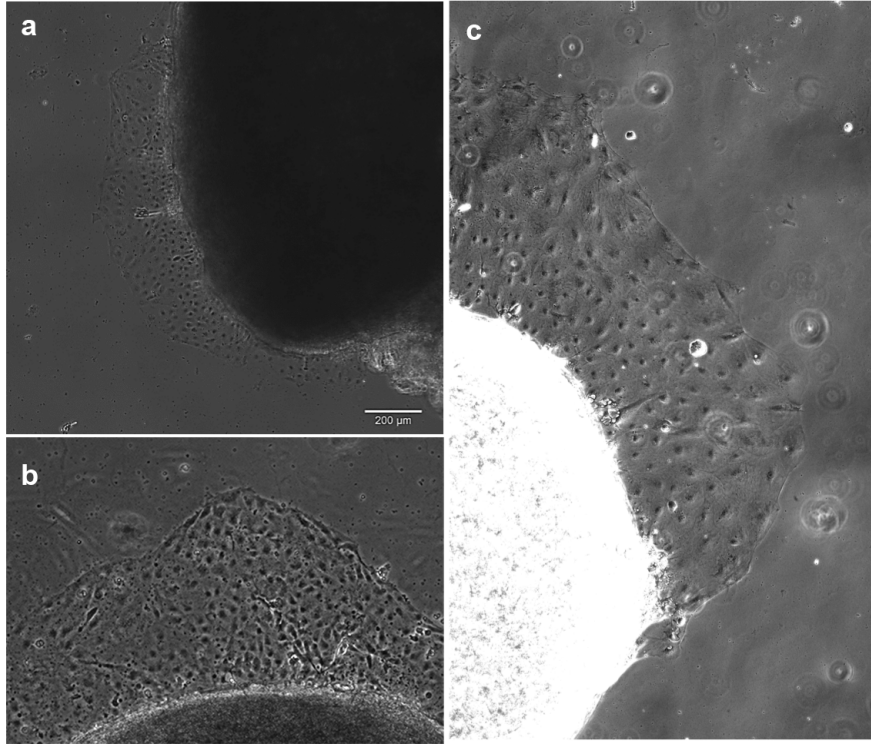


Figure 21. Epicardial explants from different hearts.

In the initial epicardial cell cultures, we removed the atrium and the outflow tract, and we seeded only the ventricles. However, we realized that when we seeded hearts with the outflow tract, the frequency of explantation was much higher, up to around 80% in non-contaminated wells.

Contamination, both fungal and bacterial, turned out to be one of the biggest problems in epicardial cell cultures even though we performed heart collection and seeding under a biological safety cabinet. We observed that when the seeding was done in six-well plates, a potential contamination spread to the neighboring wells, often contaminating the whole plate. In order to prevent this, we took several precautions. First, we started using 35 mm culture plates instead of six-well plates in order to prevent the spreading

4 Results

of a possible contamination. However, our principal aim was to prevent even a single contamination. For this, we took extra precautions while extracting the heart since the outer part of the fish body and fish water may contain many bacteria and fungi. Just before opening the cardiac cavity, we cleaned the fish skin with 70% ethanol. In addition, we used different sets of tweezers to open the cardiac cavity and to extract the heart for not to introduce outer microorganisms to the heart. And finally, we doubled the amount of antibiotics and antifungals in the medium. All of these improvements decreased the contamination frequency under 5%.

4.3.2 Optimization of surface coating

Once the epicardial cell culture protocol was optimized to obtain explanting hearts at a high and constant ratio on a tissue culture plate, different cell surface coatings were used to determine which one is more suitable for culturing these cells. We tried collagen, fibrinogen, gelatin, and fibronectin coatings. Among these coatings, we did not observe any significant differences in terms of cell explantation time or the amount of epicardial cells explanted, however in the fibrinogen coated plates, we observed easier attachment of the heart to the surface.

In the final set up, these coatings were planned to be applied on top of the fluorescent bead containing polyacrylamide gels prepared in glass-bottom tissue plates. This system allows calculation of traction forces, the forces that the cells exert on the surface. For this, time-lapse images of the fluorescent beads are taken and the traction forces are calculated by using the displacement of the beads with respect to their final position. When different coatings were applied on top of the polyacrylamide gel, collagen worked the best since it produces a very fine layer and allows measuring tractions. In contrast, fibrinogen produced a thick coating, interfering with the correct transmission of the traction forces onto the gel.

4.3.3 Characterization of zebrafish epicardial cells from uninjured hearts

Once the cells explanted onto the polyacrylamide gel coated with collagen, time-lapse images of the cells and the beads were taken every 10 minutes during approximately 15h to be able to perform physical and biological characterizations.

Cell migration velocity and traction force measurements

Cell migration velocity and traction forces are two important physical characteristics that determine cell movement. They are measured in epicardial cell sheet obtained from uninjured zebrafish heart with the aim of comparing them with the values from regenerating hearts at different time points after regeneration.

Cell migration velocities of the epicardial explants were calculated by manual tracking using Image J. 10 randomly selected cells from each heart were tracked using Image J and the trajectory was graphed (Fig. 22). From this tracking, average velocity of the cells from each heart was calculated (Fig. 23). It was observed that the cells from different uninjured, control hearts migrated with a similar velocity, since the calculated velocities were within the same range. This is important since it characterizes epicardial cells from a control heart, and can be used to compare them with regenerating hearts at different time points after regeneration.

Similar to cell migration velocity, cell tractions may determine the migratory behavior of cells. They are the forces that cells apply on top of a substrate in order to move, and can be different between epicardial cells from normal zebrafish hearts and the regenerating ones. Measurement of these forces was done by a technique called traction microscopy in collaboration with Dr. Xavier Trepats' group. Our aim here was to see if it was possible to measure these forces in epicardial explants mainly because heart beating could interfere with their detection. Since this method is based on the deformation of the polyacrylamide gel as the cells move, the stiffness of the gel is important. Therefore, we tested three different stiffnesses (6 kPa, 9 kPa, and 12 kPa). Among these, the 12 kPa gel worked the best, and we were able to measure tractions without interference from

4 Results

the heart beating. This method will be used in future to characterize zebrafish epicardial cells and to compare their behavior with epicardial cells from regenerating hearts.

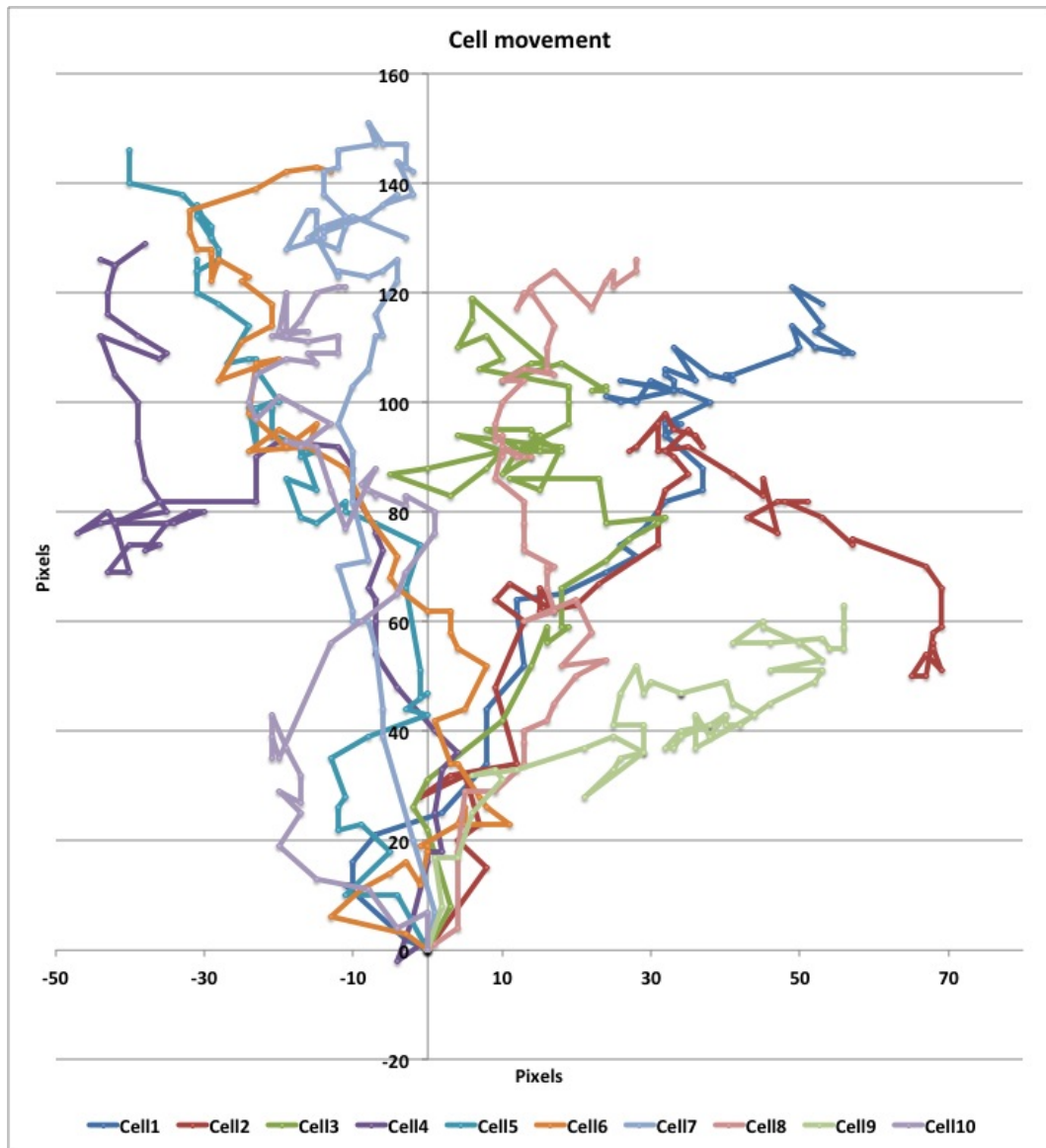


Figure 22. Cell movement graphed through manual tracking by Image J. Time-lapse images of the epicardial explant were taken every 10 minutes during approximately 15 hours. These 10 cells were selected randomly from one of the filmed heart and tracked by using Image J.

4.3 Development of an ex vivo method to study epicardial cell migration

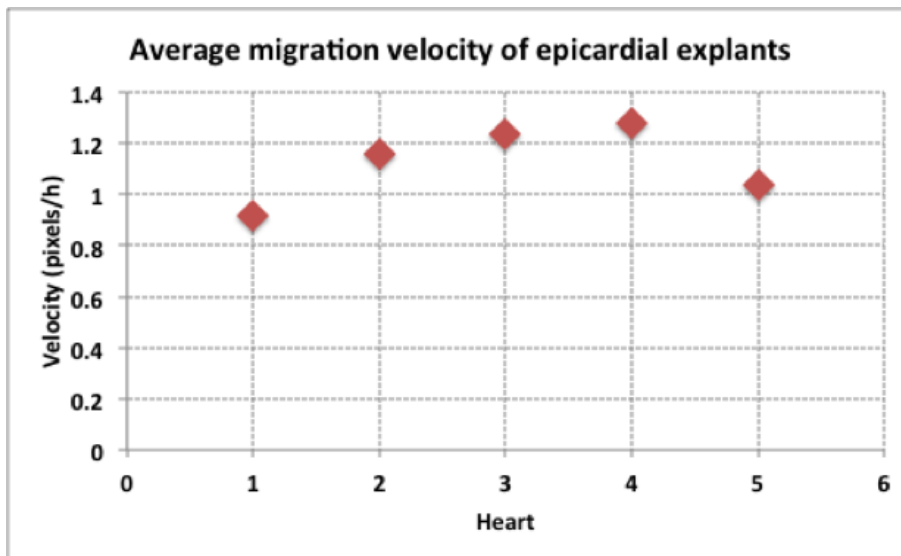


Figure 23. Average migration velocity of epicardial explants.

Characterization of cell movement through transgenic zebrafish lines

In order to understand how myosin II and F-actin fibers interact during epicardial cell movement, epicardial explants from transgenic zebrafish lines were obtained. Fish that express GFP and mCherry fluorescent proteins under the promoter of *myl12* to label myosin II, and fish of the *lifect* line, which label F-actin with GFP, and double transgenic fish that express both GFP-labeled F-actin and mCherry labeled myosin II were used.

Epicardial cells from these transgenic fish hearts allowed us to visualize F-actin and myosin II, eliminating the need of immunofluorescence analyses and enabling visualization of F-actin-myosin II interactions in living cells over time as they migrated. We observed that epicardial cells contained many myosin II fibers, and this characteristic will be compared with the epicardial cells from regenerating hearts.

4 Results

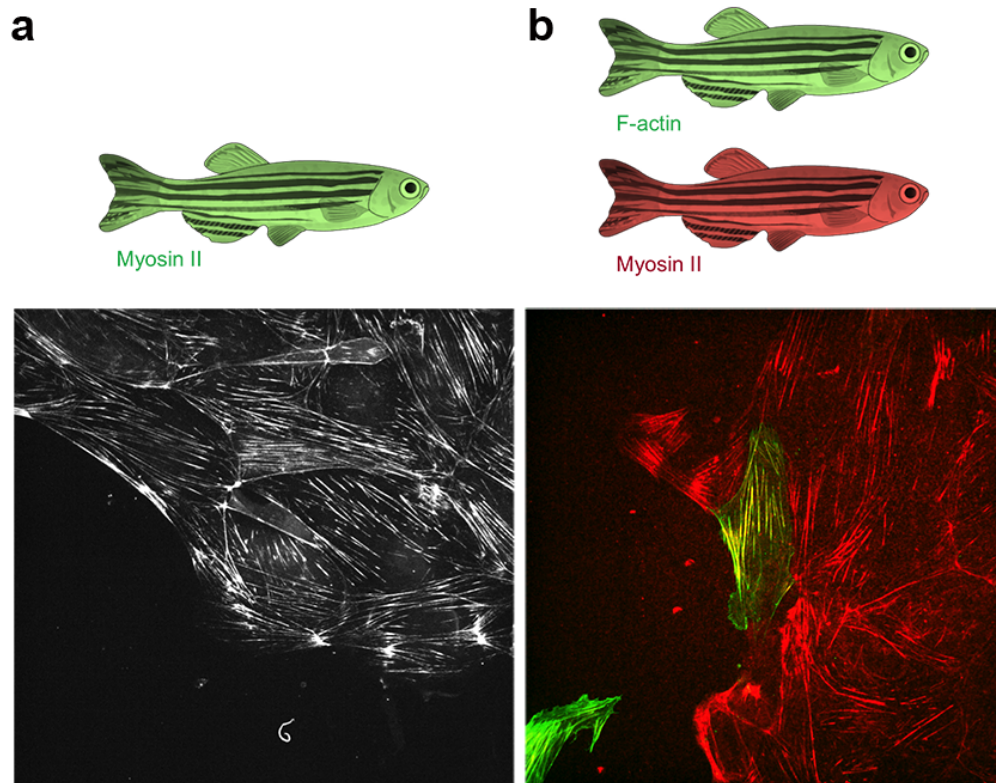


Figure 24. Epicardial explants obtained from transgenic zebrafish lines. (a) Fish that express GFP under the promoter of *myl12* to label myosin II, and (b) double transgenic fish that express both mCherry under the promoter of *myl12* to label myosin II and GFP in the *lifeact* line to label F-actin

These results showed that we developed, optimized, and validated a practical bioengineering tool which can measure important physical features of epicardial cell migration. Characterization of normal, uninjured zebrafish epicardial explant gave us the possibility to compare these characteristics with the ones that will be obtained from epicardial explant from regenerating hearts. Considering the high proliferation rate of epicardial cells during the first three days after amputation, high cell division would be expected in 1 to 3 dpa hearts. Similarly, the epicardial cells from these hearts would be expected to migrate faster. In addition, this system can be used to test different signaling molecules, or growth factors that might affect epicardial cell division or cell migration, and play role in regeneration.

5 Discussion

Zebrafish heart regeneration remains one of the most interesting phenomena of the 21st century. Considering the extremely high rate of deaths due to cardiovascular diseases in the developed countries, 1 out of every 3 people, understanding natural cardiac regeneration would address a worldwide challenge. Even though many aspects of zebrafish heart regeneration have been elucidated, there are still many open questions to be answered. Among these, the work presented here focuses on understanding cell migration mechanisms of cardiomyocytes and epicardial cells during heart regeneration.

5.1 Discussion of lineage tracing of zebrafish cardiomyocytes during development and regeneration

As demonstrated by lineage-tracing approaches, following heart damage newly generated cardiomyocytes arise from pre-existing ones, and therefore cell proliferation appears to be the primary mechanism for heart muscle regeneration after amputation or injury [Jopling et al., 2010, Kikuchi et al., 2010]. However, which cardiomyocytes build the new myocardium, and whether proliferating cardiomyocytes located distant to the injury site can actually migrate and contribute to myocardial regeneration was until now unknown. Outstanding questions in this respect include: do proliferating cardiomyocytes located distant to the injury site actually contribute to myocardial regeneration? Are there specific, regeneration-competent areas within the myocardium where the cardiomyocytes proliferate?, Or all of the cardiomyocytes have the capacity to divide and form new cardiomyocytes?

5 Discussion

In order to address these questions, lineage tracing of cardiomyocytes during heart regeneration was necessary. Cyclofen-based genetic labeling was described as proof of concept, however it had not been used for investigating a process. This work presents the first example of using this photoinducible genetic labeling system to track few cells within the same tissue. The advantage of using this system is that a direct relationship can be made between the originally labeled cells and the final clone, however, to do this only one labeled area per heart should be achieved. Even though we selected embryos with a single labeled area, since heart development is a dynamic process, it is difficult to predict the labeled outcome of the adult heart. To overcome this limitation, we tried labeling adult hearts by caged-cyclofen administration through injection followed by UV irradiation, however we could not achieve recombination. It is likely that the illumination time necessary to achieve uncaging of the caged-cyclofen in the adult heart could not be fulfilled, or the concentration of caged-cyclofen did not reach to a necessary value through the injections we performed.

Despite these setbacks, the lineage tracing analysis we performed allowed us to reach important conclusions. Lineage tracing of cardiomyocytes during development provided the first confirmation of the presence of primordial, trabecular, and cortical layers in the adult zebrafish heart by using a technique complementary to the one used in the original description of these layers [Gupta and Poss, 2012]. In addition, consistent with previous studies showing that only around 50% of the embryonic cardiomyocytes form the juvenile zebrafish myocardium [Gupta and Poss, 2012], we observed that approximately 50% of the labeled primordial cardiomyocytes did not contribute to the juvenile myocardium. Moreover, previous studies had suggested that the trabecular heart muscle originates from primordial cardiomyocytes, which detach from the myocardial wall and then reattach, sometimes even at distant places, giving rise to trabeculae [Gupta and Poss, 2012, Liu et al., 2010, Staudt et al., 2014]. The relative distribution of GFP-labeled areas found in our studies is consistent with this scenario, and further indicates that most primordial cardiomyocytes should be able to give rise to trabecular muscle, even though they do not contribute to the adult primordial layer.

Cell tracing during adult heart regeneration showed that only cardiomyocytes very close to the injury site gave rise to the cardiomyocytes in the regenerated myocardium, whereas those located farther away, even though they may undergo cell proliferation in response

5.2 Discussion about three photon-based cell photoactivation in living embryos

to the injury, did not contribute to the regenerated tissue. These results are in agreement with recent findings showing that 50% of mitotic cardiomyocytes are found within the first 100 μm adjacent to the injury zone at 7 dpa [Sallin et al., 2015]. Cardiomyocytes proliferation accounts for the regular hemostasis of the zebrafish heart [Wills et al., 2008], so it is likely that the proliferating cardiomyocytes that we show do not contribute to the regenerated tissue could instead serve to provide higher mechanical force to compensate for the lost tissue. In any case, our combined findings strongly argue against the existence of specific regeneration-competent areas in the adult zebrafish myocardium.

The overall picture that emerges from our studies of direct cardiomyocytes lineage tracing during adult heart regeneration is of a rather static process, in sharp contrast with the highly dynamic cardiomyocyte fate reprogramming described to take place during embryonic heart regeneration [Zhang et al., 2013]. Furthermore, our results showed that the predetermination of cardiomyocyte fate during adult heart regeneration is so prevailing that even their identity of layer of origin is retained, and subsequently reproduced in the regenerated tissue. In conclusion, our results revealed important differences in the cellular bases (and probably molecular mechanisms as well) that underlie the process of heart regeneration in developing embryos and in the adult setting, and highlight the key role that short-range signals should have for controlling the latter.

5.2 Discussion about three photon-based cell photoactivation in living embryos

In parallel to UV-based uncaging of caged-cyclofen, we investigated alternative ways. Our aim was to achieve prospective labeling, and we thought to do this through multi-photon excitation. Two-photon excitation was shown to work to uncage caged-cyclofen in cells or superficial structures [Sinha et al., 2010a], however the challenge here was reaching the heart. Theoretically, we calculated that three-photon photolysis would be much more effective than two-photon photolysis in deeper tissues.

In agreement with these theoretical results, we could successfully achieve uncaging of caged-cyclofen in the hearts of zebrafish embryos by using three-photon illumination at

5 Discussion

1064 nm wavelength. On the other hand, uncaging by two-photon illumination of 750 nm wavelength did not occur in our hands.

Even though we were successful in applying three-photon illumination to label a group of cardiomyocytes prospectively in the hearts of zebrafish embryos, it should be underlined that successful uncaging is not very straightforward, and depends on many factors.

The focal spot where three-photon excitation occurs should be small enough to allow this phenomenon to happen, but at the same time it should be large enough to contain sufficient amount of caged cyclofen that can be uncaged. In addition, this focal spot should be located on top of the heart wall, which at this stage is composed of a single layer of cardiomyocytes. Achieving this was a hard task considering the beating nature of the heart, and it was not possible to keep the heart wall focused during the whole illumination time. Therefore, we combined the heart beating rate with the movement of the beam, by adding z-oscillation of the objective, to produce a pulsed photo-activation, with ~ 25 -50 ms pulse width and ~ 2 -3 Hz repetition rate.

Overall, this system is based on one-by-one embryo manipulation, and very much depends on the positioning and morphology of each particular embryo. Due to these variables, we observed high variability in the rate of GFP-positive labeled hearts obtained by this method. Considering all experiments combined, the rate of obtaining GFP-positive cardiomyocytes ranged from 7 to 50 % between different experiments.

On the other hand, the embryo survival rate evaluated 24h after illumination was very high in all of the experiments, varying between 85% and 100%. This, together with the damage threshold testing, showed that the conditions we set for three-photon illumination were suitable to obtain uncaging without severely affecting embryo survival.

In summary, despite all the limitations outlined above, our results demonstrate that three-photon illumination can be used to photoactivate cells located deep within tissues, and in our case, has been very useful for labeling zebrafish cardiomyocytes in a prospective manner. Similarly, the techniques developed here could be applicable for labeling and tracing the lineage of other cell types or organs placed inside the body.

5.3 Discussion about development of an *ex vivo* method to study epicardial cell migration behavior during zebrafish heart regeneration

Upon cardiac damage, epicardium undergoes an extremely rapid and dynamic response. It becomes activated to proliferate, and migrates towards the injury site, in response to epicardium-derived signals to cover the wound within a few days [Lepilina et al., 2006]. It was demonstrated that the epicardium takes a very active role in myocardium regeneration, since, during regeneration cardiomyocytes were found to migrate to the injury site [Itou et al., 2012]. This finding uncovers an active communication between epicardial cells and cardiomyocytes, which appears to be essential for heart regeneration. Moreover, very recent evidences have shown that epicardial cell migration is essential for the regeneration of the myocardium in zebrafish [Wang et al., 2015].

The method presented here aims to provide an important bioengineering tool that allows measuring and comparing physical characteristics of epicardial explants from control and regenerating hearts at different time points after amputation. Through this technique, the differences in the amount of cell divisions, migration velocities, and the magnitude of the forces that the cells apply to the surface in order to move can be detected. It is important to measure these physical characteristics of epicardial cells, since the possible changes in these features regarding migration may reveal some of the key factors about their role during regeneration.

In addition, this technique can be used to discover molecules or factors that play roles during regeneration. Different signaling molecules, or growth factors that are known to play roles during regeneration can be added to the culture medium to detect and measure the changes in the cell division rate or their migratory behavior. Moreover, epicardial cells can be co-cultured with cardiomyocytes from regenerating hearts to study signaling between cardiomyocytes and epicardium, and this system can be used to measure their migratory behavior at the same time. Similarly, epicardial cells can be seeded on top of extracellular matrix obtained from control and regenerating hearts to study their interactions with extracellular matrix proteins.

5.4 General discussion

The discovery that zebrafish regenerates its heart by utilizing pre-existing cardiomyocytes as the primary source for new cardiac muscle, lead researches to investigate this mechanism in mammals. Shortly after, it was found that neonatal mice regenerate their hearts as well through the proliferation of pre-existing cardiomyocytes [Porrello et al., 2011]. The adult mammalian heart was once believed to be a post-mitotic organ, but this finding suggested that the ability of cardiomyocytes to re-enter the cell cycle and proliferate in response to injury was conserved in mammals, but was shut off during the first days after birth [Porrello et al., 2011]. This encourages us to think that there may be other regeneration-related mechanisms conserved between zebrafish and mammals, and that knowledge gained from investigating zebrafish heart regeneration may have implications for improving the regenerative ability of the human heart.

In this respect, the finding that only adjacent cardiomyocytes can contribute to the new tissue after regeneration is a very important conclusion that can be translated to the mammalian setting. A similar lineage tracing and fate-mapping approach in neonatal mice could show whether this mechanism is also conserved in mammals. These results highlight the key role that short-range signals should have for controlling cell proliferation and migration to the injury site during zebrafish heart regeneration, which should be further studied. Moreover, absence of specific regeneration-competent areas within the zebrafish heart indicates that the ability of de-differentiation and re-entry into the cell cycle is not specific to a specific area within the myocardium, and most probably all cardiomyocytes have this potential. Even though further evidence are necessary to validate this hypothesis, the idea of all zebrafish cardiomyocytes possess regenerative potential, encourages the notion that this potential can be re-gained in mammals through the activation or deactivation of the factors that regulate this mechanism.

Finally, the strategies developed in this work can be applied to answer other zebrafish heart regeneration related questions. For instance, the photo-inducible genetic labeling strategy can be used to label other cell types of zebrafish heart, such as epicardial, and endocardial cells to investigate their fate during heart development and regeneration. Similarly, the epicardium-related techniques can be further developed to understand

5.4 General discussion

their relation with cardiomyocytes through different signaling mechanisms. All of these approaches and the knowledge obtained with them are targeted to better understanding zebrafish heart regeneration, with the ultimate aim of translating this knowledge to achieve mammalian heart regeneration.

6 Conclusions

1. A genetic labeling method based on the activation of Cre/*lox* recombination by UV-irradiation was implemented. This method depended on UV-mediated uncaging of caged cyclofen, a caged tamoxifen analogue, in the hearts of zebrafish from double transgenic line Tg(*myl7*:ERT2-Cre-ERT2)/(*myl7*:LOXP-STOP-LOXP-EGFP).
2. Labeling resolution of up to single cardiomyocytes was achieved in the hearts of 2 dpf zebrafish larvae by using this novel technique.
3. Cardiomyocytes labeled in zebrafish larvae maintained GFP expression in adult hearts indicating that our labeling technique is suitable for lineage tracing and prospective fate mapping.
4. During zebrafish heart regeneration, only cardiomyocytes adjacent to the amputation plane contribute to new cardiomyocytes in the regenerating area.
5. Our results did not support the existence of regeneration-competent areas in the zebrafish heart.
6. Theoretical calculations predicted that three-photon photolysis was more effective for uncaging in deep tissues than two-photon.
7. We confirmed the theoretical prediction by successful uncaging of caged cyclofen in embryonic hearts by three-photon photolysis. To our knowledge, this was the first example of cell photoactivation *in vivo* using three-photon excitation.
8. Embryos labeled by three-photon excitation were survived to adulthood, and the progeny of the labeled cardiomyocytes was identified.

6 Conclusions

9. We have obtained explanted epicardial cultures from non-injured control hearts, and hearts from transgenic lines that display green or red fluorescence in myosin II or F-actin, using a system that allows analyzing the migration behavior of epicardial cells.

Bibliography

- C. P. Adler. Relationship between deoxyribonucleic acid content and nucleoli in human heart muscle cells and estimation of cell number during cardiac growth and hyperfunction. *Recent Adv Stud Cardiac Struct Metab*, 8:373–86, 1975.
- C. P. Adler and H. Friedburg. Myocardial dna content, ploidy level and cell number in geriatric hearts: post-mortem examinations of human myocardium in old age. *J Mol Cell Cardiol*, 18(1):39–53, 1986.
- S. R. Ali, S. Hippenmeyer, L. V. Saadat, L. Luo, I. L. Weissman, and R. Ardehali. Existing cardiomyocytes generate cardiomyocytes at a low rate after birth in mice. *Proc Natl Acad Sci U S A*, 111(24):8850–5, 2014.
- D. C. Andersen, S. Ganesalingam, C. H. Jensen, and S. P. Sheikh. Do neonatal mouse hearts regenerate following heart apex resection? *Stem Cell Reports*, 2(4):406–13, 2014.
- D. Bader and J. Oberpriller. Autoradiographic and electron microscopic studies of minced cardiac muscle regeneration in the adult newt, *notophthalmus viridescens*. *J Exp Zool*, 208(2):177–93, 1979.
- J. M. Bailey, B. A. Creamer, and M. A. Hollingsworth. What a fish can learn from a mouse: principles and strategies for modeling human cancer in mice. *Zebrafish*, 6(4): 329–37, 2009.
- J. Bakkers. Zebrafish as a model to study cardiac development and human cardiac disease. *Cardiovasc Res*, 91(2):279–88, 2011.

Bibliography

- T. Becker and C. G. Becker. Axonal regeneration in zebrafish. *Curr Opin Neurobiol*, 27:186–91, 2014.
- T. Becker, M. F. Wullimann, C. G. Becker, R. R. Bernhardt, and M. Schachner. Axonal regrowth after spinal cord transection in adult zebrafish. *J Comp Neurol*, 377(4): 577–95, 1997.
- Alexandra E Bely and Kevin G Nyberg. Evolution of animal regeneration: re-emergence of a field. *Trends in Ecology & Evolution*, 25(3):161–170, 2010.
- O. Bergmann, R. D. Bhardwaj, S. Bernard, S. Zdunek, F. Barnabe-Heider, S. Walsh, J. Zupicich, K. Alkass, B. A. Buchholz, H. Druid, S. Jovinge, and J. Frisen. Evidence for cardiomyocyte renewal in humans. *Science*, 324(5923):98–102, 2009.
- R. R. Bernhardt, E. Tongiorgi, P. Anzini, and M. Schachner. Increased expression of specific recognition molecules by retinal ganglion cells and by optic pathway glia accompanies the successful regeneration of retinal axons in adult zebrafish. *J Comp Neurol*, 376(2):253–64, 1996.
- M. Bettencourt-Dias, S. Mittnacht, and J. P. Brockes. Heterogeneous proliferative potential in regenerative adult newt cardiomyocytes. *J Cell Sci*, 116(Pt 19):4001–9, 2003.
- Jeremy P Brockes, Anoop Kumar, and Cristiana P Velloso. Regeneration as an evolutionary variable. *Journal of anatomy*, 199(1&2):3–11, 2001.
- D. M. Bryant, C. C. O’Meara, N. N. Ho, J. Gannon, L. Cai, and R. T. Lee. A systematic analysis of neonatal mouse heart regeneration after apical resection. *J Mol Cell Cardiol*, 79:315–8, 2015.
- P. B. Burton, M. C. Raff, P. Kerr, M. H. Yacoub, and P. J. Barton. An intrinsic timer that controls cell-cycle withdrawal in cultured cardiac myocytes. *Dev Biol*, 216(2): 659–70, 1999.
- Bruce M. Carlson. *Principles of regenerative biology*. Academic Press, 2011.

- F. Chablais, J. Veit, G. Rainer, and A. Jazwinska. The zebrafish heart regenerates after cryoinjury-induced myocardial infarction. *BMC Dev Biol*, 11:21, 2011.
- M. Chalfie, Y. Tu, G. Euskirchen, W. W. Ward, and D. C. Prasher. Green fluorescent protein as a marker for gene expression. *Science*, 263(5148):802–5, 1994.
- E. P. Creaser. Some notes on north american crayfish. *Science*, 79(2051):364, 1934.
- S. Curado, R. M. Anderson, B. Jungblut, J. Mumm, E. Schroeter, and D. Y. Stainier. Conditional targeted cell ablation in zebrafish: a new tool for regeneration studies. *Dev Dyn*, 236(4):1025–35, 2007.
- A. Darehzereshki, N. Rubin, L. Gamba, J. Kim, J. Fraser, Y. Huang, J. Billings, R. Mohammadzadeh, J. Wood, D. Warburton, V. Kaartinen, and C. L. Lien. Differential regenerative capacity of neonatal mouse hearts after cryoinjury. *Dev Biol*, 399(1): 91–9, 2015.
- W. Denk, J. H. Strickler, and W. W. Webb. Two-photon laser scanning fluorescence microscopy. *Science*, 248(4951):73–6, 1990.
- C. Q. Diep and A. J. Davidson. Transplantation of cells directly into the kidney of adult zebrafish. *J Vis Exp*, 0(51):e2725, May 2011.
- W. Driever, L. Solnica-Krezel, A. F. Schier, S. C. Neuhauss, J. Malicki, D. L. Stemple, D. Y. Stainier, F. Zwartkruis, S. Abdelilah, Z. Rangini, J. Belak, and C. Boggs. A genetic screen for mutations affecting embryogenesis in zebrafish. *Development*, 123: 37–46, 1996.
- G. M. Ellison, C. Vicinanza, A. J. Smith, I. Aquila, A. Leone, C. D. Waring, B. J. Henning, G. G. Stirparo, R. Papait, M. Scarfo, V. Agosti, G. Viglietto, G. Condorelli, C. Indolfi, S. Ottolenghi, D. Torella, and B. Nadal-Ginard. Adult c-kit(pos) cardiac stem cells are necessary and sufficient for functional cardiac regeneration and repair. *Cell*, 154(4):827–42, 2013.
- R. Feil, J. Wagner, D. Metzger, and P. Chambon. Regulation of cre recombinase activity by mutated estrogen receptor ligand-binding domains. *Biochem Biophys Res Commun*, 237(3):752–7, 1997.

Bibliography

- M. A. Goldstein, W. C. Claycomb, and A. Schwartz. Dna synthesis and mitosis in well-differentiated mammalian cardiocytes. *Science*, 183(4121):212–3, 1974.
- J. M. Gonzalez-Rosa, V. Martin, M. Peralta, M. Torres, and N. Mercader. Extensive scar formation and regression during heart regeneration after cryoinjury in zebrafish. *Development*, 138(9):1663–74, 2011.
- J. M. Gonzalez-Rosa, M. Peralta, and N. Mercader. Pan-epicardial lineage tracing reveals that epicardium derived cells give rise to myofibroblasts and perivascular cells during zebrafish heart regeneration. *Dev Biol*, 370(2):173–86, 2012.
- Maria Göppert-Mayer. Über elementarakte mit zwei quantensprüngen. *Annalen der Physik*, 401(3):273–294, 1931.
- V. Gupta and K. D. Poss. Clonally dominant cardiomyocytes direct heart morphogenesis. *Nature*, 484(7395):479–84, 2012.
- V. Gupta, M. Gemberling, R. Karra, G. E. Rosenfeld, T. Evans, and K. D. Poss. An injury-responsive gata4 program shapes the zebrafish cardiac ventricle. *Curr Biol*, 23(13):1221–7, 2013.
- S. Hans, J. Kaslin, D. Freudenreich, and M. Brand. Temporally-controlled site-specific recombination in zebrafish. *PLoS One*, 4(2):e4640, 2009.
- S. Hata, M. Namae, and H. Nishina. Liver development and regeneration: from laboratory study to clinical therapy. *Dev Growth Differ*, 49(2):163–70, 2007.
- B. J. Haubner, M. Adamowicz-Brice, S. Khadayate, V. Tiefenthaler, B. Metzler, T. Aitman, and J. M. Penninger. Complete cardiac regeneration in a mouse model of myocardial infarction. *Aging (Albany NY)*, 4(12):966–77, 2012.
- S. W. Hell, K. Bahlmann, M. Schrader, A. Soini, H. M. Malak, I. Gryczynski, and J. R. Lakowicz. Three-photon excitation in fluorescence microscopy. *J Biomed Opt*, 1(1):71–4, 1996.
- N. G. Horton, K. Wang, D. Kobat, C. G. Clark, F. W. Wise, C. B. Schaffer, and C. Xu. three-photon microscopy of subcortical structures within an intact mouse brain. *Nat Photonics*, 7(3):205–209, January 2013.

- K. Howe, M. D. Clark, C. F. Torroja, J. Torrance, C. Berthelot, M. Muffato, J. E. Collins, S. Humphray, K. McLaren, L. Matthews, S. McLaren, I. Sealy, M. Caccamo, C. Churcher, C. Scott, J. C. Barrett, R. Koch, G. J. Rauch, S. White, W. Chow, B. Kilian, L. T. Quintais, J. A. Guerra-Assuncao, Y. Zhou, Y. Gu, J. Yen, J. H. Vogel, T. Eyre, S. Redmond, R. Banerjee, J. Chi, B. Fu, E. Langley, S. F. Maguire, G. K. Laird, D. Lloyd, E. Kenyon, S. Donaldson, H. Sehra, J. Almeida-King, J. Loveland, S. Trevanion, M. Jones, M. Quail, D. Willey, A. Hunt, J. Burton, S. Sims, K. McLay, B. Plumb, J. Davis, C. Clee, K. Oliver, R. Clark, C. Riddle, D. Elliot, G. Threadgold, G. Harden, D. Ware, S. Begum, B. Mortimore, G. Kerry, P. Heath, B. Phillimore, A. Tracey, N. Corby, M. Dunn, C. Johnson, J. Wood, S. Clark, S. Pelan, G. Griffiths, M. Smith, R. Glithero, P. Howden, N. Barker, C. Lloyd, C. Stevens, J. Harley, K. Holt, G. Panagiotidis, J. Lovell, H. Beasley, C. Henderson, D. Gordon, K. Auger, D. Wright, J. Collins, C. Raisen, L. Dyer, K. Leung, L. Robertson, K. Ambridge, D. Leongamornlert, S. McGuire, R. Gilderthorp, C. Griffiths, D. Manthravadi, S. Nichol, G. Barker, et al. The zebrafish reference genome sequence and its relationship to the human genome. *Nature*, 496(7446):498–503, 2013.
- P. C. Hsieh, V. F. Segers, M. E. Davis, C. MacGillivray, J. Gannon, J. D. Molkenin, J. Robbins, and R. T. Lee. Evidence from a genetic fate-mapping study that stem cells refresh adult mammalian cardiomyocytes after injury. *Nat Med*, 13(8):970–4, 2007.
- N. Hu, H. J. Yost, and E. B. Clark. Cardiac morphology and blood pressure in the adult zebrafish. *Anat Rec*, 264(1):1–12, 2001.
- J. Itou, I. Oishi, H. Kawakami, T. J. Glass, J. Richter, A. Johnson, T. C. Lund, and Y. Kawakami. Migration of cardiomyocytes is essential for heart regeneration in zebrafish. *Development*, 139(22):4133–42, 2012.
- S. A. Jesty, M. A. Steffey, F. K. Lee, M. Breitbart, M. Hesse, S. Reining, J. C. Lee, R. M. Doran, A. Y. Nikitin, B. K. Fleischmann, and M. I. Kotlikoff. c-kit⁺ precursors support postinfarction myogenesis in the neonatal, but not adult, heart. *Proc Natl Acad Sci U S A*, 109(33):13380–5, 2012.
- S. L. Johnson and J. A. Weston. Temperature-sensitive mutations that cause stage-specific defects in zebrafish fin regeneration. *Genetics*, 141(4):1583–95, 1995.

Bibliography

- C. Jopling, E. Sleep, M. Raya, M. Marti, A. Raya, and J. C. Izpisua Belmonte. Zebrafish heart regeneration occurs by cardiomyocyte dedifferentiation and proliferation. *Nature*, 464(7288):606–9, 2010.
- Chris Jopling, Stephanie Boue, and Juan Carlos Izpisua Belmonte. Dedifferentiation, transdifferentiation and reprogramming: three routes to regeneration. *Nature reviews Molecular cell biology*, 12(2):79–89, 2011.
- W Kaiser and CGB Garrett. Two-photon excitation in calcium: Eu²⁺. *Physical review letters*, 7(6):229, 1961.
- J. Karlsson, J. von Hofsten, and P. E. Olsson. Generating transparent zebrafish: a refined method to improve detection of gene expression during embryonic development. *Mar Biotechnol (NY)*, 3(6):522–7, 2001.
- R. N. Kettleborough, E. M. Busch-Nentwich, S. A. Harvey, C. M. Dooley, E. de Bruijn, F. van Eeden, I. Sealy, R. J. White, C. Herd, I. J. Nijman, F. Fenyes, S. Mehroke, C. Scahill, R. Gibbons, N. Wali, S. Carruthers, A. Hall, J. Yen, E. Cuppen, and D. L. Stemple. A systematic genome-wide analysis of zebrafish protein-coding gene function. *Nature*, 496(7446):494–7, 2013.
- K. Kikuchi, J. E. Holdway, A. A. Werdich, R. M. Anderson, Y. Fang, G. F. Egnaczyk, T. Evans, C. A. Macrae, D. Y. Stainier, and K. D. Poss. Primary contribution to zebrafish heart regeneration by gata4(+) cardiomyocytes. *Nature*, 464(7288):601–5, 2010.
- K. Kikuchi, V. Gupta, J. Wang, J. E. Holdway, A. A. Wills, Y. Fang, and K. D. Poss. tcf21+ epicardial cells adopt non-myocardial fates during zebrafish heart development and regeneration. *Development*, 138(14):2895–902, 2011a.
- K. Kikuchi, J. E. Holdway, R. J. Major, N. Blum, R. D. Dahn, G. Begemann, and K. D. Poss. Retinoic acid production by endocardium and epicardium is an injury response essential for zebrafish heart regeneration. *Dev Cell*, 20(3):397–404, 2011b.
- J. Kim, Q. Wu, Y. Zhang, K. M. Wiens, Y. Huang, N. Rubin, H. Shimada, R. I. Handin, M. Y. Chao, T. L. Tuan, V. A. Starnes, and C. L. Lien. Pdgf signaling is required for

- epicardial function and blood vessel formation in regenerating zebrafish hearts. *Proc Natl Acad Sci U S A*, 107(40):17206–10, 2010.
- C. B. Kimmel. Patterning the brain of the zebrafish embryo. *Annu Rev Neurosci*, 16: 707–32, 1993.
- C. B. Kimmel, D. A. Kane, C. Walker, R. M. Warga, and M. B. Rothman. A mutation that changes cell movement and cell fate in the zebrafish embryo. *Nature*, 337(6205): 358–62, 1989.
- C. B. Kimmel, K. Hatta, and W. K. Metcalfe. Early axonal contacts during development of an identified dendrite in the brain of the zebrafish. *Neuron*, 4(4):535–45, 1990.
- K. Konig. Multiphoton microscopy in life sciences. *J Microsc*, 200(Pt 2):83–104, 2000.
- K. Kretzschmar and F. M. Watt. Lineage tracing. *Cell*, 148(1-2):33–45, 2012.
- V. Kroehne, D. Freudenreich, S. Hans, J. Kaslin, and M. Brand. Regeneration of the adult zebrafish brain from neurogenic radial glia-type progenitors. *Development*, 138 (22):4831–41, 2011.
- K. M. Kwan, E. Fujimoto, C. Grabher, B. D. Mangum, M. E. Hardy, D. S. Campbell, J. M. Parant, H. J. Yost, J. P. Kanki, and C. B. Chien. The tol2kit: a multisite gateway-based construction kit for tol2 transposon transgenesis constructs. *Dev Dyn*, 236(11): 3088–99, 2007.
- M. A. Laflamme and C. E. Murry. Heart regeneration. *Nature*, 473(7347):326–35, 2011.
- A. Lepilina, A. N. Coon, K. Kikuchi, J. E. Holdway, R. W. Roberts, C. G. Burns, and K. D. Poss. A dynamic epicardial injury response supports progenitor cell activity during zebrafish heart regeneration. *Cell*, 127(3):607–19, 2006.
- F. Li, X. Wang, J. M. Capasso, and A. M. Gerdes. Rapid transition of cardiac myocytes from hyperplasia to hypertrophy during postnatal development. *J Mol Cell Cardiol*, 28(8):1737–46, 1996.
- C. L. Lien, M. R. Harrison, T. L. Tuan, and V. A. Starnes. Heart repair and regeneration: recent insights from zebrafish studies. *Wound Repair Regen*, 20(5):638–46, 2012.

Bibliography

- J. Liu, M. Bressan, D. Hassel, J. Huisken, D. Staudt, K. Kikuchi, K. D. Poss, T. Mikawa, and D. Y. Stainier. A dual role for *erbb2* signaling in cardiac trabeculation. *Development*, 137(22):3867–75, 2010.
- J. Livet, T. A. Weissman, H. Kang, R. W. Draft, J. Lu, R. A. Bennis, J. R. Sanes, and J. W. Lichtman. Transgenic strategies for combinatorial expression of fluorescent proteins in the nervous system. *Nature*, 450(7166):56–62, 2007.
- H. Masaki and H. Ide. Regeneration potency of mouse limbs. *Dev Growth Differ*, 49(2):89–98, 2007.
- Shanthi Mendis, Pekka Puska, Bo Norrving, World Health Organization., World Heart Federation., and World Stroke Organization. *Global atlas on cardiovascular disease prevention and control*. World Health Organization in collaboration with the World Heart Federation and the World Stroke Organization, Geneva, 2011.
- C. Mosimann and L. I. Zon. Advanced zebrafish transgenesis with *tol2* and application for *cre/lox* recombination experiments. *Methods Cell Biol*, 104:173–94, 2011.
- J. B. Moss, P. Koustubhan, M. Greenman, M. J. Parsons, I. Walter, and L. G. Moss. Regeneration of the pancreas in adult zebrafish. *Diabetes*, 58(8):1844–51, 2009.
- A. Nagy. Cre recombinase: the universal reagent for genome tailoring. *Genesis*, 26(2):99–109, 2000.
- N. Naqvi, M. Li, J. W. Calvert, T. Tejada, J. P. Lambert, J. Wu, S. H. Kesteven, S. R. Holman, T. Matsuda, J. D. Lovelock, W. W. Howard, S. E. Iismaa, A. Y. Chan, B. H. Crawford, M. B. Wagner, D. I. Martin, D. J. Lefer, R. M. Graham, and A. Husain. A proliferative burst during preadolescence establishes the final cardiomyocyte number. *Cell*, 157(4):795–807, 2014.
- J. Oberpriller and J. C. Oberpriller. Mitosis in adult newt ventricle. *J Cell Biol*, 49(2):560–3, 1971.
- J. O. Oberpriller and J. C. Oberpriller. Response of the adult newt ventricle to injury. *J Exp Zool*, 187(2):249–53, 1974.

- J. O. Oberpriller, J. C. Oberpriller, D. G. Matz, and M. H. Soonpaa. Stimulation of proliferative events in the adult amphibian cardiac myocyte. *Ann N Y Acad Sci*, 752: 30–46, 1995.
- E. R. Porrello, A. I. Mahmoud, E. Simpson, J. A. Hill, J. A. Richardson, E. N. Olson, and H. A. Sadek. Transient regenerative potential of the neonatal mouse heart. *Science*, 331(6020):1078–80, 2011.
- E. R. Porrello, A. I. Mahmoud, E. Simpson, B. A. Johnson, D. Grinsfelder, D. Canseco, P. P. Mammen, B. A. Rothermel, E. N. Olson, and H. A. Sadek. Regulation of neonatal and adult mammalian heart regeneration by the mir-15 family. *Proc Natl Acad Sci U S A*, 110(1):187–92, 2013.
- K. D. Poss. Getting to the heart of regeneration in zebrafish. *Semin Cell Dev Biol*, 18(1):36–45, 2007.
- K. D. Poss, L. G. Wilson, and M. T. Keating. Heart regeneration in zebrafish. *Science*, 298(5601):2188–90, 2002.
- A. Raya, C. M. Koth, D. Buscher, Y. Kawakami, T. Itoh, R. M. Raya, G. Sternik, H. J. Tsai, C. Rodriguez-Esteban, and J. C. Izpisua-Belmonte. Activation of notch signaling pathway precedes heart regeneration in zebrafish. *Proc Natl Acad Sci U S A*, 100 Suppl 1:11889–95, 2003.
- Ángel Raya, Antonella Consiglio, Yasuhiko Kawakami, Concepcion Rodriguez-Esteban, and Juan Carlos Izpisúa-Belmonte. The zebrafish as a model of heart regeneration. *Cloning and stem cells*, 6(4):345–351, 2004.
- Peter W Reddien and Alejandro Sánchez Alvarado. Fundamentals of planarian regeneration. *Annu. Rev. Cell Dev. Biol.*, 20:725–757, 2004.
- Randall W Reyer, Robert A Woolfitt, and Loraine T Withersty. Stimulation of lens regeneration from the newt dorsal iris when implanted into the blastema of the regenerating limb. *Developmental biology*, 32(2):258–281, 1973.
- H. A. Sadek, J. F. Martin, J. K. Takeuchi, J. Leor, Y. Nie, M. Giacca, and R. T. Lee. Multi-investigator letter on reproducibility of neonatal heart regeneration following apical resection. *Stem Cell Reports*, 3(1):1, 2014.

Bibliography

- K. C. Sadler, K. N. Krahn, N. A. Gaur, and C. Ukomadu. Liver growth in the embryo and during liver regeneration in zebrafish requires the cell cycle regulator, *uhrf1*. *Proc Natl Acad Sci U S A*, 104(5):1570–5, 2007.
- P. Sallin, A. S. de Preux Charles, V. Duruz, C. Pfefferli, and A. Jazwinska. A dual epimorphic and compensatory mode of heart regeneration in zebrafish. *Dev Biol*, 399(1):27–40, 2015.
- Alejandro Sánchez Alvarado. Regeneration in the metazoans: why does it happen? *Bioessays*, 22(6):578590, 2000.
- B. Sauer. Inducible gene targeting in mice using the cre/lox system. *Methods*, 14(4):381–92, 1998.
- K. Schnabel, C. C. Wu, T. Kurth, and G. Weidinger. Regeneration of cryoinjury induced necrotic heart lesions in zebrafish is associated with epicardial activation and cardiomyocyte proliferation. *PLoS One*, 6(4):e18503, 2011.
- David Sedmera. Function and form in the developing cardiovascular system. *Cardiovascular research*, 91(2):252–259, 2011.
- S. E. Senyo, M. L. Steinhauser, C. L. Pizzimenti, V. K. Yang, L. Cai, M. Wang, T. D. Wu, J. L. Guerquin-Kern, C. P. Lechene, and R. T. Lee. Mammalian heart renewal by pre-existing cardiomyocytes. *Nature*, 493(7432):433–6, 2013.
- S. E. Senyo, R. T. Lee, and B. Kuhn. Cardiac regeneration based on mechanisms of cardiomyocyte proliferation and differentiation. *Stem Cell Res*, 13(3 Pt B):532–41, 2014.
- Xavier Serra-Picamal, Vito Conte, Romaric Vincent, Ester Anon, Dhananjay T Tambe, Elsa Bazellieres, James P Butler, Jeffrey J Fredberg, and Xavier Trepac. Mechanical waves during tissue expansion. *Nature Physics*, 8(8):628–634, 2012.
- W. Shi, Z. Fang, L. Li, and L. Luo. Using zebrafish as the model organism to understand organ regeneration. *Sci China Life Sci*, 58(4):343–51, 2015.

- X. Shi and D. J. Garry. Muscle stem cells in development, regeneration, and disease. *Genes Dev*, 20(13):1692–708, 2006.
- D. K. Sinha, P. Neveu, N. Gagey, I. Aujard, C. Benbrahim-Bouzidi, T. Le Saux, C. Rampon, C. Gauron, B. Goetz, S. Dubruille, M. Baaden, M. Volovitch, D. Bensimon, S. Vríz, and L. Jullien. Photocontrol of protein activity in cultured cells and zebrafish with one- and two-photon illumination. *Chembiochem*, 11(5):653–63, 2010a.
- D. K. Sinha, P. Neveu, N. Gagey, I. Aujard, T. Le Saux, C. Rampon, C. Gauron, K. Kawakami, C. Leucht, L. Bally-Cuif, M. Volovitch, D. Bensimon, L. Jullien, and S. Vríz. Photoactivation of the creer t2 recombinase for conditional site-specific recombination with high spatiotemporal resolution. *Zebrafish*, 7(2):199–204, 2010b.
- L. Solnica-Krezel, A. F. Schier, and W. Driever. Efficient recovery of enu-induced mutations from the zebrafish germline. *Genetics*, 136(4):1401–20, 1994.
- Hans Spemann and Hilde Mangold. Über induktion von embryonalanlagen durch implantation artfremder organisatoren. *Development Genes and Evolution*, 100(3):599–638, 1924.
- D. Y. Stainier. Zebrafish genetics and vertebrate heart formation. *Nat Rev Genet*, 2(1):39–48, 2001.
- D. Y. Stainier, R. K. Lee, and M. C. Fishman. Cardiovascular development in the zebrafish. i. myocardial fate map and heart tube formation. *Development*, 119(1):31–40, 1993.
- D. Y. Stainier, B. Fouquet, J. N. Chen, K. S. Warren, B. M. Weinstein, S. E. Meiler, M. A. Mohideen, S. C. Neuhaus, L. Solnica-Krezel, A. F. Schier, F. Zwartkruis, D. L. Stemple, J. Malicki, W. Driever, and M. C. Fishman. Mutations affecting the formation and function of the cardiovascular system in the zebrafish embryo. *Development*, 123:285–92, 1996.
- D. W. Staudt, J. Liu, K. S. Thorn, N. Stuurman, M. Liebling, and D. Y. Stainier. High-resolution imaging of cardiomyocyte behavior reveals two distinct steps in ventricular trabeculation. *Development*, 141(3):585–93, 2014.

Bibliography

- G. Streisinger, C. Walker, N. Dower, D. Knauber, and F. Singer. Production of clones of homozygous diploid zebra fish (*brachydanio rerio*). *Nature*, 291(5813):293–6, 1981.
- E. G. Strungs, E. L. Ongstad, M. P. O’Quinn, J. A. Palatinus, L. J. Jourdan, and R. G. Gourdie. Cryoinjury models of the adult and neonatal mouse heart for studies of scarring and regeneration. *Methods Mol Biol*, 1037:343–53, 2013.
- J. Summerton and D. Weller. Morpholino antisense oligomers: design, preparation, and properties. *Antisense Nucleic Acid Drug Dev*, 7(3):187–95, 1997.
- Elly M Tanaka and Peter W Reddien. The cellular basis for animal regeneration. *Developmental cell*, 21(1):172–185, 2011.
- R. Thummel, T. J. Bailey, and D. R. Hyde. In vivo electroporation of morpholinos into the adult zebrafish retina. *J Vis Exp*, 0(58):e3603, December 2011.
- Panagiotis A Tsonis. Regeneration in vertebrates. *Developmental biology*, 221(2):273–284, 2000.
- Panagiotis A Tsonis, Mayur Madhavan, Emily E Tancous, and Katia Del Rio-Tsonis. A newt’s eye view of lens regeneration. *Int J Dev Biol*, 48(8-9):975–980, 2004.
- A. Ustione and D. W. Piston. A simple introduction to multiphoton microscopy. *J Microsc*, 243(3):221–6, 2011.
- J. H. van Berlo, O. Kanisicak, M. Maillet, R. J. Vagnozzi, J. Karch, S. C. Lin, R. C. Middleton, E. Marban, and J. D. Molkentin. *c-kit*⁺ cells minimally contribute cardiomyocytes to the heart. *Nature*, 509(7500):337–41, 2014.
- T. S. Vihtelic and D. R. Hyde. Light-induced rod and cone cell death and regeneration in the adult albino zebrafish (*danio rerio*) retina. *J Neurobiol*, 44(3):289–307, 2000.
- Walther Vogt. Gestaltungsanalyse am amphibienkeim mit örtlicher vitalfärbung. *Wilhelm Roux’Archiv für Entwicklungsmechanik der Organismen*, 120(1):384–706, 1929.
- B. G. Wang, K. Konig, and K. J. Halhuber. Two-photon microscopy of deep intravital tissues and its merits in clinical research. *J Microsc*, 238(1):1–20, 2010.

- J. Wang, D. Panakova, K. Kikuchi, J. E. Holdway, M. Gemberling, J. S. Burris, S. P. Singh, A. L. Dickson, Y. F. Lin, M. K. Sabeh, A. A. Werdich, D. Yelon, C. A. Macrae, and K. D. Poss. The regenerative capacity of zebrafish reverses cardiac failure caused by genetic cardiomyocyte depletion. *Development*, 138(16):3421–30, 2011.
- J. Wang, J. Cao, A. L. Dickson, and K. D. Poss. Epicardial regeneration is guided by cardiac outflow tract and hedgehog signalling. *Nature*, 522(7555):226–30, 2015.
- Irving L Weissman, David J Anderson, and Fred Gage. Stem and progenitor cells: origins, phenotypes, lineage commitments, and transdifferentiations. *Annual review of cell and developmental biology*, 17(1):387–403, 2001.
- Monte Westerfield. *The zebrafish book: a guide for the laboratory use of zebrafish (Danio rerio)*. University of Oregon Press, 2000.
- C.O. Whitman. a contribution to the history of the germ-layers in clepsine. *Journal of Morphology*, 1:105, 1887.
- R. M. Williams, D. W. Piston, and W. W. Webb. Two-photon molecular excitation provides intrinsic 3-dimensional resolution for laser-based microscopy and microphotochemistry. *FASEB J*, 8(11):804–13, 1994.
- Airon A Wills, Jennifer E Holdway, Robert J Major, and Kenneth D Poss. Regulated addition of new myocardial and epicardial cells fosters homeostatic cardiac growth and maintenance in adult zebrafish. *Development*, 135(1):183–192, 2008.
- Edmund Beecher Wilson. *The cell-lineage of Nereis*. Ginn & Company, 1892.
- N. Witman, B. Murtuza, B. Davis, A. Arner, and J. I. Morrison. Recapitulation of developmental cardiogenesis governs the morphological and functional regeneration of adult newt hearts following injury. *Dev Biol*, 354(1):67–76, 2011.
- C. Wyatt, E. M. Bartoszek, and E. Yaksi. Methods for studying the zebrafish brain: past, present and future. *Eur J Neurosci*, 42(2):1746–63, 2015.
- C Xu and WW Webb. Nonlinear and two-photon induced fluorescence. *Topics in Fluorescence Spectroscopy*, page 475, 1997.

Bibliography

- C. Xu, W. Zipfel, J. B. Shear, R. M. Williams, and W. W. Webb. Multiphoton fluorescence excitation: new spectral windows for biological nonlinear microscopy. *Proc Natl Acad Sci U S A*, 93(20):10763–8, 1996.
- R. Zhang, P. Han, H. Yang, K. Ouyang, D. Lee, Y. F. Lin, K. Ocorr, G. Kang, J. Chen, D. Y. Stainier, D. Yelon, and N. C. Chi. In vivo cardiac reprogramming contributes to zebrafish heart regeneration. *Nature*, 498(7455):497–501, 2013.

Appendix I. Three-photon illumination calculations

Following calculations were done by our collaborator Dra. Dobryna Zalvidea

N-photon photolysis

Excitation rate: fraction of molecules found per simple pulse

$$k_e = \frac{\alpha \cdot \eta}{T}, \quad \alpha = \frac{N_e}{N_t}$$

N_t : total number of molecules
 η : quantum efficiency
 T : pulse time

Numbers of absorbed photons:

$$dN_{abs} = \sigma_n \cdot \Phi^n \cdot dN_t \cdot dt \quad \sigma_n: n \text{ cross-section} \quad C_0: \text{molecule concentration}$$

$$N_t = C_0 \cdot N_A \cdot V \quad V: \text{volume of photolysis} \quad N_A: \text{Avogadro's number}$$

Photon flux per unit area unit time:

$$\Phi = I(r, z, t) \cdot \frac{\lambda}{h \cdot c}, \quad dN_{abs} = \frac{\sigma_n \cdot I(r, z, t)^n \cdot \lambda^n \cdot C_0 \cdot N_A}{h^n \cdot c^n} \alpha V \cdot dt$$

Numbers of molecules excited in V per pulse is $1/n^{th}$ numbers of photons:

$$N_e = \frac{N_{abs}}{n} = \frac{\sigma_n \cdot \lambda^n \cdot C_0 \cdot N_A}{n \cdot h^n \cdot c^n} \int_T I_0(t)^n \cdot dt \int_V S(r, z)^n \cdot dV$$

taking into account the temporal coherence:

Appendix I

$$\delta^n = \frac{\langle I_0(t)^n \rangle}{\langle I_0(t) \rangle^n} = g^n \left(\frac{T}{\tau} \right)^{n-1}$$

$$k_e^{(n)} = \frac{\sigma_n \cdot \lambda^n \cdot \eta}{n \cdot h^n \cdot c^n \cdot \mathcal{F}} g_n \left(\frac{T}{\tau} \right)^{n-1} \cdot \langle I_0 \rangle^n \cdot \mathcal{F} \cdot \frac{\int S(r,z)^n \cdot dV}{V}$$

$$VF = \frac{\int S(r,z)^n \cdot dV}{V}$$

$$k_e^{(n)} = \frac{\sigma_n \cdot \lambda^n \cdot \eta}{n \cdot h^n \cdot c^n} g_n \left(\frac{T}{\tau} \right)^{n-1} \cdot \frac{P_0^n}{(\pi \cdot \omega_0^2)^n} \cdot VF$$

For $n = 2$

$$k_e^{(2)} = \frac{\sigma_2 \cdot \lambda^2 \cdot \eta}{2 \cdot h^2 \cdot c^2} g_2 \left(\frac{T}{\tau} \right) \cdot \frac{P_0^2}{\pi^2 \cdot \omega_0^4} \cdot VF$$

For $n = 3$

$$k_e^{(3)} = \frac{\sigma_3 \cdot \lambda^3 \cdot \eta}{3 \cdot h^3 \cdot c^3} g_3 \left(\frac{T}{\tau} \right)^2 \cdot \frac{P_0^3}{\pi^3 \cdot \omega_0^6} \cdot VF$$

To estimate VF :

The molecules used $\tau_v \cong 20ms$ to travel $\sim 10\mu m$, so $V = 0.5\mu m/ms$

If the focal volume is $\sim 1\mu m^3$, it will take for them $\sim 1ms$ to get out or in, in this volume.

We are considering the uncaging rate per pulse, that is $< 0.5ps$, in this time these molecules did not move.

Consequently, the volume V can be approximated to the excitation volume and $VF \sim 1$.

Measurement of the three-photon uncaging cross section

The three-photon uncaging reaction taking place within the illuminated volume V_{exc} resulting from laser focusing is:



where A is the active substrate, G the caging group and cA the caged compound. The corresponding uncaging rate within the photolysis volume is:

$$k_{3p}^{unc} = \frac{\sigma_{3p} \cdot \eta_{3p}}{n} \frac{\lambda^3}{h^3 c^3} g_{3p} \left(\frac{T}{\tau} \right)^2 \frac{P_0^3}{(\pi \cdot \omega_0^2)^3} VF \quad (2)$$

where σ_{3p} is the three-photon absorption cross-section, η_{3p} is the quantum efficiency of uncaging, and $\delta_{3p} = \sigma_{3p} \cdot \eta_{3p}$, $\omega_0 = 0.55 \mu m$ is the measured focal radius at the xy-plane, $T = 50 ns$ the periodicity and $\tau = 280 fs$ the duration of the pulses, $\lambda = 1064 nm$ the central wavelength, h the Planck constant, c the velocity of light, $n_0 = 1.33$ the refractive index of the propagating medium, $g_{3p} = 0.41$ is a measurement of the 3-order of temporal coherence of the excitation source and VF is the fraction of the excitation volume in the photolysis volume. Considering the diffusion coefficient of DMNB expected to be in the $10^{-10} m^2 s^{-1}$ range, the time for diffusing in or out of the focal radius for DMNB is $\sim 1 ms$. For pulse durations $\lesssim 0.5 ps$, the excitation volume is the photolysis volume, and $VF = 1$.

Neglecting diffusion of the reactant and products of the reaction (1) in and out of a single cell inside the fish embryo within the uncaging time scales, each cell can be assumed as a closed system. The uncaging rate ke^{3p} in the photolysis volume/excitation volume is related with the measured uncaging rate k in a closed volume $V = 500 \pm 50 \mu m^3$ (cell) that contains the focal volume V_{exc} by:

$$ke^{3p} = k(V/V_{exc}) \quad (3)$$

where the reactant and products of the reaction can be considered to be homogeneously distributed within the cell. Then the concentrations in cA (DMNB-coumarin) and A (coumarin) obey:

$$\frac{dcA}{dt} = -\frac{dA}{dt} = -k \cdot cA \quad (4)$$

which solution is:

$$A(t) = cA_0 (1 - e^{-kt}) \quad (5)$$

Appendix I

Measuring the increase of the fluorescence intensity of photo-releasing the fluorescent substrate A in a single cell of the zebrafish embryo that was previously incubated with cA , the rate constant k can be estimated. We illuminated a superficial single cell in a 48 hpf zebrafish with 280fs pulses at 1064nm ($\sim 20nm$ bandwidth) with repetition rate 20 MHz using the above described set up. For these experiments, the beam was fixed to a predetermined position in the embryo using a $60xNA = 1.0$ water objective and the epifluorescence was detected using a photon counting (H9319, Hamamatsu). In fig. 16 (b) it is shown that the intensity exhibits an exponential growth as predicted by the expression (5) derived from the kinetic model.

The fluorescence intensity growth can be fitted with:

$$I(t) = I_{max} (1 - e^{-kt}) \quad (6)$$

where $k = 0.07s^{-1}$ for input power 37.5mW and $k = 0.02s^{-1}$ for input power 24.6mW. Both k values satisfactorily fulfil the expected cubic dependence of k on the input power. From equations (3) and (2), the three-photon uncaging cross-section of DMNB is:

$$\delta_{3p} = (4 \pm 2) \times 10^{-85} cm^6 (s/photon)^2.$$

Calculation of two- and three-photon uncaging rate

We calculated the two- and three-photon uncaging rate from the equation

$$k_{np}^{unc} = \frac{\sigma_{np} \cdot \eta_{np}}{n} \frac{\lambda^n}{h^n c^n} g_{np} \left(\frac{T}{\tau} \right)^{n-1} \frac{P_0^n}{(\pi \cdot \omega_0^2)^n} VF \cdot e^{-\frac{nz}{l_{np}}}$$

for $n = 3$ three- and $n = 2$ two-photon uncaging rates for DMNB

($\delta_{2p} = 4 \times 10^{-53} cm^4 s/photon$ and $\delta_{3p} = 4 \times 10^{-85} cm^6 s^2/photon^2$) illuminating with pulses with $T = 50ns$, $\tau = 180fs$, $w_0 = 0.25\mu m$, $\lambda = 730nm$ and $g_2 = 0.59$ for two-photon, and $\lambda = 1064nm$ and $g_2 = 0.41$ for three-photon uncaging. The scattering lengths $l_{2p} = 235\mu m$ and $l_{3p} = 500\mu m$ were calculated with Mie approximation considering

a solution containing $1\mu m$ spheres, $n_s = 1.5$, in water $n_m = 1.33$ with concentration $5.4 \times 10^{-3} \text{ spheres}/\mu m^3$, for $\lambda = 730nm$ in the two- and $\lambda = 1064nm$ in the three-photon case.

Appendix II

Publications

This section consists of the manuscripts of two articles that are currently submitted for publication in the following order:

Article 1

Long-term *in vivo* single cell lineage tracing of deep structures by three-photon activation

Submitted on July 28th, 2015 to the journal *Light: Science & Applications* with impact factor (2014): 14.603

Article 2

Fate predetermination of cardiac myocytes during zebrafish heart regeneration

Submitted on September 17th, 2015 to the journal *Developmental Biology* with impact factor (2014): 3.547

Long-term *in vivo* single cell lineage tracing of deep structures by three-photon activation

Isil Tekeli ¹, Isabelle Aujard ^{2,3,4}, Xavier Trepât ^{5,6}, Ludovic Jullien ^{2,3,4}, Angel Raya ^{1,6,7,8*},
Dobryna Zalvidea ^{5*}

¹ Control of Stem Cell Potency Group, Institute for Bioengineering of Catalonia (IBEC), Barcelona Science Park, Baldiri Reixac 15-21, 08028 Barcelona, Spain

² École Normale Supérieure – PSL Research University, Department of Chemistry, 24 rue Lhomond, F-75005 Paris, France.

³ Sorbonne Universités, UPMC Univ Paris 06, PASTEUR, F-75005 Paris, France.

⁴ CNRS, UMR 8640 PASTEUR, F-75005 Paris, France.

⁵ Integrative Cell and Tissue Dynamics Group, Institute of Bioengineering of Catalonia (IBEC), Barcelona, Spain.

⁶ Institució Catalana de Recerca i Estudis Avançats (ICREA)

⁷ Center for Networked Biomedical Research on Bioengineering, Biomaterials and Nanomedicine (CIBER-BBN)

⁸ Center of Regenerative Medicine in Barcelona (CMRB), Barcelona Biomedical Research Park, Dr. Aiguader 88, 08003 Barcelona, Spain.

* Address for correspondence: Angel Raya, Phone: +34 934 020 537; Fax: +34 934 020 183; Email: araya@ibecbarcelona.eu

OR Dobryna Zalvidea, Phone: +34 934 037 068; Fax: +34 934 037 181; Email: dzalvidea@ibecbarcelona.eu

Keywords: multi-photon microscopy, photo-activation, zebrafish, three-photon microscopy

Abstract

Genetic labeling techniques allow non-invasive lineage tracing of cells *in vivo*. Two-photon-inducible activators provide spatial resolution for superficial cells, but labeling cells located deep within tissues is precluded by scattering of the far-red illumination required for two-photon photolysis. Three-photon illumination has been shown to overcome the limitations of two-photon microscopy for *in vivo* imaging of deep structures, but whether it can be used for photo-activation remains to be tested. Here we show, theoretically and experimentally, that three-photon illumination surpasses scattering problems by combining longer wavelength excitation with high uncaging three-photon cross-section molecules. We prospectively labeled heart muscle cells in zebrafish embryos, and found permanent labeling in their progeny in adult animals, with negligible tissue damage. This technique allows non-invasive genetic manipulation *in vivo* with spatial, temporal, and cell-type specificity, and may have wide applicability for experimental biology.

Introduction

Controlling cell behavior by manipulating the expression of proteins has become a fundamental tool in biology^{1,2}. Whether triggering their expression by using chemical means or irradiating heat or light^{3,4}, the predetermination of cells/tissues selected for undergoing a given modification is as important as predicting the moment of the event. Photo-activation of protein expression allows cell or subcellular spatial resolution as well as high temporal precision^{5,6}. An attractive system to study long-term effects of photo-activation in depth tissues *in vivo* is the Cre-loxP genetic switch system^{7,8}, which is widely used in biology for controlling protein expression. It controls protein expression by modifying precise sites in the DNA, allowing the use of specific promoters for

targeting specific cell types and using external stimulus for triggering it. Because it is a DNA modification, it persists through the cell lifespan and is also transmitted to its progeny. It has been genetically implemented in mice⁷, and more recently in zebrafish⁸. A non-invasive, photo-inducible Cre-loxP system shown by Sinha *et al.*^{9,10} permits activation of the expression of green fluorescent protein (GFP) with temporal and single-cell spatial resolution (Fig. 1). This system uses an inactive, caged inducer that penetrates the whole organism, but only becomes functional when it is uncaged in a region of interest (Fig. 1b and 1c). It was reported that uncaging of the inducer can be achieved by UV illumination, without resolution along the beam path. Using femtosecond pulses at 750 nm, two-photon photolysis allowed 3D spatial resolution, successfully labeling single cells at the

eye and somites in 24-hours post fertilization (hpf) zebrafish embryos^{9,10}. However, investigation of internal organs during development requires accessibility to cells masked by more complex tissues, as well as maintaining long-term viability of labeled cells. The efficiency of photo-activation in a selected cell is a function of the number of effective photons, not affected by the scattering, that reach it (*ballistic photons*). Far-red photons at 700-750 nm already suffer significant scattering¹¹, therefore resulting in sub-optimal photo-activation for powers below the damage threshold.

Here, inspired by previous works for increasing imaging depth,^{11,12} we demonstrate that illuminating at longer wavelengths results in lower scattering when traveling through tissues, while still inducing nonlinear photo-activation.

Methods

Numerical Results

We calculated the n -photon uncaging rate when the laser illuminates a thick sample is k_{np}^{unc} ¹³:

$$k_{np}^{unc} = \frac{\sigma_{np} \eta_{np}}{n} \frac{\lambda^n}{h^n c^n} g_{np} \left(\frac{T}{\tau} \right)^{n-1} \frac{P_0^n}{(\pi w_0^2)^n} VF \cdot e^{-\frac{nz}{l_c}} \quad (1)$$

for $n = 3$ three- and $n = 2$ two-photon uncaging rates for DMNB (with $\delta_{2p} = 4 \times 10^{-53} \text{ cm}^4 \text{ s/photon}$ and $\delta_{3p} = 4 \times 10^{-85} \text{ cm}^6 \text{ s}^2/\text{photon}^2$) illuminating with pulses with $T = 50 \text{ ns}$, $\tau = 180 \text{ fs}$, $w_0 = 0.25 \text{ } \mu\text{m}$, $\lambda = 730 \text{ nm}$ and $g_2 = 0.59$ for two-photon, and $\lambda = 1064 \text{ nm}$ and $g_3 = 0.41$ for three-photon uncaging. The scattering lengths $l_{2p} = 235 \text{ } \mu\text{m}$ and $l_{3p} = 500 \text{ } \mu\text{m}$ were calculated with Mie approximation considering a solution containing $1 \text{ } \mu\text{m}$ spheres, $n_s = 1.5$, in water $n_m = 1.33$ with concentration $5.4 \times 10^{-3} \text{ spheres}/\mu\text{m}^3$, for $\lambda = 730 \text{ nm}$ in the two- and $\lambda = 1064 \text{ nm}$ in the three-photon case.

Zebrafish

Zebrafish were maintained at 28.5°C, raised according to standard methods¹⁴. All experiments were conducted following procedures approved by the Ethics Committee on Experimental Animals of the Barcelona Research Park. The generation and characterization of the transgenic zebrafish line used in this study: Tg-cmlc2a-Cre-Ert2/Tg-lox-STOP-lox-GFP has been previously described¹⁵.

Animal Procedures

We inhibited the pigmentation by using 75 μM 1-phenyl 2-thiourea (PTU) at 22 hpf (28 somite stage), as previously described¹⁶.

Caged 4-hydroxy-cyclofen was synthesized as described previously^{9,10}. Zebrafish embryos were incubated in embryo medium containing 2 μM caged-cyclofen (DMNB-cyclofen) during 12 hours prior to photoactivation. Before illumination, the embryos were thoroughly washed with fresh embryo medium to avoid any possible interference originating from photorelease of caged-cyclofen in the medium.

For positive control, embryos were incubated in 2 μM 4-Hydroxy-tamoxifen (4-OHT) (Sigma).

Prior to illumination, zebrafish were anesthetized using 4.2 ml tricaine solution (4 mg/ml) per 100 ml of fish tank water¹⁴.

Set up for measuring three-photon cross-section

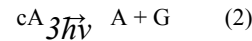
The set up used for the measurement of the cross-sections was the following: the 280 fs pulses at 1064 nm ($\square 20 \text{ nm}$ bandwidth) with repetition rate 20 MHz generated by a fiber laser (Femtopower, Fianium It) were sent to an inverted microscope, through a telescope to overfill the back aperture of the objective. The light was focused with a 60x NA = 1.0 water objective to a femtoliter volume. The emission fluorescence was collected in epifluorescence configuration using a photon counting (H9319, Hamamatsu).

Three-photon behavior

In order to test the three-photon behavior for the excitation wavelength of our experimental set up, we measured the 3-photon excited fluorescence vs. excitation power using blue fluospheres (FluoSpheres® Carboxylate-Modified Microspheres, 1 μm , blue fluorescent (365/415)) in suspension (0.02% solids in water) (Fig. 2a).

Measurement of the three-photon uncaging cross section

The three-photon uncaging reaction taking place within the illuminated volume V_{exc} resulting from laser focusing is¹⁷:



where A is the active substrate, G the caging group and cA the caged compound. The corresponding uncaging rate within the photolysis volume is:

$$k_{3p}^{unc} = \frac{\sigma_{3p} \eta_{3p}}{n} \frac{\lambda^3}{h^3 c^3} g_{3p} \left(\frac{T}{\tau} \right)^2 \frac{P_0^3}{(\pi w_0^2)^3} VF \quad (3)$$

where σ_{3p} is the three-photon absorption cross-section, η_{3p} is the quantum efficiency of uncaging, and $\delta_{3p} = \sigma_{3p} \eta_{3p}$, $w_0 = 0.55 \text{ } \mu\text{m}$ is the measured focal radius at the xy -plane, $T = 50 \text{ ns}$ the periodicity and $\tau = 280 \text{ fs}$ the duration of the pulses, $\lambda = 1064 \text{ nm}$ the central wavelength, h the Planck constant, c the velocity of light, $n_0 = 1.33$ the refractive index of the propagating medium, $g_{3p} = 0.41$ is a measurement of the 3-order of temporal coherence of the excitation source and VF is the fraction of the excitation volume in the photolysis volume. Considering the diffusion coefficient of DMNB expected to be in the $10^{-10} \text{ m}^2 \text{ s}^{-1}$ range, the time for diffusing in or out of the focal radius for DMNB is $\square 1 \text{ ms}$. For pulse durations $\square 0.5 \text{ ps}$, the excitation volume is the photolysis volume, and $VF = 1$.

Neglecting diffusion of the reactant and products of the reaction (2) in and out of a single cell inside the fish embryo within the uncaging timescales, each cell can be assumed as a closed system. The uncaging rate k_e^{3p} in the photolysis volume/excitation volume is related with the measured uncaging rate k in a closed volume $V = 500 \pm 50 \text{ } \mu\text{m}^3$ (cell) that contains the focal volume V_{exc} by:

$$k_e^{3p} = k (V/V_{exc}) \quad (4)$$

where the reactant and products of the reaction can be considered to be homogeneously distributed within the

cell. Then the concentrations in cA (DMNB-coumarin) and A (coumarin) obey:

$$\frac{dcA}{dt} = -\frac{dA}{dt} = -k \cdot cA \quad (5)$$

which solution is:

$$A(t) = cA_0 (1 - e^{-kt}) \quad (6)$$

Measuring the increase of the fluorescence intensity of photo-releasing the fluorescent substrate A in a single cell of the zebrafish embryo that was previously incubated with cA, the rate constant k can be estimated. We illuminated a superficial single cell in a 48 hpf zebrafish with 280 fs pulses at 1064 nm (□20 nm bandwidth) with repetition rate 20 MHz using the above described set up. For these experiments, the beam was fixed to a predetermined position in the embryo using a 60 x NA = 1.0 water objective and the epifluorescence was detected using a photon counting (H9319, Hamamatsu). In fig. 2b it is shown that the intensity exhibits an exponential growth as predicted by the expression (6) derived from the kinetic model.

The fluorescence intensity growth can be fitted with:

$$I(t) = I_{\max} (1 - e^{-kt}) \quad (7)$$

where $k = 0.07 \text{ s}^{-1}$ for input power 37.5 mW and $k = 0.02 \text{ s}^{-1}$ for input power 24.6 mW. Both k values satisfactorily fulfil the expected cubic dependence of k on the input power. From equations (4) and (3), the three-photon uncaging cross-section of DMNB is $\delta_{3p} = (4 \pm 2) \times 10^{-85} \text{ cm}^6(\text{s/photon})^2$.

In vitro damage assay

Fibroblasts cells were plate on glass-bottom dishes (MatTek) and imaged for 100 s using 280 fs pulses at 1064 nm, to study cell damage. After 24 hours we counted the dead cells. Results are shown in fig. 2c. We defined “damage threshold” as the power where more than 50% of the cells survived.

Control experiments

Control experiments were done by exposing the animals to: 1. cyclofen, without illumination; 2. 280 fs pulses illumination without previous treatment with DMNB-cyclofen and, finally, 3. DMNB-cyclofen without illumination (Fig. 2d).

Three-photon activation set up

The photoactivation of the DMNB-cyclofen was performed using 280 fs duration pulses at 1064 nm, with a repetition rate of 20 MHz, generated by a fiber laser (FemtoPower, Fianium lt.). The pulses were sent by a set of galvo-scanners (Thorlabs, GVSM002/M) through a telescope, in order to fulfil the back aperture of the objective, to an inverted microscope (Olympus) equipped with a motorized xy-stage (Marzhauser, SCAN IM 120 x 80) and a motorized objective holder (Marzhauser, MA42). The usual objective used was a 40x with 1.3 NA (Olympus, UPLFLN 40 XO). Targeting the specific tissue was achieved with a custom software (Labview) and a PCI board (National Instrument, NI PCI-6024E) by

controlling the galvo-scanners and the motorized stage. A CCD (EverFocus, EQ200E) was used for wide-field imaging of the animal during the experiment. A custom software make the focal spot follow a 3D sinusoid. Typical patches targeted at the heart were of 15x15, 15x20, 20x20 μm^2 with 0.1 patch/s, by raster scanning. It was shown that the transient increment in temperature inside the focal volume generated by femtosecond pulses is accumulative in time¹⁸. For minimizing this effect we combined the heart beating rate with the movement of the beam, by adding z -oscillation of the objective, to produce a pulsed photoactivation, with ~ 25 -50 ms pulse width and ~ 2 -3 Hz repetition rate.

Illumination experiments

48-80-hpf zebrafish embryos were placed in a glass-bottom petri dish (MatTek) after 2 min in embryo medium with anaesthesia. The zone of photoactivation was previously chosen from a schematic of the ventricle of the zebrafish heart divided in top, central and bottom part. The illumination experiment consisted in the three-photon activation by using the dedicated software with parameters described above, and it lasted 2 to 4 min. After illumination, embryos were transferred to individual tanks for further follow up. 24 hours later, they were imaged under a fluorescence microscope, classified according to GFP expression, and transferred to rearing tanks.

Microscopy, in vivo imaging and image processing

General screening of GFP-positive zebrafish embryos was done by using a fluorescence stereomicroscope (Leica), and for detailed in vivo imaging a spinning-disk confocal microscope (PerkinElmer UltraViewERS Spinning-Disk microscopy system mounted on a Zeiss Axiovert 200M microscope) equipped with a Hamamatsu C9100-50 EMCCD camera was used. Images and videos were processed with the software Adobe Photoshop and Volocity, respectively.

Immunohistochemistry and imaging

Immunohistochemistry was performed on 10 μm cryosections using the antibodies MF20 (DSHB) and anti-GFP (GFP-1020; Aves Labs). Images of the heart sections were taken by using a Leica SP5 microscope.

Results and Discussion

To address whether three-photon absorption at longer wavelengths is efficient at deeper tissues when excited with powers below the damage threshold, we first calculated the rate of n -uncaging as a function of the quantity of *ballistic* photons that reach the target cell. The power of the *ballistic* photons contributing to nonlinear absorption follows a Lambert-Beer like exponential decline,

$$P = P_0 e^{-z/l_s} \quad (8)$$

with depth z , characteristic length l_s , calculated through Mie theory, and P_0 power at the surface of the sample. The n -photon uncaging rate when the laser illuminates a thick sample is k_{unc}^{np} ¹³:

$$k_{unc}^{np} = \frac{\sigma_{np} \eta_{np}}{n} \frac{\lambda^n}{h^n c^n} g_{np} \left(\frac{T}{\tau} \right)^{n-1} \frac{P_0^n}{(\pi w_0^2)^n} VF \cdot e^{-\frac{nc}{l_{np}}} \quad (9)$$

where σ_{np} is the n -photon absorption cross-section, η_{np} is the quantum efficiency of uncaging, and $\delta_{np} = \sigma_{np} \eta_{np}$ is the action uncaging cross-section, T the periodicity and τ the duration of the pulses, λ the central wavelength, h the Planck constant, c the velocity of light, w_0 the focal radius at the xy -plane, g_{np} is a measure of the n -order of temporal coherence of the excitation source, VF is the fraction of the excitation volume in the photolysis volume and l_{np} the scattering length at the wavelength for n -photon absorption. The uncaging rates depend on the molecule by δ_{np} , and on the illumination, through λ , τ , T , w_0 and P_0 . A compromise of the uncaging efficiency and damage constricts the illumination parameters for each tissue.

Several moieties can be used for caging the activating molecule^{19,20}. We chose 4,5 dimethoxy-2-nitrobenzyl (DMNB) because it was likely to be photoactive around 1 μm when excited with three photons. The choice of 1 μm excitation is based on minimization of scattering effects while using caged molecules that will not be one- and/or two-photon activated in the visible/very near-IR wavelength, allowing their combination with any fluorescent label that is excited within this range. Furthermore, 1 μm is a suitable wavelength for three-photon photo-activation of most caging groups. We measured the three-photon action uncaging cross-section for DMNB (see Methods), $\delta_{3p} = (4 \pm 2) \times 10^{-85} \text{ cm}^6(\text{s/photon})^2$. To our knowledge, there are no measurements of the three-photon action uncaging cross-section and very few three-photon excitation cross-sections¹³ values in the literature. From the characterization of one-photon uncaging of DMNB,¹⁹ we could expect $\eta_{3p} \square \eta_{1p} \square 0.01$ and therefore $\sigma_{3p} \square 10^{-83} \text{ cm}^6(\text{s/photon})^2$. The latter order of magnitude satisfactorily compares with typical values extracted from three-photon excitation cross-sections of molecules used

in functional imaging, like fura-2 with Ca^{2+} , $\sigma_{3p} \eta_{3p}^{exc} = 30 \times 10^{-83} \text{ cm}^6(\text{s/photon})^2$ or indo-1 with Ca^{2+} , $\sigma_{3p} \eta_{3p}^{exc} = 6 \times 10^{-83} \text{ cm}^6(\text{s/photon})^2$,¹³ assuming $\eta_{3p}^{exc} \square \eta_{1p}^{exc} \square 1$,²¹. Moreover the value obtained for three-photon action uncaging cross-section of DMNB is in a range suitable for efficient uncaging with three-photon excitation.

Next, to investigate whether three-photon excitation could improve the uncaging rate for cells within tissues, we compared it with two-photon uncaging using $\delta_{2p} = 4 \times 10^{-53} \text{ cm}^4 \text{ s/photon}$,⁴ (see Methods for details on the parameters used). We calculated the ratio between DMNB uncaging rates for two- and three-photon excitation, and predicted three-photon excitation for deeply embedded cells to be up to 5 times more efficient than two-photon illumination (Fig. 3a), while being below the damage threshold and above a minimum production rate of the uncaged molecule (Fig. 1c). Specifically, our calculations predict higher efficiency of two-photon uncaging for superficial tissues and the

opposite behavior the deeper the cells are within the tissue, for powers still below the damage threshold (Fig. 3b). Moreover, higher efficiency of three- compared to two-photon uncaging can be achieved by decreasing the focal spot size (Fig. 3c), although limited by the damage threshold for a specific depth (Fig. 3d). In summary, our calculations predict that three-photon uncaging at longer wavelengths could be a solution for photo-activation in tissues located deep inside the animal, where two-photon absorption suffers strong scattering that affects the efficiency of activation vs. damage threshold²².

We confirmed and applied our predictions by investigating *in vivo* three-photon activation of cardiomyocytes of 48-80 hpf zebrafish embryos transgenic for a Cre-loxP system that labels cardiomyocytes by expressing GFP (Fig. 4a and b). These embryos expressed inducible Cre in cardiomyocytes, and were treated with DMNB-cyclofen. Successful uncaging of the DMNB-cyclofen would initiate the Cre-loxP recombination process, leading to the expression of GFP in photo-activated cardiomyocytes. We built a custom set up and designed a protocol with *ad hoc* photo-activation strategies for optimizing the quantity of molecules uncaged while avoiding tissue damage (see Methods for details). Targeted cells at $>150 \mu\text{m}$ were successfully labeled and found to express GFP (Fig. 4 and Supplementary Video 1). We also accessed different parts of the heart at varying depths, and labeled distinct areas (Fig. 4 and Supplementary Video 2).

To investigate the long-term survival of the labeled cells and their progeny, we allowed some of the fish to develop until adulthood, when their hearts were harvested for analysis. Fig. 4c shows a heart harvested 3 months after three-photon illumination, which originally affected an area of 0.01 mm^2 in a central part of the heart ventricle. The final labeled area in the adult heart was $\sim 0.126 \text{ mm}^2$ with a signal to noise ratio (SNR_{dB}) of 20 dB (Fig. 4c). Photo-activated cardiomyocytes and their progeny were identified in the adult myocardium, and shown to contribute to all three recently²³ identified primordial, cortical and trabecular layers (Fig. 4c). Negligible damage occurred during three-photon uncaging in cardiomyocytes at the embryo stage, as labeled cells were able to survive, divide and their progeny was found after 3 months in the heart of the adult zebrafish, indistinguishable from unlabeled cardiomyocytes.

Conclusions

In summary, we stipulated and confirmed, theoretically and experimentally, that three-photon illumination of a typical caging group provides a solution to the ubiquitous scattering problem, and effectively activates proteins in deep tissues without damage along the lifetime of the animal. We have demonstrated, for the first time, that three-photon illumination at $\sim 1 \mu\text{m}$ of caged-cyclofen results in successful uncaging of the compound in deep tissue cells. In combination with a genetic Cre-loxP labeling system, three-photon activation enables long-term cell lineage tracing of cells embedded in deep

tissues or structures. This methodology, demonstrated in the heart of the zebrafish, can be extended to other tissues and animal models, as well as for activating, with time and space resolution, the expression of different proteins that can provide long-term control of individual or multiple cells behavior *in vivo*.

Acknowledgments

We thank Cristina García for excellent technical assistance with zebrafish husbandry. IT and DZ were partially supported by a pre-doctoral fellowship from MINECO and the I3 program, respectively. Additional support was provided by grants from MINECO (SAF2012-33526, BFU2012-38146), ISCIII (Red de Terapia Celular - TerCel RD12/0019/0019), and ERC (Grant Agreement 242993).

References

- Buckingham M. E. & Meilhac S. M. Tracing cells for tracking cell lineage and clonal behaviour. *Developmental Cell* **21**, 394-409 (2011).
- Weber T. & Köster R. Genetic tools for multicolor imaging in zebrafish larvae. *Methods* **62**, 279–291 (2013).
- Bugai L. J., Choksi A. T., Mesuda C. K., Kane R. S. & Schaffer C. B. Optogenetic protein clustering and signaling activation in mammalian cells. *Nat Methods* **10**, 249-252 (2013).
- Madisen L., Mao, T., Koch H., Zhuo J. M., Berenyi A., Fujisawa S., Hsu Y. W., Garcia A. J., Gu X., Zanella S., Kidney J., Gu H., Mao Y., Hooks B. M., Boyden E. S., Buzsáki G., Ramirez J. M., Jones A. R., Svoboda K., Han X., Turner E. E. & Zeng H. A toolbox of Cre-dependent optogenetic transgenic mice for light-induced activation and silencing. *Nat Neuroscience* **15**, 793-802 (2012).
- Gautier A., Gauron C., Volovitch M., Bensimon D., Jullien L. & Vríz S. How to control proteins with light in living systems. *Nat Chemical Biology* **10**, 533–541 (2014).
- Ellis-Davies G. C. Caged compounds: photorelease technology for control of cellular chemistry and physiology. *Nat Methods* **4**, 619-628 (2007).
- Feil R., J. Brocard B. Mascrez M. LeMeur D. Metzger P. Chambon. Ligand-activated site-specific recombination in mice. *Proc. Natl. Acad. Sci. USA* **93**, 10887–10890 (1996).
- Pan X., Wan H., Chia W., Tong Y. & Gong Z. Demonstration of site-directed recombination in transgenic zebrafish using the Cre/loxP system. *Transgenic Res* **14**, 217-223 (2005).
- Sinha D. K., Neveu P., Gagey N., Aujard I., Le Saux T., Rampon C., Gauron C., Kawakami K., Leucht C., Bally-Cuif L., Volovitch M., Bensimon D., Jullien L. & Vríz S. Photoactivation of the CreER T2 recombinase for conditional site-specific recombination with high spatiotemporal resolution. *Zebrafish* **7**, 199-204 (2010).
- Sinha D. K., Neveu P., Gagey N., Aujard I., Benbrahim-Bouzidi C., Le Saux T., Rampon C., Gauron C., Goetz B., Dubruille S., Baaden M., Volovitch M., Bensimon D., Vríz S., Jullien L. Photocontrol of protein activity in cultured cells and zebrafish with one- and two-photon illumination. *Chembiochem* **11**, 653-663 (2010).
- Kobat D., Durst M. E., Nishimura N., Wong A. W., Schaffer C. B. & Xu C. Deep tissue multiphoton microscopy using longer wavelength excitation. *Opt. Express* **17**, 13354–13364 (2009).
- Horton N. G., Wang K., Kobat D., Clark C. G., Wise F. W., Schaffer C. B. & Xu C. *In vivo* three-photon microscopy of subcortical structures within an intact mouse brain. *Nat Photonics* **7**, 205-209 (2013).
- Xu C. & Webb W. W. *Topics in Fluorescence Spectroscopy: Volume 5. Nonlinear and Two-photon-Induced Fluorescence*, edited by Lakowicz, J. Plenum Press, New York (1997).
- Westerfield M. *The Zebrafish Book: A Guide for the Laboratory use of Zebrafish (Danio Rerio)*, 4th ed. Eugene: Univ. of Oregon Press (2000).
- Jopling C., Sleep E., Raya M., Marti M., Raya A. & Izpisua Belmonte, J.C. Zebrafish heart regeneration occurs by cardiomyocyte dedifferentiation and proliferation. *Nature* **464**, 606-609 (2010).
- Karlsson J., von Hofsten J., & Olsson P.E. Generating transparent zebrafish: a refined method to improve detection of gene expression during embryonic development. *Mar Biotechnol* **464**, 522-527 (2001).
- Neveu P., Aujard I., Benbrahim C., Le Saux T., Allemand J-F., Vríz S., Bensimon D., Jullien L. A caged retinoic acid for use with one- and two-photon excitation in zebrafish embryos. *Angew. Chem. Int. Ed.*, **47**, 3744–3746 (2008).
- Vogel A., Noack J., Huettman G., Paltauf G. Mechanisms of femtosecond laser nanosurgery of cells and tissues. *Appl. Phys B* **81**, 1015-1047 (2005).
- Aujard I., Benbrahim C., Gouget M., Ruel O., Baudin J. B., Neveu P. & Jullien L. o-nitrobenzyl photolabile protecting groups with red-shifted absorption: syntheses and uncaging cross-sections for one- and two-photon excitation. *Chem. Eur. J* **12**, 6865-6879 (2006).
- Bort G., Gallavardin T., Ogden D. & Dalko P. I. From One-Photon to Two-Photon Probes: “Caged” Compounds, Actuators, and Photoswitches. *Angew. Chem. Int. Ed.* **52**, 4526-4537 (2013).
- Grynkiewicz G., Poenie M., Tsien R. Y. A new generation of Ca²⁺ indicators with greatly improved fluorescence properties. *J Biol. Chem.* **260**, 3440-3450 (1985).
- Kiskin N. I., Chillingworth R., McCray J. A., Piston D. & Ogden, D. The efficiency of two-photon photolysis of a "caged" fluorophore, o-1-(2-nitrophenyl)ethylpyranine, in relation to photodamage of synaptic terminals. *Eur Biophys J* **30**, 588-604 (2002).
- Poss K.D. & Gupta V. Clonally dominant cardiomyocytes direct heart morphogenesis. *Nature* **484**, 479-485 (2012).

Figures

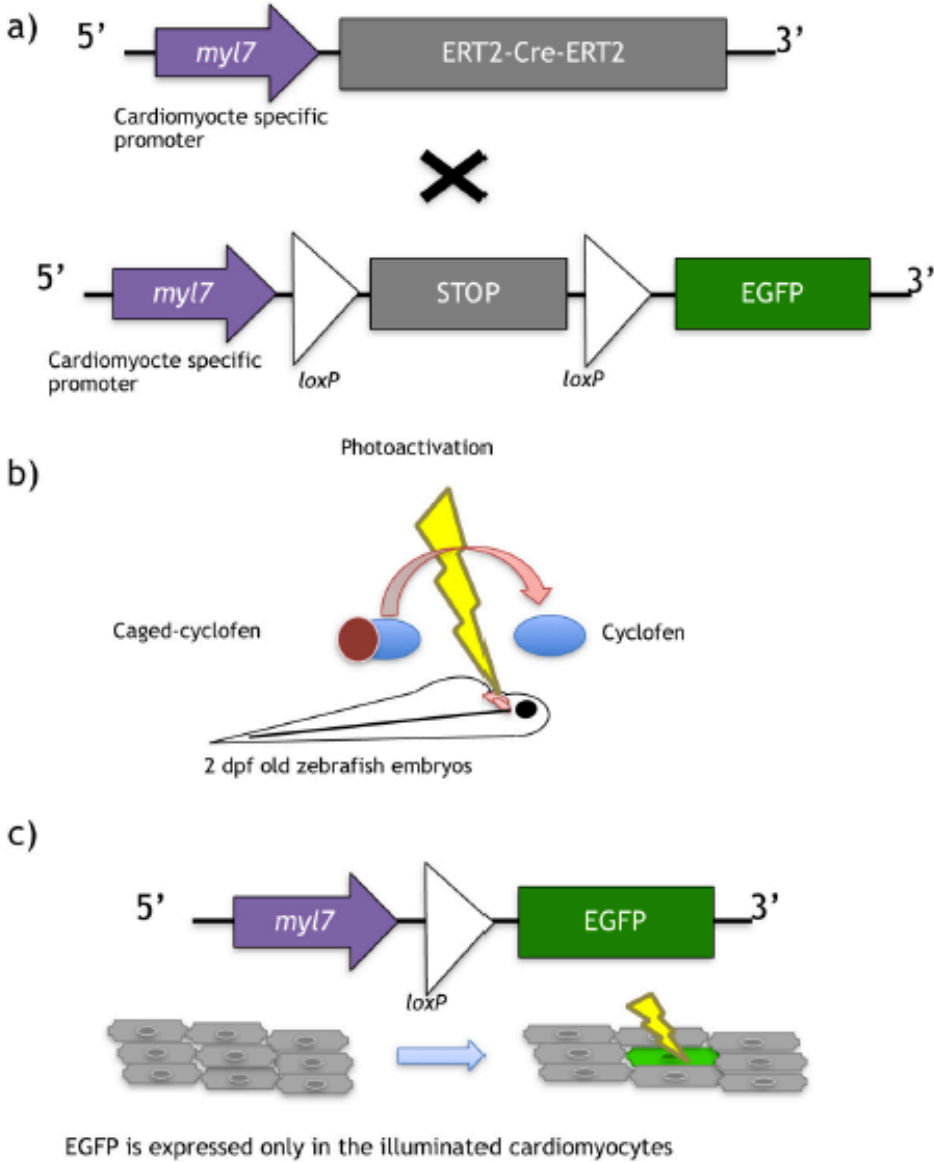


Fig. 1. Photo-inducible Cre-lox system. In this system, Cre activity is controlled by fusing it to a modified fragment of the estrogen receptor (ERT2), which sequesters Cre outside of the nucleus where it cannot perform recombination. In the presence of an estrogen receptor antagonist, Cre enters the nucleus where it mediates recombination. a) shows the transgenic lines used; b) represents uncaging of caged-cyclofen; c) is the final transgene resulting from Cre-mediated recombination in photo-activated cardiomyocytes.

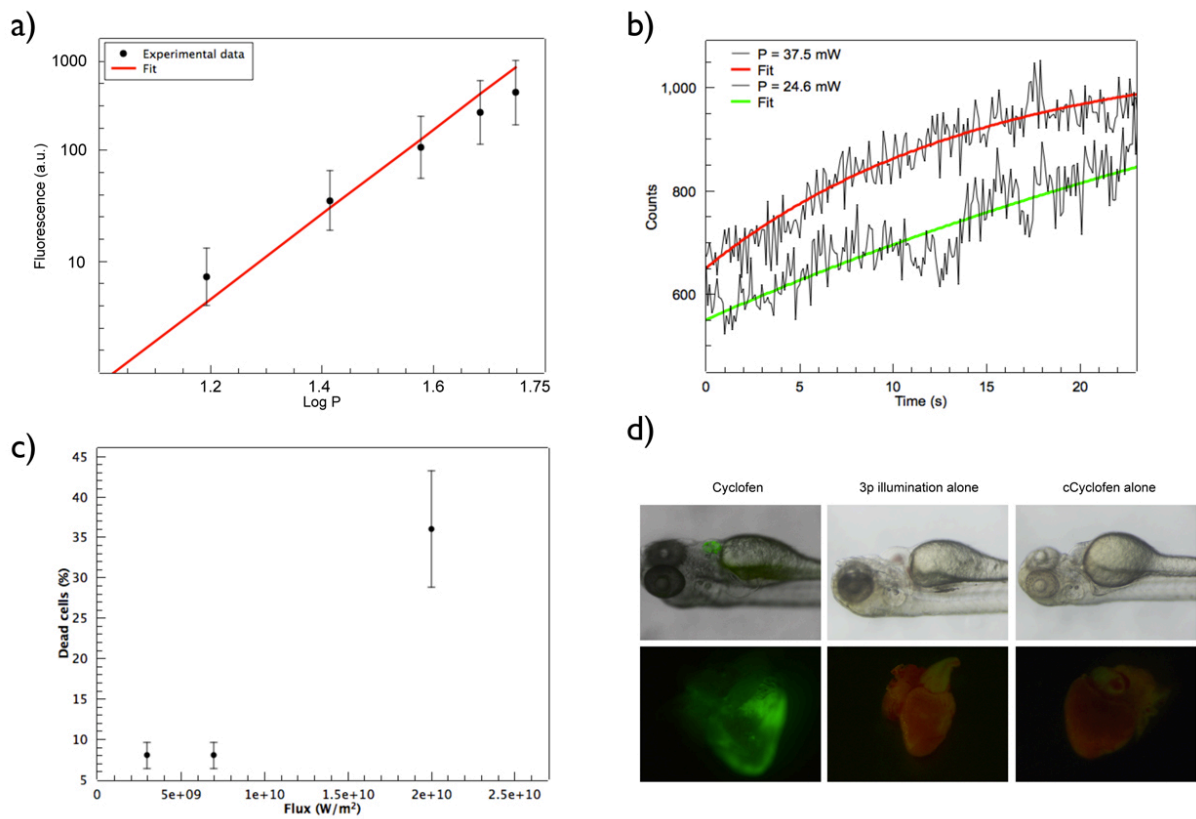


Fig. 2. a) Three-photon excitation fluorescence from blue Fluospheres in suspension (slope of the linear fit, $m = 2.95$) vs. input power at 1064 nm. b) Three-photon uncaging of DMNB-coumarin. Fluorescence increase observed upon illumination of a single cell with 24.6 mW (lower curve) and 37.5 mW (upper curve). c) Percentage of dead cells as function of laser flux for illumination at 1064 nm. d) Control experiments showing activated heart when the animal is exposed to cyclofen, non-activated heart when the animal was illuminated with the three-photon source but not treated with DMNB-cyclofen, and when the animal was treated with DMNB-cyclofen.

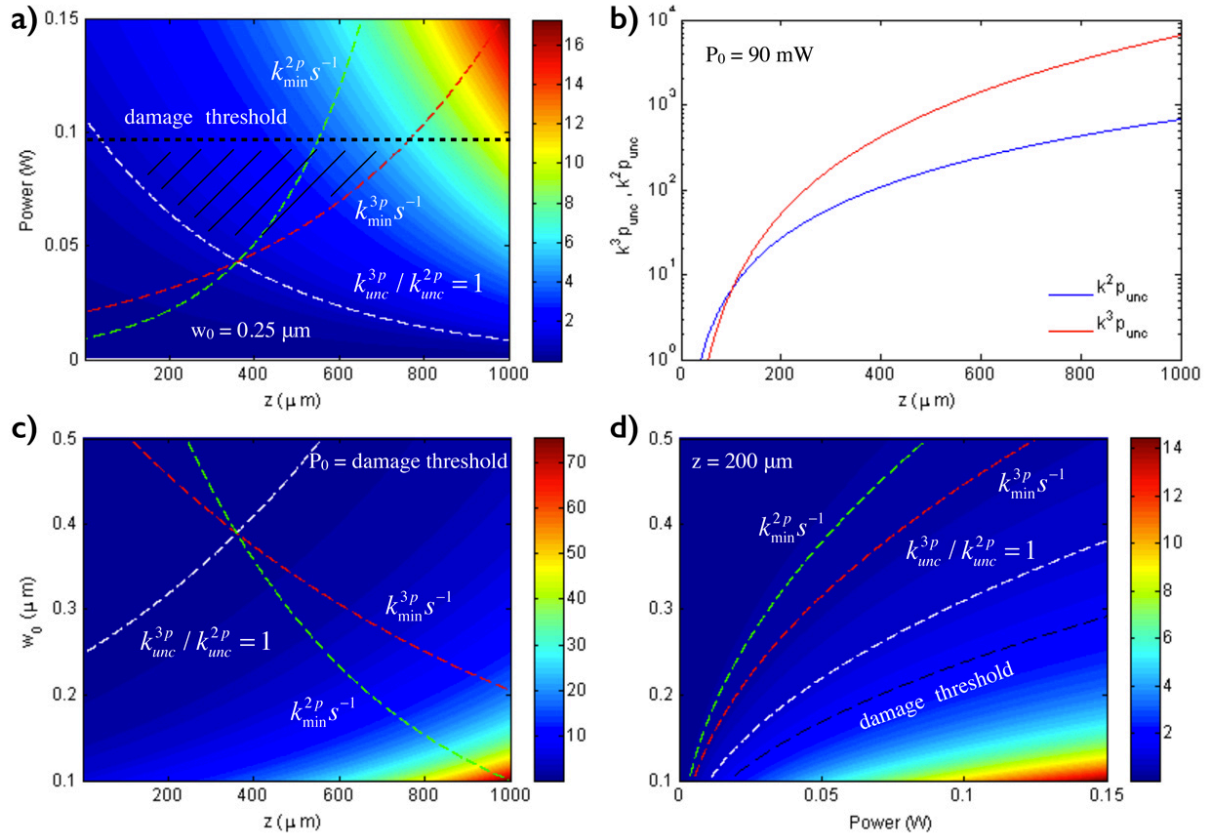


Fig. 3. Numerical results of the ratio between three- and two-photon uncaging rates for DMNB (see Methods for details on the parameters used). Ratio between three- and two-photon uncaging rates for DMNB: a) as function of input power and depth inside the embryo (black dashed line is the damage threshold); b) three- (red) and two- (black) photon uncaging rates for DMNB for $P_0 = 90 \text{ mW}$ as function of depth; and c) ratio between three- and two-photon uncaging rates for DMNB for the same parameters as in a) but at $P_0 = 90 \text{ mW}$ as function of the focal spot radius w_0 ; and d) as function of power and the focal spot radius w_0 for $z = 200 \mu\text{m}$. In all the plots the curves represent the damage threshold (black), $k_{3p}^{unc} / k_{2p}^{unc} = 1$ (white), $k_{3p}^{unc} = k_{3p}^{min} s^{-1}$ (red) and $k_{2p}^{unc} = k_{2p}^{min} s^{-1}$ (green).

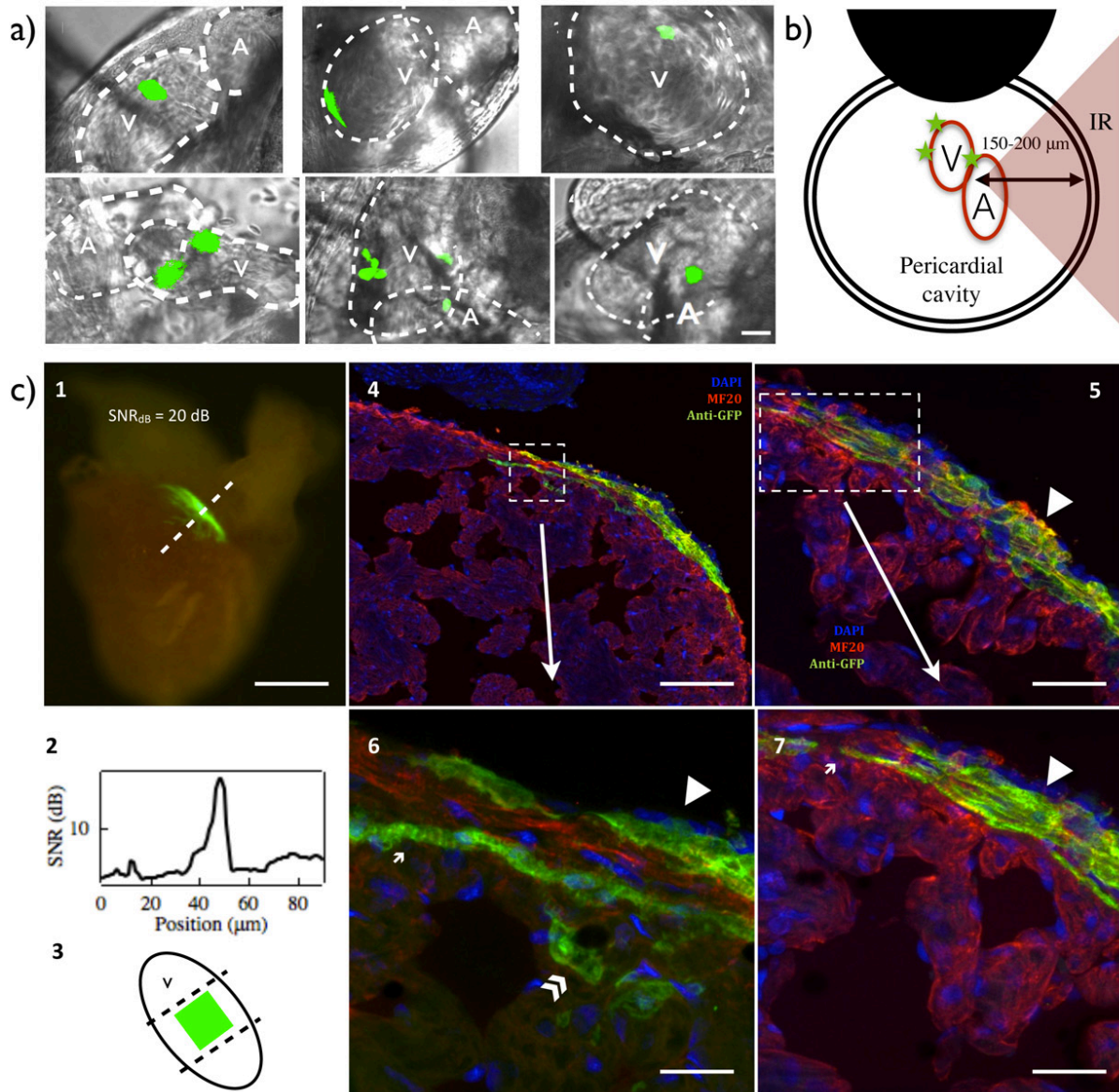


Fig. 4. Long-term *in vivo* lineage tracing of zebrafish cardiomyocytes. a) Selected areas labeled in the heart of the zebrafish embryo in order of accessibility (scale bar 10 μm , for more details see Methods): images 1 and 2 show $\sim 10\text{-}20 \mu\text{m}^2$ labeled areas; 3 shows a single cell of $5 \mu\text{m}^2$; 4 to 6 show multiple labeled areas at different locations; and b) shows a labeled area behind inhomogeneous tissue, at $\sim 150 \mu\text{m}$. c) Excised heart of an adult zebrafish. The original $\sim 10\text{-}20 \mu\text{m}^2$ labeled area was extended to $\sim 0.125 \text{mm}^2$ (scale bar is 250 μm) c.2) shows a fluorescence SNR $\sim 20 \text{dB}$ and c.3) position of the original labeled zone. From c.4) to c.7) immunostaining images of the adult zebrafish heart show the participation of the photoactivated cardiomyocytes in the three layers of the heart wall (scale bar: c.4) 50 μm , c.5) 20 μm , c.6) 5 μm and c.7) 10 μm).

Fate predetermination of cardiac myocytes during zebrafish heart regeneration

Isil Tekeli ^{1,2}, Mario Notari ^{1,2}, Anna Garcia-Puig ^{1,2}, Cristina García-Pastor ^{1,2}, Isabelle Aujard ^{3,4,5},

Ludovic Jullien ^{3,4,5}, Angel Raya ^{1,2,6,7*}

¹ Center of Regenerative Medicine in Barcelona (CMRB), Barcelona Biomedical Research Park, Dr. Aiguader 88, 08003 Barcelona, Spain.

² Control of Stem Cell Potency Group, Institute for Bioengineering of Catalonia (IBEC), Barcelona Science Park, Baldiri Reixac 15-21, 08028 Barcelona, Spain.

³ École Normale Supérieure – PSL Research University, Department of Chemistry, 24 rue Lhomond, F-75005 Paris, France.

⁴ Sorbonne Universités, UPMC Univ Paris 06, PASTEUR, F-75005 Paris, France.

⁵ CNRS, UMR 8640 PASTEUR, F-75005 Paris, France.

⁶ Institució Catalana de Recerca i Estudis Avançats (ICREA).

⁷ Center for Networked Biomedical Research on Bioengineering, Biomaterials and Nanomedicine (CIBER-BBN).

* Address for correspondence: Angel Raya, Phone: +34 933 160 320; Fax: +34 933 160 332; Email: araya@cmrb.eu

Keywords: Cardiomyocytes; Lineage-tracing; Cell migration; Heart development; Cre/lox recombination

Adult zebrafish have the remarkable ability to regenerate their heart upon injury, a process that involves limited dedifferentiation and proliferation of spared cardiomyocytes, and migration of their progeny. During regeneration, proliferating cardiomyocytes are detected throughout the myocardium, including areas distant to the injury site, but whether all of them are able to contribute to the regenerated tissue remains unknown. Here, we developed a cardiomyocyte-specific, photoinducible genetic labeling system, and show that cardiomyocytes labeled in embryonic hearts survive and contribute to all three (primordial, trabecular, and cortical) layers of the adult zebrafish heart. Next, using this system to investigate the fate of cardiomyocytes from different parts of the myocardium during regeneration, we show that only cardiomyocytes immediately adjacent to the injury site contributed to the regenerated tissue. Finally, our results show an extensive predetermination of cardiomyocyte fate during adult heart regeneration, with cells from each myocardial layer giving rise to cells that retain their layer identity in the regenerated myocardium. Overall, our studies indicate that adult heart regeneration in the zebrafish is a rather static process governed by short-range signals, in contrast to the highly dynamic plasticity of cardiomyocyte fates that takes place during embryonic heart regeneration.

INTRODUCTION

The zebrafish has positioned itself as a valuable model for investigating heart regeneration due to its intrinsic capacity to restore large portions of this organ after amputation (Poss et al., 2002; Raya et al., 2003), cryoinjury (Chablais et al., 2011; Gonzalez-Rosa et al., 2011; Schnabel et al., 2011), or genetic ablation (Wang et al., 2011). Following damage of up to 20% of the heart ventricle, adult zebrafish can fully regenerate it through multiple mechanisms that involve limited dedifferentiation of spared cardiomyocytes (CMs), sarcomere disassembly, and CM proliferation through the re-expression of cell cycle regulators such as *plk1* and *mps1*. As demonstrated by lineage-tracing approaches, newly generated CMs arise from pre-existing ones, and therefore CM proliferation appears to be the primary mechanism for CM regeneration after amputation or injury (Jopling et al., 2010; Kikuchi et al., 2010). Cell proliferation assays such as 5-bromo-2'-deoxyuridine (BrdU) or 5-ethynyl-2'-deoxyuridine (EdU) incorporation have shown that most proliferating CMs are located close to the injury site (between 65-75%), although some can also be found throughout the entire myocardium (from 10% up to 30%) (Itou et al., 2012; Jopling et al., 2010; Sallin et al., 2015). Whether proliferating CMs located distant to the injury site actually contribute to myocardial regeneration is currently unknown. However, two pieces of indirect evidence support that this might be the case. First, in the adult zebrafish active migration of CMs toward the injury site was shown to be essential for heart regeneration (Itou

et al., 2012). Second, in zebrafish larvae, CMs from the atrium transdifferentiated into ventricular CMs and migrated all the way to the ventricle, where they contributed to myocardial regeneration (Zhang et al., 2013).

At any rate, it should be noted that this type of cell proliferation assay provides information as to the location of BrdU- or EdU-labeled cells at the time of analysis, which may be different from their original position when they begun proliferating and incorporated BrdU/EdU. This raises the intriguing possibility that CMs could proliferate in specific, perhaps distant zones of the heart, and migrate toward the regenerating area where they would contribute to the newly formed myocardium. An analogous situation has been long known in the context of lens regeneration in newts, where only the pigmented epithelial cells from the dorsal iris contribute to the regenerative process by transdifferentiating into lens cells (Eguchi and Shingai, 1971). In contrast, planarian neoblasts are absent in the most anterior part of the head and the pharynx, making these regions regeneration-incompetent (Salveti et al., 2009). The existence of such regeneration-competent (or regeneration-incompetent) areas has not been previously explored in the context of zebrafish heart regeneration. In the present study, we sought to address these two outstanding questions: whether the CMs that proliferate at places distant to the injury site actually contribute to the regenerated myocardium, and if so, whether they are distributed randomly throughout the zebrafish heart, or they make up specific, regeneration-competent areas.

For this purpose, we have developed a genetic lineage-tracing strategy based on the conditional expression of a fluorescent reporter transgene in a single or few CMs by *Cre/lox* recombination. Since this genetic modification is permanent and inherited by the progeny of the labeled CMs, this system allows lineage tracing of labeled CMs during development and regeneration. Our results show that CMs display a short-range migration, and only CMs immediately adjacent to the injury site contribute to the regenerating myocardium.

RESULTS AND DISCUSSION

Genetic labeling of zebrafish CMs

In order to label specific CMs in different regions of the zebrafish heart, we developed a myocardium-specific UV-inducible *Cre/lox* recombination system. In this system, CM labeling is based on green fluorescent protein (GFP) expression only in the CMs of transgenic zebrafish upon Cre recombination. For this, we first generated a double transgenic zebrafish line by crossing Tg(my17:ERT2-Cre-ERT2) and Tg(-1my17:LOXP-STOP-LOXP-EGFP) (Jopling et al., 2010) (Fig. S1). In these transgenic fish, GFP is expressed only in CMs when a recombination event is induced by tamoxifen administration. In order to label CMs in a specific area, we took advantage of cyclofen, a synthetic analogue of tamoxifen, which can be synthesized as inactive (caged-cyclofen) and turned into its active form by freeing it from its caging group upon UV illumination (Sinha et al., 2010). This feature of the system allows *Cre/lox* recombination to take place only in the cells that are photoactivated.

To test whether cyclofen was able to induce *Cre/lox* recombination in our system, we treated 2-day post-fertilization (dpf) embryos with uncaged cyclofen and assessed GFP-expression two days later. After confirming that the recombination occurred successfully and specifically in CMs (Fig. 1A), these embryos were raised to adulthood to verify that GFP expression was permanent (Fig. 1E,I). To test the existence of leakage in our system, we treated 2-dpf embryos with caged-cyclofen and did not expose them to UV light. In those hearts, no recombination events were induced, as judged by the absence of GFP expression at 4 dpf (Fig. 1B), and in adult animals (Fig. 1F,J). In contrast, we observed successful recombination and strong GFP expression in confined areas of embryonic zebrafish hearts upon UV illumination (Fig. 1C,D). By optimizing the time of illumination and distance from the UV light source, we could obtain hearts with single GFP-labeled areas of an average diameter size of 17.2 μm (n=7), indicating that each GFP-positive area comprised 1-2 CMs (Fig. S2). As expected, these labeled embryos maintained GFP expression in their hearts as adults, demonstrating that labeled CMs survived and passed the recombined construct onto their progeny (Fig. 1G,K,H,L). So far, these results show that our myocardium-specific photoinducible genetic labeling system is suitable to label one or two CMs in the embryonic zebrafish heart for further lineage tracing analysis during development and regeneration.

Genetically labeled CMs were found in primordial, trabecular, and cortical layers

The traditional view of the zebrafish ventricle consisting of two types of cardiac muscle, a peripheral wall of compact muscle and inner trabecular muscle, has been revised by the observation of primordial and cortical muscle lineages within the compact layer (Gupta and Poss, 2012). Analyses of GFP-positive areas in adult hearts labeled as embryos with our novel genetic system provided further evidence for their existence. Thus, we could observe GFP-positive CMs in the innermost

part of the compact myocardium forming a one-cell thick layer (Fig. 2A,A'), highly reminiscent of the primordial layer described by Gupta and Poss (Gupta and Poss, 2012). Surprisingly, this structure was never found labeled alone in our labeled hearts, but always accompanied by labeled CMs in the trabecular zone (n = 16), suggesting that primordial CMs gave rise to trabecular CMs in all of the hearts analyzed. Additionally, we could detect GFP-positive areas located in the outer part of the compact myocardium in adult hearts (Fig. 2C,C'), which would correspond to the cortical layer (Gupta and Poss, 2012). Therefore, our results provide independent confirmation of the visualization of three myocardial layers (primordial, trabecular, and cortical) in the zebrafish heart, using a direct lineage tracing system, and demonstrate that CMs labeled in embryonic hearts survive and contribute to all three layers in adult myocardium.

Out of 30 hearts that were successfully labeled at 2 dpf and verified to contain GFP-positive CMs at 4 dpf, when analyzed as adults, 23 hearts still maintained GFP-labeled areas (Table S1). The absence of GFP-positive CMs in the remaining 7 hearts indicates that either labeled embryonic cells died before giving rise to progeny, or they did not produce progeny at all. This is consistent with previous studies showing that from around 115 embryonic CMs, only around 55 (roughly 50%) go on to form the juvenile zebrafish myocardium (Gupta and Poss, 2012). Among the adult hearts that maintained GFP-labeled areas, approximately 1/3 (7 out of 23, 30%) showed labeled CMs distributed along the three myocardial layers, whereas 40% (9 out of 23) occupied both primordial and trabecular layers, and the remaining 30% (7 out of 23) of GFP-positive areas contained exclusively trabecular CMs (Table S1). It is interesting to note that all labeled areas in adult hearts comprised trabecular muscle, even when no GFP-positive CMs were found in the primordial layer. Previous studies have suggested that the trabecular heart muscle originates from primordial CMs, which detach from the myocardial wall and then reattach, sometimes even at distant places, giving rise to trabeculae (Gupta and Poss, 2012; Liu et al., 2010; Staudt et al., 2014). The relative distribution of GFP-labeled areas found in our studies is consistent with this scenario, and further points out that most primordial CMs should be able to give rise to trabecular muscle, even though they do not contribute to the adult primordial layer. Finally, the GFP-positive areas comprising cortical myocardium detected in our studies ranged in size from 1.2% to 11% of the ventricular surface (Fig. S3), indicating that none of them had labeled a dominant clone in agreement with their reported low frequency (Gupta and Poss, 2012).

Short-range migration of CMs during adult heart regeneration

To analyze the contribution of different GFP-labeled areas to regeneration, we amputated the ventricular apex of 3-month-old fish that had been labeled at 2 dpf and verified to contain GFP-positive CMs at 4 dpf (n=21). We then analyzed the presence of GFP-labeled CMs in the regenerated tissue at 30 days post-amputation (dpa), a time when the regenerative process is well underway and most *de novo* CMs have been produced (Poss et al., 2002; Raya et al., 2003). In 6 of the 21 hearts processed and analyzed in this way, the amputation plane passed through a GFP-labeled area, as shown by the presence of GFP-positive cells in the piece of excised apex tissue (Fig. 3A,B). In 4 of these 6 cases, the GFP-labeled areas affected by the amputation comprised trabecular and primordial myocardial layers, and the regenerated tissue after 30 dpa also contained GFP-positive CMs in the same layers (Fig. 3A',A'). Similarly, the amputation plane cut through labeled trabecular and cortical layers in the remaining 2 hearts, and the regenerated tissue

contained labeled CMs from these two layers (Fig. 3B',B''). In all cases, the seamless continuation of labeled cells from the spared myocardium into the regenerated tissue indicates that CMs in the primordial, trabecular, and cortical layers give rise to new CMs in the corresponding layers of the regenerated myocardium.

With the aim of investigating the existence of specific regeneration-competent areas within the myocardium, and whether the migration of CMs from such zones toward the injury site would occur during regeneration, we performed ventricular amputation in 15 adult zebrafish in which the GFP-labeled areas were located away from the apex. Taken together, the GFP-labeled areas in these hearts covered the vast majority of the ventricular surface, but the amputation plane did not cut through them (Fig. 4A,B). When we analyzed the regenerated area at 30 dpa, we could not find GFP-labeled CMs in any of these hearts (Fig. 4D,E). Thus, our results indicate that CMs proliferating at a distance from the regenerating area (which were found in several GFP-labeled clones; data not shown) do not contribute to the regenerated myocardium. CM proliferation accounts for the regular hemostasis of the zebrafish heart (Wills et al., 2008), so it is likely that the proliferating CMs that we show do not contribute to the regenerated tissue could instead serve to provide higher mechanical force to compensate for the lost tissue. In any case, our combined findings strongly argue against the existence of specific regeneration-competent areas in the adult zebrafish myocardium.

CONCLUSIONS

The present studies take advantage of the direct lineage tracing of CMs during development and regeneration, made possible thanks to a novel myocardium-specific, photoinducible genetic labeling system. Lineage tracing of CMs during development provides independent confirmation of the presence of primordial, trabecular, and cortical layers in the adult zebrafish heart by using a technique complementary to the one used in the original description of these layers (Gupta and Poss, 2012). Cell tracing during adult heart regeneration showed that CMs adjacent to the injury site gave rise to the CMs in the regenerated myocardium, whereas those located farther away, even though they may undergo cell proliferation in response to the injury, did not contribute to the regenerated tissue. These results are in agreement with recent findings showing that 50% of mitotic CMs are found within the first 100 μm adjacent to the injury zone at 7 dpa (Sallin et al., 2015). The overall picture that emerges from our studies of direct CM lineage tracing during adult heart regeneration is of a rather static process, in sharp contrast with the highly dynamic CM fate reprogramming described to take place during embryonic heart regeneration (Zhang et al., 2013). According to our results, only CMs very close to the injury site would be able to proliferate, migrate (perhaps through a *cxcl12a-cxcr4b*-dependent mechanism) (Itou et al., 2012), and give rise to new CMs in the regenerated myocardium. Furthermore, our results show that the predetermination of CM fate during adult heart regeneration is so prevailing that even their identity of layer of origin is retained, and subsequently reproduced in the regenerated tissue. Our combined results reveal important differences in the cellular bases (and probably molecular mechanisms as well) that underlie the process of heart regeneration in developing embryos and in the adult setting, and highlight the key role that short-range signals should have for controlling the latter.

MATERIALS AND METHODS

Zebrafish maintenance and surgical procedures

AB strain wild type and transgenic zebrafish were maintained and raised according to standard protocols (Westerfield, 2000). The generation and characterization of the transgenic zebrafish lines Tg(*myl7:ERT2-Cre-ERT2*) and Tg(-1*myl7:LOXP-STOP-LOXP-EGFP*) were described previously (Jopling et al., 2010). The ventricular amputations were done according to the published protocol (Raya et al., 2003). All experiments were conducted following procedures approved by the Ethics Committee on Experimental Animals of the Barcelona Science Park and/or the Barcelona Biomedical Research Park.

Application of cyclofen and caged-cyclofen

Cyclofen and caged-cyclofen were synthesized and prepared as described previously (Sinha et al., 2010). Zebrafish embryos were incubated overnight in the embryo medium containing 2 μM caged-cyclofen prior to UV exposure. Before UV irradiation, the embryos were washed with fresh embryo medium to avoid any possible interference, which could originate from photoreleasing the caged-cyclofen in the medium.

UV illumination

Zebrafish embryos were treated with 75 μM 1-phenyl 2-thiourea (PTU) at 22 hpf (28 somite stage) as previously described (Karlsson et al., 2001), in order to inhibit pigmentation and allow UV light to reach the heart tissue. Prior to UV illumination, 2-dpf zebrafish were anesthetized using 4.2 ml tricaine solution (4 mg/ml) per 100 ml of fish tank water (Westerfield, 2000). UV illumination was achieved using a bench-top UV lamp (Spectroline FC-100) that emits light of wavelength 365nm. Screening for positive or negative results was done one and two days following each experiment.

Immunofluorescence analyses

Hearts were fixed overnight in 4% paraformaldehyde at 4°C, washed with PBS several times, equilibrated in 30% sucrose in PBS, and frozen in OCT (Tissue-Tek) for cryosectioning. Immunohistochemistry was performed on 10 μm cryosections by using MF20 (DSHB), and anti-GFP (GFP-1020; Aves Labs) primary antibodies; and DyLight 488 (Jackson Immuno Research Laboratories) and Cy3 (Jackson Immuno Research Laboratories) as secondary antibodies.

Microscopy, in vivo imaging and image processing

General screening of the zebrafish larvae for GFP-positive labeled CMs was done under a stereomicroscope (Leica). Detailed images of the positive larvae were done by a spinning-disk confocal microscopy system (PerkinElmer UltraViewERS Spinning-Disk) mounted on a Zeiss Axiovert 200M microscope equipped with a Hamamatsu C9100-50 EMCCD camera. Whole-mount hearts and the heart sections were imaged using a stereomicroscope (Leica), and a confocal microscope (Leica SP5), respectively. Images and videos were processed with the software Adobe Photoshop and Velocity, respectively.

Acknowledgements

We thank Adriana Rodriguez-Marí for help and advice, and Sylvia Bedford-Guaus for critical reading of the manuscript. IT and AG-P were partially supported by pre-doctoral fellowships from FPU and FPI programs, respectively. MN was partially supported by a MINECO Postdoctoral Fellowship (FPDI-2013-18459). Additional support was provided by grants from MINECO (SAF2012-33526), ISCIII-FEDER (TerCel RD12/0019/0019), and AGAUR (2014-SGR-1460).

REFERENCES

- Chablais, F., Veit, J., Rainer, G., Jazwinska, A., 2011. The zebrafish heart regenerates after cryoinjury-induced myocardial infarction. *BMC developmental biology* 11, 21.
- Eguchi, G., Shingai, R., 1971. Cellular analysis on localization of lens forming potency in the newt iris epithelium. *Dev Growth Differ* 13, 337-349.
- Gonzalez-Rosa, J.M., Martin, V., Peralta, M., Torres, M., Mercader, N., 2011. Extensive scar formation and regression during heart regeneration after cryoinjury in zebrafish. *Development* 138, 1663-1674.
- Gupta, V., Poss, K.D., 2012. Clonally dominant cardiomyocytes direct heart morphogenesis. *Nature* 484, 479-484.
- Itou, J., Oishi, I., Kawakami, H., Glass, T.J., Richter, J., Johnson, A., Lund, T.C., Kawakami, Y., 2012. Migration of cardiomyocytes is essential for heart regeneration in zebrafish. *Development* 139, 4133-4142.
- Jopling, C., Sleep, E., Raya, M., Marti, M., Raya, A., Izpisua Belmonte, J.C., 2010. Zebrafish heart regeneration occurs by cardiomyocyte dedifferentiation and proliferation. *Nature* 464, 606-609.
- Karlsson, J., von Hofsten, J., Olsson, P.E., 2001. Generating transparent zebrafish: a refined method to improve detection of gene expression during embryonic development. *Marine biotechnology* 3, 522-527.
- Kikuchi, K., Holdway, J.E., Werdich, A.A., Anderson, R.M., Fang, Y., Egnaczyk, G.F., Evans, T., Macrae, C.A., Stainier, D.Y., Poss, K.D., 2010. Primary contribution to zebrafish heart regeneration by *gata4*(+) cardiomyocytes. *Nature* 464, 601-605.
- Liu, J., Bressan, M., Hassel, D., Huisken, J., Staudt, D., Kikuchi, K., Poss, K.D., Mikawa, T., Stainier, D.Y., 2010. A dual role for ErbB2 signaling in cardiac trabeculation. *Development* 137, 3867-3875.
- Poss, K.D., Wilson, L.G., Keating, M.T., 2002. Heart regeneration in zebrafish. *Science* 298, 2188-2190.
- Raya, A., Koth, C.M., Buscher, D., Kawakami, Y., Itoh, T., Raya, R.M., Sternik, G., Tsai, H.J., Rodriguez-Esteban, C., Izpisua-Belmonte, J.C., 2003. Activation of Notch signaling pathway precedes heart regeneration in zebrafish. *Proceedings of the National Academy of Sciences of the United States of America* 100 Suppl 1, 11889-11895.
- Sallin, P., de Preux Charles, A.S., Duruz, V., Pfefferli, C., Jazwinska, A., 2015. A dual epimorphic and compensatory mode of heart regeneration in zebrafish. *Developmental biology* 399, 27-40.
- Salveti, A., Rossi, L., Bonuccelli, L., Lena, A., Pugliesi, C., Rainaldi, G., Evangelista, M., Gremigni, V., 2009. Adult stem cell plasticity: neoblast repopulation in non-lethally irradiated planarians. *Dev Biol* 328, 305-314.
- Schnabel, K., Wu, C.C., Kurth, T., Weidinger, G., 2011. Regeneration of cryoinjury induced necrotic heart lesions in zebrafish is associated with epicardial activation and cardiomyocyte proliferation. *PloS one* 6, e18503.
- Sinha, D.K., Neveu, P., Gagey, N., Aujard, I., Benbrahim-Bouzidi, C., Le Saux, T., Rampon, C., Gauron, C., Goetz, B., Dubruille, S., Baaden, M., Volovitch, M., Bensimon, D., Vrız, S., Jullien, L., 2010. Photocontrol of protein activity in cultured cells and zebrafish with one- and two-photon illumination. *ChemBiochem : a European journal of chemical biology* 11, 653-663.
- Staudt, D.W., Liu, J., Thorn, K.S., Stuurman, N., Liebling, M., Stainier, D.Y., 2014. High-resolution imaging of cardiomyocyte behavior reveals two distinct steps in ventricular trabeculation. *Development* 141, 585-593.
- Wang, J., Panakova, D., Kikuchi, K., Holdway, J.E., Gemberling, M., Burris, J.S., Singh, S.P., Dickson, A.L., Lin, Y.F., Sabeh, M.K., Werdich, A.A., Yelon, D., Macrae, C.A., Poss, K.D., 2011. The regenerative capacity of zebrafish reverses cardiac failure caused by genetic cardiomyocyte depletion. *Development* 138, 3421-3430.
- Westerfield, M., 2000. *The zebrafish book: a guide for the laboratory use of zebrafish (Danio rerio)*. University of Oregon Press.
- Wills, A.A., Holdway, J.E., Major, R.J., Poss, K.D., 2008. Regulated addition of new myocardial and epicardial cells fosters homeostatic cardiac growth and maintenance in adult zebrafish. *Development* 135, 183-192.
- Zhang, R., Han, P., Yang, H., Ouyang, K., Lee, D., Lin, Y.F., Ocorr, K., Kang, G., Chen, J., Stainier, D.Y., Yelon, D., Chi, N.C., 2013. In vivo cardiac reprogramming contributes to zebrafish heart regeneration. *Nature* 498, 497-501.

FIGURES

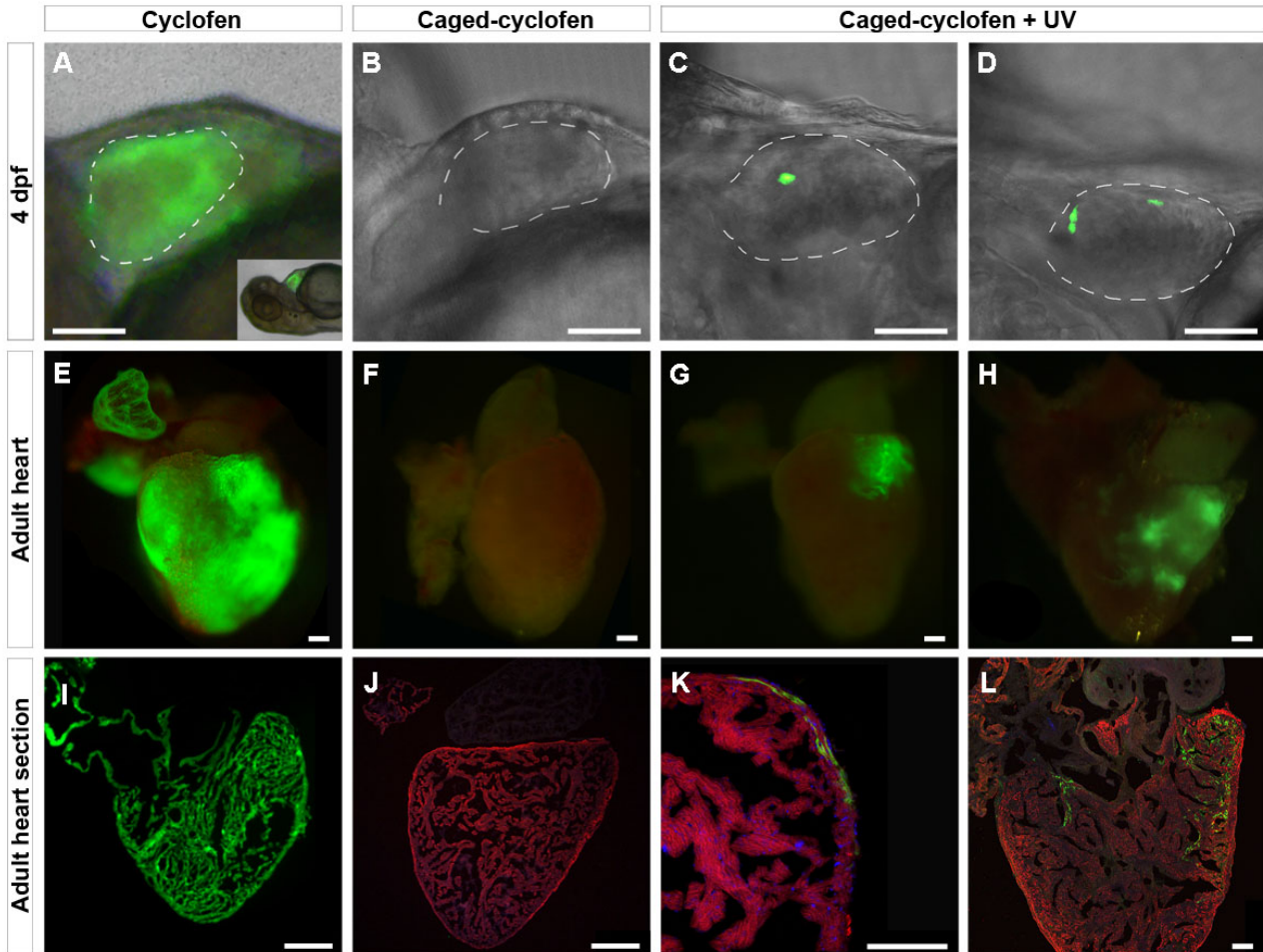


Fig. 1. Genetic labeling of zebrafish CMs using a UV-inducible Cre/lox recombination system. Doubly transgenic embryos [$Tg(myl7:ERT2-Cre-ERT2 \times Tg-Imyl7:LOXP-STOP-LOXP-EGFP)$] were treated at 2 dpf with (A) uncaged cyclofen ($n \sim 100$), (B) caged-cyclofen without UV exposure ($n \sim 100$), and (C,D) caged-cyclofen followed by UV exposure ($n \sim 100$). One fish tank per condition (approximately 40 larvae) was raised to adulthood. Cyclofen works as a tamoxifen analogue and induces recombination in CMs as observed by GFP expression at 4 dpf (A) and at adult stage (E,I). (B,F,J) Caged-cyclofen cannot induce recombination unless it is uncaged by UV exposure (C,D,G,H,K,L). Adult heart sections were processed for immunofluorescence with antibodies against MF20 and GFP. Nuclei were counterstained with DAPI. Scale bars: 150 μm in A-D; 250 μm in E-J; 100 μm in K-L.

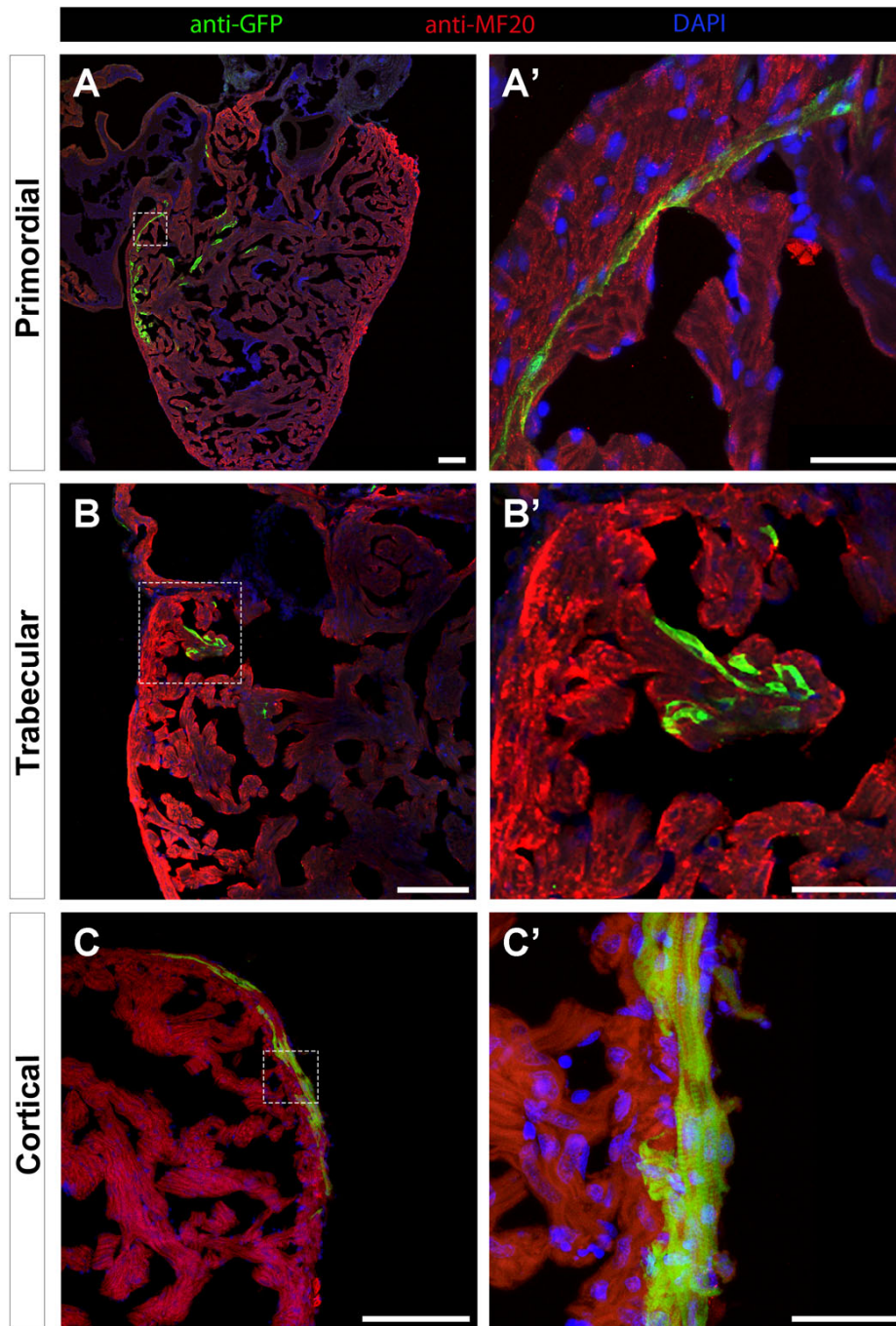


Fig. 2. Genetically labeled CMs are found in all three myocardium layers. Adult zebrafish hearts labeled at 2 dpf were sectioned and processed for immunofluorescence with antibodies against MF20 and GFP. (**A,A'**) GFP-labeled CMs were identified in the primordial layer, (**B,B'**) the trabecular layer, and (**C,C'**) the cortical layer. Nuclei were counterstained with DAPI. Scale bars: 100 μ m in A-C; 25 μ m in A'-C'.

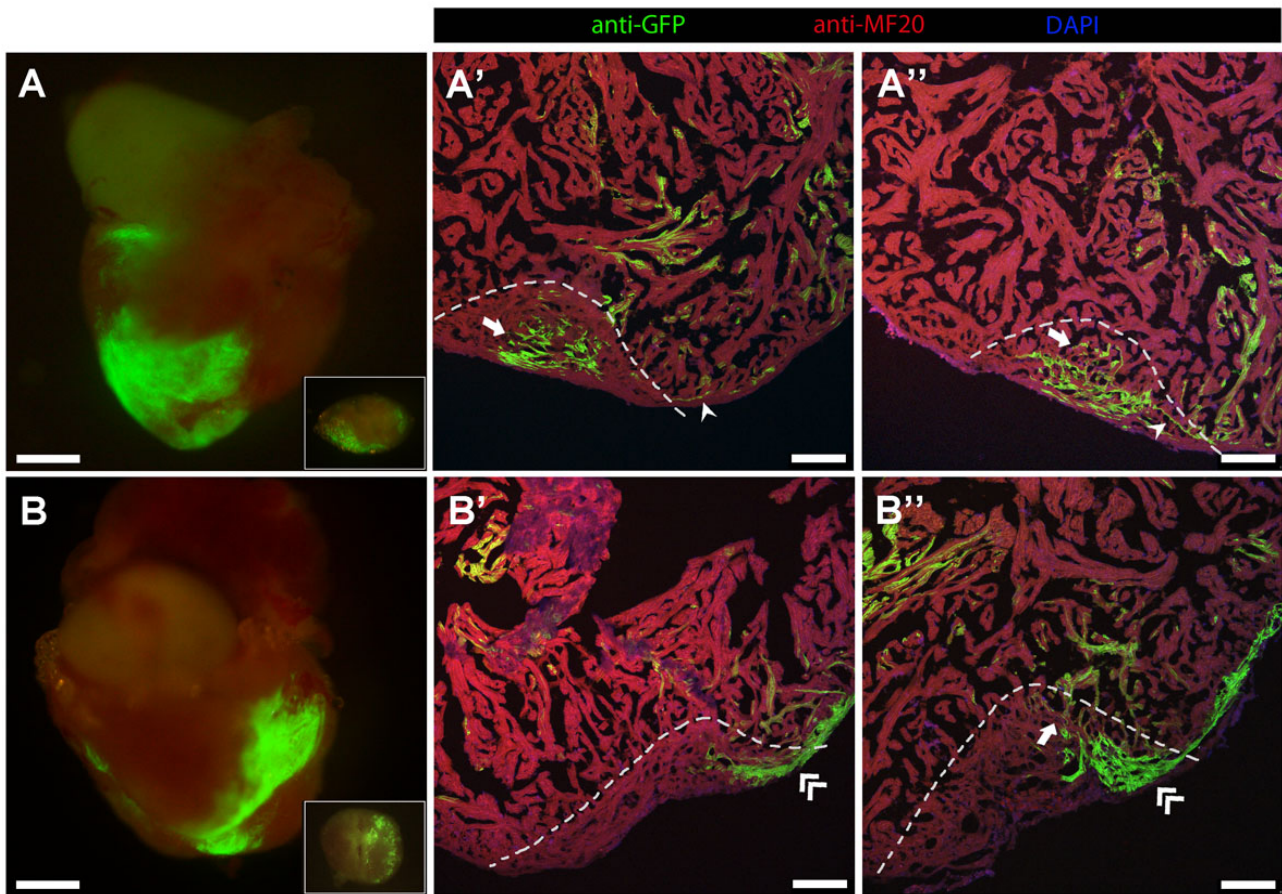


Fig. 3. Cell fate of labeled CMs during regeneration. 3-month-old adult zebrafish labeled at 2 dpf were subjected to ventricular amputation, and after 30 dpa the hearts were collected. (**A,B**) Epifluorescence images of representative hearts where the amputation plane passed through GFP-positive areas. The excised portion of tissue is shown in insert. (**A'-B''**) Collected hearts were sectioned, and processed for immunofluorescence with antibodies against MF20 and GFP. (**A',A''**) Sections of the regenerated myocardium of the heart shown in (**A**), where primordial (arrowhead) and trabecular (arrow) labeled CMs were observed. (**B',B''**) Sections of the regenerated myocardium of the heart shown in (**B**), where trabecular (arrow) and cortical (double-arrowhead) GFP-positive CMs were detected. The amputation plane is indicated by dashed lines. Nuclei were counterstained with DAPI. Scale bars: 500 μm in whole-mount hearts; 100 μm in sections.

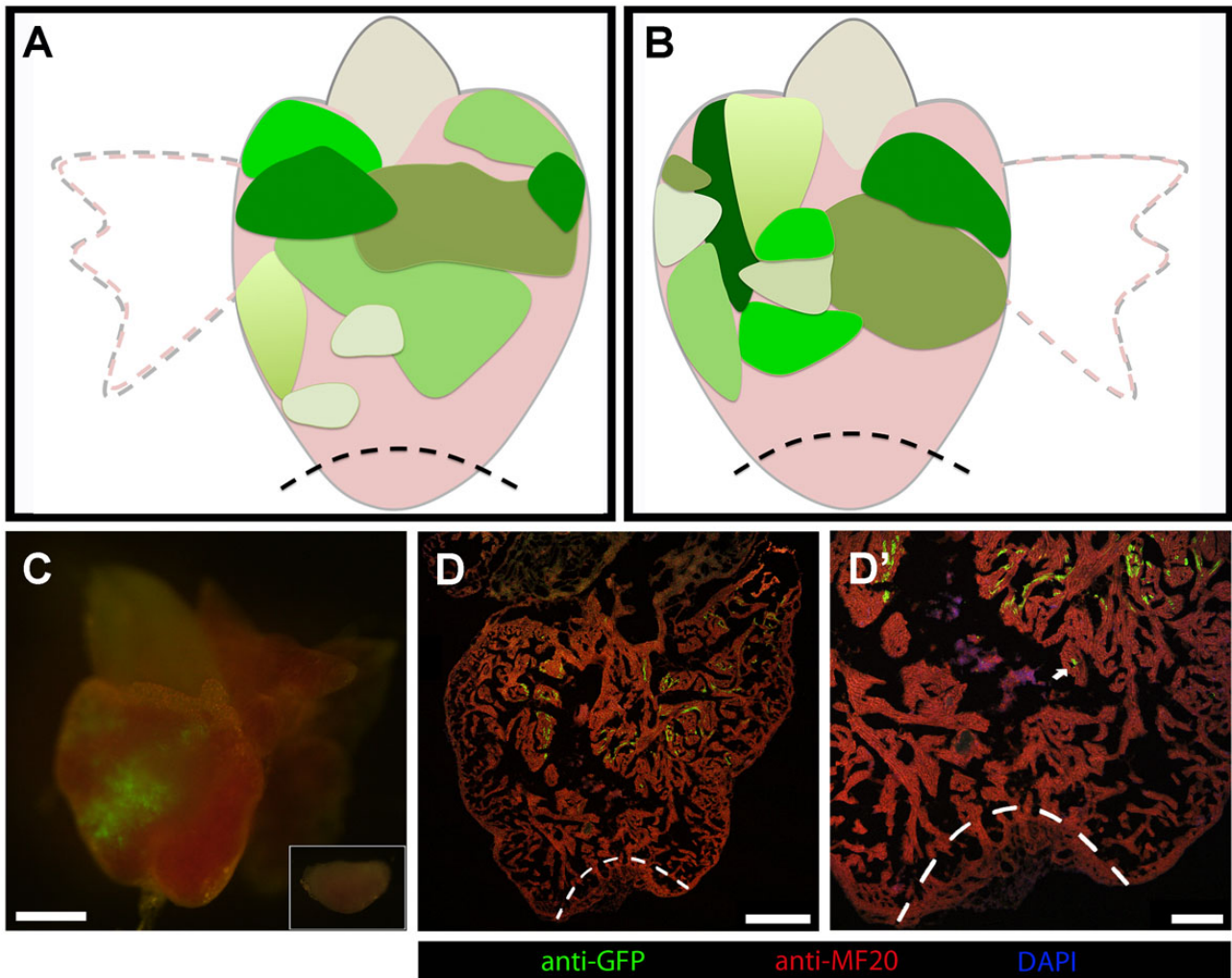


Fig. 4. CMs distant from the amputation site do not contribute to the regenerated tissue. (A,B) Diagram summarizing the size and location of GFP-positive areas from different hearts, which did not contribute to regeneration (n=15). (C) Epifluorescence image of a representative heart where the amputation plane did not pass through the GFP-positive area. The excised portion of tissue is shown in insert. (D-D') Collected hearts were sectioned, and processed for immunofluorescence with antibodies against MF20 and GFP. GFP-labeled CMs are absent in the regenerated area. The amputation plane is indicated by dashed lines. Nuclei were counterstained with DAPI. Scale bars: 500 μm in C; 250 μm in D; 100 μm in D'.

Resumen

El pez cebra (*Danio rerio*) se ha convertido en uno de los modelos más importantes de regeneración del corazón debido a la capacidad intrínseca de restaurar grandes porciones del corazón en caso de una lesión. El corazón humano no tiene esta capacidad regenerativa y por lo tanto, cada 1 de 3 personas sufren de enfermedades cardíacas. Una mejor comprensión de los mecanismos que dirigen este proceso complejo ayudaría a desarrollar estrategias para regenerar el corazón humano y curar las enfermedades cardíacas. Con este objetivo, en este trabajo, hemos creado nuevas aproximaciones de bioingeniería para comprender los mecanismos de migración celular de los cardiomiocitos y de las células epicárdicas durante la regeneración del corazón.

La regeneración del corazón en el pez cebra adulto implica desdiferenciación limitada y la proliferación de los cardiomiocitos, y la migración de su progenie. Durante la regeneración, en todo el miocardio se encuentran cardiomiocitos en proliferación, incluyendo zonas distantes a la herida, pero aún sigue siendo desconocido si todos ellos son capaces de contribuir al tejido regenerado.

El objetivo general de esta tesis ha sido desarrollar estrategias basadas en la aproximación de bioingeniería para estudiar el papel de la migración celular durante la regeneración del corazón del pez cebra. En este aspecto, los objetivos específicos son:

1. Desarrollar un sistema de seguimiento del linaje de los cardiomiocitos del pez cebra basado en técnicas de marcaje genético inducible.
2. Realizar el seguimiento del linaje de los cardiomiocitos durante el desarrollo y la regeneración del corazón del pez cebra mediante la técnica desarrollada en el Objetivo 1.

Resumen

3. Evaluar las capacidades de migración de cardiomiocitos basandose en los datos obtenidos por el seguimiento del linaje de los cardiomiocitos en el Objetivo 2.
4. Desarrollar un método *ex vivo* para analizar la migración de las células del epicardio durante la regeneración del corazón del pez cebra.

Para alcanzar estos objetivos, hemos realizado tres tareas principales.

Primero, hemos desarrollado un sistema photo-inducible de marcaje genética específico para el seguimiento del linaje de los cardiomiocitos y hemos demostrado que los cardiomiocitos marcados en los corazones embrionarios sobreviven y contribuyen a las tres capas musculares (primordial, trabecular y cortical) del corazón del pez cebra adulto. A continuación, utilizando este sistema, hemos investigado el destino de los cardiomiocitos de diferentes partes del miocardio durante la regeneración y hemos demostrado que sólo los cardiomiocitos inmediatamente adyacentes a la lesión contribuyen al tejido regenerado. Finalmente, nuestros resultados han mostrado una extensa predeterminación del destino de los cardiomiocitos durante la regeneración de corazón adulto, es decir, las células de cada capa del miocardio dan lugar a las células de la misma capa y retienen su identidad en el miocardio regenerado. En general, nuestros estudios indican que la regeneración del corazón del pez cebra adulto es un proceso más bien estático, gobernado por señales y migración de corto alcance, contrario a la plasticidad en el destino de los cardiomiocitos que tiene lugar durante la regeneración del corazón embrionario.

A continuación, hemos acoplado este novedoso sistema de marcaje genética a un sistema de activación por microscopía de tres-fotones con el objetivo de aumentar la resolución espacial. Se había demostrado que la iluminación de tres-fotones supera las limitaciones de microscopía de dos-fotones, tales como la dispersión, a la hora de hacer imágenes *in vivo* de estructuras profundas, pero esta técnica nunca había sido utilizado para la foto-activación. En este trabajo, hemos mostrado teóricamente y experimentalmente que la iluminación de tres-fotones supera problemas de dispersión mediante la combinación de excitación con luz de mayor longitud de onda y moléculas con alto corte transversal de “uncaging” por tres-fotones. Hemos utilizado la iluminación de tres fotones en combinación con el sistema de etiquetado genético foto-inducible para marcar las células musculares del corazón en embriones de pez cebra de forma prospectiva. Esta técnica permite la recombinación genética no invasiva con especificidad espacial,

temporal y de tipo celular, y puede tener una amplia aplicación para otros fines de marcaje genética de tejidos profundos.

Por último, hemos desarrollado un sistema *ex vivo* para caracterizar el comportamiento migratorio de las células epicárdicas de corazones de pez cebra con el fin de investigar las características físicas de la migración celular de las células de epicardio durante la regeneración. Este método nos permite medir las características físicas esenciales para la migración celular, tales como la velocidad migratoria y las fuerzas de tracción en las células epicárdicas de corazones no lesionados y corazones regenerando en diferentes etapas de regeneración.

Estas aproximaciones presentadas aquí ofrecen nuevas herramientas de bioingeniería para estudiar la regeneración del corazón del pez cebra y revelar nuevos conocimientos sobre la comprensión de este proceso. Por otra parte, estas técnicas presentan una amplia aplicabilidad para realizar seguimiento del linaje o estudiar el comportamiento migratorio de otros tipos de células durante la regeneración del corazón del pez cebra, u otros procesos biológicos.

Agradecimientos

Escribir estas líneas significa que, por fin, he llegado al final de una etapa muy importante de mi vida. Llegar aquí significa mucho y debo admitir que no ha sido nada fácil, pero hubiera sido imposible sin la ayuda y el apoyo de gente maravillosa que me ha rodeado a lo largo de este trayecto.

Primero que todo, quiero darle mis sinceros agradecimientos a mi director de tesis Ángel Raya. Ángel, gracias por darme la oportunidad de ser parte de tu laboratorio, permitirme dejar mi pequeña huella en el mundo científico, ayudarme a luchar en los momentos más difíciles y siempre confiar en que iba a salir adelante. He aprendido mucho de ti y sin tu apoyo y paciencia sería imposible llegar a este punto. Muchísimas gracias por todo!

A Dobryna y a Marina por vuestra colaboración tan valiosa y la ayuda con la parte técnica de los experimentos. A Mario por tu gran ayuda en la última recta. A todos los que han pasado por el laboratorio de stem cell potency, pero especialmente a mis chicas peces Senda, Adriana, Cristina y Anna; y a Claudia, Yvonne, Juan, Juanlu, Isaac, Raquel, América, Marcel, Sergio y Eduard, por ser tan buenos compañeros, por ideas científicas, por toda la ayuda y el apoyo, por compartir risas, lagrimas, comidas, cafés, cañas, fiestas, resacones, algún viaje por allí, por los momentos buenos y no tan buenos, pero sobretodo por llegar a ser mi familia durante todo este tiempo.

A los vecinos con quien también he compartido mucho, especialmente a Anto, Adriana, Roger, Carles, Irene, Carla, Francesca y los más nuevos miembros.

A Isabel y Carola, a las estudiantes del máster que he tenido el placer de ayudar con sus trabajos. Gracias por vuestra contribución! He aprendido mucho de cada una de vosotras.

Agradecimientos

A la comunidad del IBEC y la de CMRB. Ha sido un placer trabajar con cada uno de vosotros!

A mis amigas Gizem y Ezgi, por todo lo compartido. A mis amigos no científicos que nunca se quejaron cuando la frase más escuchada de los fines de semana era “Nooo..Tengo que ir a dar de comer a los peces..”.

Y más importante, muchísimas gracias a mi familia por los ánimos, el apoyo y el amor que me han dado constantemente a lo largo de este camino largo; y finalmente a Carlos! No podría agradecer suficientemente lo que has hecho por mi! Muchisimas gracias!!